

Review

Open Access



Bifunctional 2D structured catalysts for air electrodes in rechargeable metal-air batteries

Chengang Pei^{1,*}, Dong Zhang^{1,#}, Jaekyum Kim¹, Xu Yu⁵, Uk Sim^{3,*}, Ho Seok Park^{1,4,*}, Jung Kyu Kim^{1,2,*}

¹School of Chemical Engineering, Sungkyunkwan University (SKKU), Suwon 16419, Republic of Korea.

²SKKU Advanced Institute of Nano Technology (SAINT), Sungkyunkwan University, Suwon 16419, Republic of Korea.

³Hydrogen Energy Technology Laboratory, Korea Institute of Energy Technology (KENTECH), Jeonnam 58330, Republic of Korea.

⁴SKKU Institute of Energy Science and Technology (SIEST), Sungkyunkwan University (SKKU), Suwon 16419, Republic of Korea.

⁵School of Chemistry and Chemical Engineering, Yangzhou University, Yangzhou 225002, Jiangsu, China.

#Authors contributed equally.

Correspondence to: Prof. Uk Sim, Hydrogen Energy Technology Laboratory, Korea Institute of Energy Technology (KENTECH), 200 Hyeoksins-ro, Naju, Jeonnam 58330, Republic of Korea. E-mail: usim@kentech.ac.kr; Prof. Ho Seok Park, School of Chemical Engineering, Sungkyunkwan University (SKKU), 2066 Seobu-Ro, Suwon 16419, Republic of Korea. E-mail: phs0727@skku.edu; Prof. Jung Kyu Kim, School of Chemical Engineering, Sungkyunkwan University (SKKU), 2066 Seobu-Ro, Suwon 16419, Republic of Korea. E-mail: legkim@skku.edu

How to cite this article: Pei C, Zhang D, Kim J, Yu X, Sim U, Park HS, Kim JK. Bifunctional 2D structured catalysts for air electrodes in rechargeable metal-air batteries. *Energy Mater* 2024;4:400003. <https://dx.doi.org/10.20517/energymater.2023.66>

Received: 31 Aug 2023 **First Decision:** 8 Oct 2023 **Revised:** 27 Oct 2023 **Accepted:** 10 Nov 2023 **Published:** 3 Jan 2024

Academic Editor: Yuhui Chen **Copy Editor:** Fangyuan Liu **Production Editor:** Fangyuan Liu

Abstract

The inherent technical challenges of metal-air batteries (MABs), arising from the sluggish redox electrochemical reactions on the air electrode, significantly affect their efficiency and life cycle. Two-dimensional (2D) nanomaterials with near-atomic thickness have potential as bifunctional catalysts in MABs because of their distinct structures, exceptional physical properties, and tunable surface chemistries. In this study, the chemistry of representative 2D materials was elucidated, and the comprehensive analysis of the primary modification techniques, including geometric structure manipulation, defect engineering, crystal facet selection, heteroatom doping, single-atom catalyst construction, and composite material synthesis, was conducted. The correlation between material structure and activity is illustrated by examples, with the aim of leading the development of advanced catalysts in MABs. We also focus on the future of MABs from the perspective of bifunctional catalysts, definite mechanisms, and standard measurement. We expect this work to serve as a guide for the design of air electrode materials that can be used in MABs.

Keywords: Two-dimensional material, metal-air battery, air electrode, bifunctional catalyst, oxygen electrochemistry



© The Author(s) 2024. **Open Access** This article is licensed under a Creative Commons Attribution 4.0 International License (<https://creativecommons.org/licenses/by/4.0/>), which permits unrestricted use, sharing, adaptation, distribution and reproduction in any medium or format, for any purpose, even commercially, as long as you give appropriate credit to the original author(s) and the source, provide a link to the Creative Commons license, and indicate if changes were made.



INTRODUCTION

The escalating concerns regarding energy shortages and environmental pollution arising from the overconsumption of fossil fuels are driving global technological development toward reducing fossil fuel dependence and CO₂ emissions^[1,2]. High-efficiency electrical energy storage is vital if we are to achieve sustainable energy, and batteries are instrumental in bridging the gap between energy collection and utilization. Although the high-energy capacity of lithium-ion batteries (LIBs) has resulted in the dominance of the consumer market, the safety issues and increasing material costs associated with these batteries remain challenging^[3]. Additionally, their limited energy density hinders commercial use, especially in electric vehicles with concerns about travel range anxiety.

To circumvent these limitations, substitute energy storage and conversion devices have gained significant attention, with metal-air batteries (MABs) standing out. Of various MABs available, alkaline Zn-air batteries (ZABs) and aprotic lithium-O₂ batteries (LOBs) have emerged as highly promising systems. ZABs offer a theoretical gravimetric energy density that far surpasses the current lithium-ion technology (1,086 W h kg⁻¹), and the abundant and corrosion-resistant Zn anode is considered particularly safe^[4]. LOBs exhibit an even higher energy density, reaching 3,500 W h kg⁻¹^[5]. Collectively, the remarkable features, including high-energy density, cost-effectiveness, and eco-friendly operation, render MABs a possible transformative solution for future energy applications.

MABs have been the subject of research since the last century; however, the development of these batteries remains nascent as compared to the well-established LIBs technologies^[1]. Various challenges, including low roundtrip efficiency, poor rate performance, and limited stability, hinder the widespread adoption of MABs. Besides the impacts stemming from the electrolyte and anode, these challenges primarily arise due to the sluggish kinetics of the oxygen reduction reaction (ORR) and oxygen evolution reaction (OER) occurring at the cathode^[6]. Hence, designing highly efficient bifunctional catalysts is key to the further development of MABs.

Two-dimensional (2D) nanomaterials with large specific surfaces full of exposed atoms and defects have received considerable attention as emerging catalysts^[7]. Broadly speaking, 2D nanomaterials include nanomaterials with 2D morphology and 2D crystal structures. Both of them provide numerous anchor sites for atoms, maximizing the reaction efficiency and facilitating accelerated charge transport by electronic modulation. As a result, 2D materials generally exhibit superior electrocatalytic performance as compared to their three-dimensional (3D) bulk counterparts. Additionally, 2D nanomaterials serve as ideal theoretical calculation models with which to gain insights into the intricate relationship between materials structure and electrocatalytic performance, enabling exploration of the essential structure-property relationship^[8,9]. The promising features of 2D nanomaterials have led to the careful design and utilization of various 2D materials as cathodes in MABs.

While several review articles have explored the possible applications of 2D nanomaterials in energy storage and conversion, a comprehensive review covering all types of 2D nanomaterials with the most commonly employed modification in both ZABs and LOBs remains unavailable. This review begins by introducing the crucial features of MABs, with a detailed explanation of the working principles behind two prominent MAB types: ZABs and LOBs. Then, we delve into the structural and property characteristics of typical 2D materials and explore various strategies for catalyst modification, including geometric structure manipulation, defect engineering, crystal facet selection, heteroatom doping, single-atom catalyst (SAC)

construction, and composite material synthesis. Furthermore, relevant research on catalyst design and its influence on the overall performance of MABs are discussed, providing valuable insights into future catalyst fabrication. Finally, we emphasize the present challenges and offer perspective on the future development of efficient bifunctional catalysts for use with MABs.

OPERATION PRINCIPLES FOR AQUEOUS AND NONAQUEOUS MABS

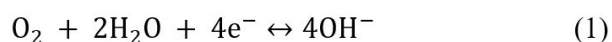
As potential cornerstones of the future energy grid, MABs have received substantial attention over the past few decades. These batteries generally consist of four fundamental components: metal electrodes, air electrodes, electrolytes, and membrane separators. Metals that have been used as anodes in MABs include alkali metals, alkaline earth metals, and first-line transition metals (TMs) with good electrochemical equivalence. Based on the inherent reactivity of the utilized metals with water, MABs are categorized into two distinct classes: aqueous MABs (e.g., Fe, Al, Mg, and Zn) and nonaqueous MABs (e.g., Li, Na, and K)^[10]. The difference in reactivity with water has led to substantial variations in their operational principles, depending on the nature of the electrolytes employed.

Mechanism of aqueous ZABs

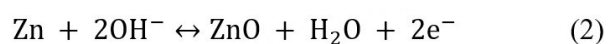
Of the many different aqueous MABs developed so far (including Fe, Al, Mg, and Zn), ZABs have emerged as the most promising. Although Fe-air batteries possess rechargeability, their practical energy density remains significantly lower, typically falling within the range of 60–80 Wh kg⁻¹, rendering them less competitive when compared to prevailing lithium-ion technology. These batteries find their niche in stationary energy storage applications, attributed to their extended cycle life (> 1,000 cycles), cost-effectiveness (< \$100 kWh⁻¹), and environmental compatibility^[2,10]. However, their feasibility for exclusive employment in pure electric vehicle applications is limited. Al-air and Mg-air batteries exhibit considerable theoretical energy densities; however, their susceptibility to severe corrosion upon contact with aqueous electrolytes restricts their practical application. Therefore, this review focuses on ZABs as a representative case to elucidate the underlying reaction principles of aqueous MABs.

As seen in [Figure 1A](#), the ZAB discharging process involves intricate redox reactions at both the Zn and air electrodes:

Air electrode reaction:



Zn electrode reaction:



Overall reaction:



During discharge, atmospheric O₂ molecules penetrate the gas diffusion layer and are reduced to OH⁻ ions on the catalytic layer (equation 1). Simultaneously, Zinc ions are generated at the Zn electrode, with concomitant electron flow to the air electrode through the external circuit. The OH⁻ ions formed at the air

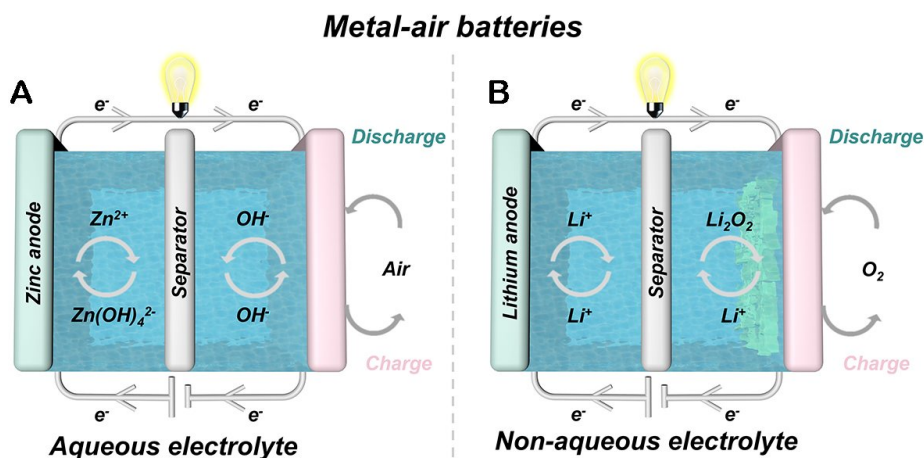
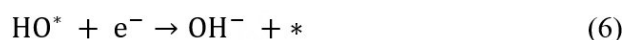


Figure 1. Schematic illustrations of device configurations and working mechanisms of aqueous ZABs and nonaqueous LOBs.

electrode then migrate across the electrolyte through a separator, forming into Zn(OH)_4^{2-} species, which subsequently undergo dehydration to yield ZnO, as illustrated in equation 2. The overall reaction is summarized in equation 3.

It is worth noting that the ORR reaction is quite complex. Verified by many *in situ* characterizations, there are two possible mechanisms of ORR: a dissociation pathway and an associative pathway. In alkaline media, if the O_2 molecule dissociates before the reduction, it belongs to the dissociation mechanism, going through the following steps:



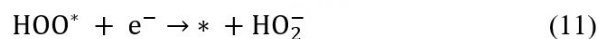
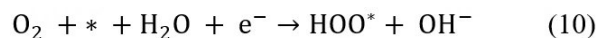
where * represents the active site on the surface of catalysts.

While the O-O bond breaks after a reduction in the associative mechanism, the elementary steps proceed as follows:



And then, the reactions from O^* to hydroxyl ions are the same as equations 5 and 6. The dissociation pathway is the preferred route under conditions of low oxygen surface coverage, whereas the association pathway is favored when the surface exhibits high oxygen coverage.

All of the above are four-electron transfer reactions. While a two-electron transfer ORR reaction often exists as a side reaction, which affects the efficiency of the reaction. In alkaline media, the pathway of two-electron ORR includes the following steps:

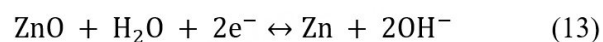


In the initial stages of the development of rechargeable ZABs, depicted reactions were confined to the forward process, characteristic of discharge. However, with the advent of bifunctional catalysts, subsequent advancements have enabled the occurrence of the reverse process, specifically, OER. The redox reactions that occur during recharge are presented as follows:

Air electrode reaction:



Zn electrode reaction:



Overall reaction:



In the charging phase, the air electrode catalyzes a four-electron transfer OER, denoted as equation 12. Concurrently, ZnO, a product from the previous discharge, undergoes reduction, reverting to its original form, Zn, as delineated in equation 13. In an ideal scenario, the charging reaction would equal the inverse of the discharge reaction, as expressed in equation 14.

Mechanism for nonaqueous LOBs

In recent decades, nonaqueous liquid alkali MABs, particularly LOBs, have emerged as prominent subjects for study due to their remarkably high-energy densities and straightforward battery architecture. The seminal work of Abraham *et al.* in 1996, showcasing the first rechargeable nonaqueous LOBs, marked the inception of alkali MABs^[11]. LOBs, which feature Li_2O_2 as the discharge product, exhibit the most promising theoretical performance, boasting a high specific capacity ($3,860 \text{ mA h g}^{-1}$) and a cell voltage of up to $2.96 \text{ V}^{[4]}$. Conversely, Na- O_2 batteries generate a discharge product comprising Na_2O_2 and NaO_2 , while K- O_2 batteries predominantly produce KO_2 . These superoxides or peroxides, insoluble in the electrolyte, tend to accumulate on the air cathode, leading to progressive blockage of the cathode surface and battery shutdown. As a result, LOBs have been selected as representatives in the subsequent discussions.

In the nonaqueous liquid system (depicted in Figure 1B), lithium metal is oxidized into a cation and subsequently shuttled through the electrolyte towards the cathode during discharge (equation 15). The desired electrochemical reaction yielding Li_2O_2 as the discharge product is articulated in equation 16. However, catalytic reactions typically encompass multiple steps rather than a singular equation. As demonstrated in equation 17, the intermediary LiO_2 is initially formed, followed by its conversion into the final discharge product Li_2O_2 . Furthermore, two disproportionation pathways exist for LiO_2 : the surface pathway (equation 18) and the solution pathway (equation 19). The solution route represents a classic electrochemical-chemical coupled reaction that was extensively explored by Savéant^[12]. In instances where LiO_2 disproportionates at the electrode surface, equations 18 and 19 are the same. At this stage,

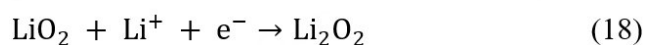
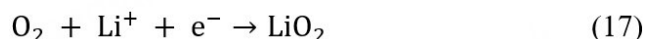
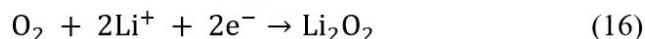
experimental differentiation between surface disproportionation and electro-reduction is challenging, in a manner akin to the Heyrovsky step and Tafel step competition in the hydrogen evolution reaction.

The discharging process of LOBs involves several intricate redox reactions:

Li electrode reaction:

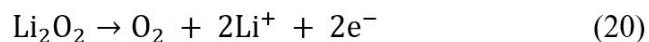


Air electrode reaction:

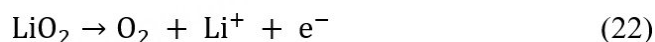
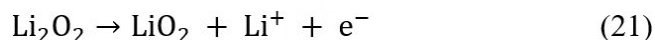


The charging process, commonly recognized as the OER process, ideally involves the entirely reversible decomposition of Li_2O_2 . However, challenges that are associated with the charging process include significant overpotential, diminished coulombic efficiency, and pronounced side reactions. These complications contribute to cathode passivation effects, voltage hysteresis, and the potential for battery deterioration over time. Experiments and theoretical calculations have yielded two primary charge reaction mechanisms for the anode surface in the nonaqueous liquid system^[12]: Mechanism I, which is a two-electron process (equation 20), and Mechanism II (equations 21 and 22), which encompasses two consecutive one-electron processes that involve the formation of LiO_2 from dissolved Li_2O_2 .

When charging, air electrode reaction I:



Air electrode reaction II:



The mechanisms underlying LOBs are considerably more intricate than those associated with ZABs. Despite the preceding summary of the fundamental mechanisms of LOBs, the actual scenarios are far more complex than depicted. Consequently, a substantial array of cutting-edge *in-situ* research tools is required to unravel the intricate reaction mechanisms of LOBs, facilitating the design of enhanced battery systems.

STRUCTURE AND CHEMISTRY OF 2D NANOMATERIALS FOR MABS

Structure and chemistry of 2D nanomaterials

Graphene has played an instrumental role in shaping the trajectory of 2D material development. In the early years, pioneering work by Landau LD and Peierls RE indicated that strictly 2D materials exhibit thermodynamic instability at non-zero temperatures^[7]. It is the discovery and characterization of 2D

graphene that has led researchers to study and explore 2D materials. Presently, the integrity of the theory stands affirmed: actual 2D materials deviate from an ideal flat structure, adopting a distinctive ripple pattern. So far, dozens of 2D materials have been engineered and classified into broad categories, including elements (e.g., graphene, graphdiyne (GDY), black phosphorus (BP), and 2D metal nanosheets), nonmetallic compounds (e.g., g-C₃N₄, h-BN), metallic compounds [e.g., TM dichalcogenides (TMDCs), layered double hydroxide (LDH), and Mxenes], and organics [e.g., metal-organic frameworks (MOF) and covalent-organic frameworks (COF)].

Graphene, characterized by sp² hybridized carbon atoms that are arranged in a 2D hexagonal lattice, offers advantages such as low density, large surface area, high electrical conductivity, and remarkable electrochemical stability. These attributes render graphene a cornerstone in energy storage and conversion. As exploration into graphene advances, there has been a burgeoning interest in designing carbon-based catalysts with heightened degrees of sp hybridization because it is proved that the introduction of ethynyl units may improve the electrochemical properties of carbon. The co-existence of sp-like and sp²-like carbon atoms in GDY endow them with uniformly distributed pores, high π -conjugation, and tunable electronic properties. In the past few decades, theoretical and experimental investigations unveiled the unique properties of GDY, demonstrating their potential in energy storage and conversion^[13]. Different from the materials mentioned so far, the cost and air sensitivity of BP limit its viability for use in MABs. Similarly, although 2D noble metal nanosheets have demonstrated potential in laboratory settings, their low crust content hinders large-scale production, precluding their detailed discussion here.

Within the realm of nonmetallic compounds, g-C₃N₄ exhibits a distinctive structural composition in which the fundamental units encompass either triazine or heptazine cores that yield layered products due to their inherently planar nature. As an n-type semiconductor material, g-C₃N₄ has sparked considerable enthusiasm across research domains, especially in MABs, as a result of its facile synthesis, attractive electronic band structure (with conduction band and valence band energy positions at -1.1 and 1.6 eV, respectively), robust physicochemical stability, and abundance in nature^[14]. Conversely, insulated h-BN, with a wide band gap, is infrequently utilized in MABs, mainly due to its lack of conductivity, which is a requirement of catalysts.

The group of 2D metallic compounds is particularly large as compared to the other three types of 2D materials. TM oxides (TMOs), hydroxides (TMOHs), sulfides (TMSs), selenides (TMSes), tellurides (TMTes), phosphides (TMPs), nitrides (TMNs), carbides (TMCs), and borides (TMBs) with nanosheet structure are all involved in this group. Many metal compounds have demonstrated prowess in catalyzing OER and ORR, with LDH, TMDC, and MXenes being the most representative. LDHs, referred to as hydrotalcite-like compounds, are a large family of 2D anionic clay materials with the formula $[M^{2+}_{(1-x)}M^{3+}_x(OH)_2]^{x+}(A^{n-})_{x/n} \cdot mH_2O$, in which M²⁺ refers to divalent cations, while M³⁺ signifies trivalent cations. As efficient and stable catalysts, LDHs are bolstered by attributes such as composition flexibility, cost-effectiveness, and ease of preparation. TMDCs, which are typified by the formula MX₂ (M = Mo, W, Re, Ti, V; X = S, Se, Te), consist of two layers of X atoms and an intervening M atom layer, with interactions between the stacked layers governed by the van der Waals forces. They have been applied in hydrogen evolution reactions, alkali metal-ion batteries, and supercapacitors and have even been used in LOBs due to their high surface area, easily controlled exposed crystal facets, and diverse compositions. However, the catalytic performance of TMDCs in terms of the traditional OER and ORR is limited, rendering its application in ZABs exceedingly uncommon. In comparison, MXenes, represented by M_{n+1}X_nT_x (M = early TMs, X = C and/or N, T = surface terminated functional groups), are a more recently explored 2D nanomaterial family. Noted for their excellent electrical conductivity and hydrophilic surfaces, MXene-

based materials have exhibited significant promise in many energy applications.

MOFs/COFs have emerged as the pivotal class of materials that are particularly promising for use in MABs^[15]. They have garnered considerable attention due to their versatile framework structures, distinctive porosity, and expansive surface areas. MOFs comprise inorganic-organic infinite frameworks via interactions between metal nodes and organic linkers, while COFs comprise ordered honeycomb-like structures that are composed of organic linkers and linkage. While most MOFs and COFs do not inherently qualify as 2D materials, the strategic design of 2D MOFs/COFs can yield distinct advantages over their 3D counterparts. Specifically, the readily available active sites that lie on the surfaces of the exfoliated 2D MOFs/COFs layers ensure unhindered access for substrates and reagents without diffusion limitations. Another unique feature of 2D MOFs/COFs is that they have defective and exchangeable coordination positions at the metal nodes, suggesting enhanced catalytic efficiency as compared to their 3D analogs. Notably, 2D MOFs/COFs often exhibit chemical and thermal stability that is akin to or even exceeds their 3D counterparts.

Approaches to the modification of 2D catalysts

It has been widely recognized that whether it is an aqueous MAB or aprotic LOB, the performances are mainly determined by the cathode ORR and OER. Yet, both ORR and OER are hindered by substantial overpotential, sluggish kinetics, and huge energy barriers. Consequently, the development of efficient electrocatalysts assumes paramount importance. When designing and fabricating catalysts, several facets must be deliberated from structural and performance perspectives, encompassing the density of active sites, intrinsic activity of each site, electrical conductivity, robust stability, and enduring durability. Nevertheless, pristine 2D materials often lack the capacity to fulfill the multifaceted demands of a catalyst, meaning that modification and enhancement are required. In the subsequent discourse, the modification strategies for 2D materials are categorized into six principal domains: geometric structure control, defect engineering, crystal facet selection, heteroatom doping, SAC construction, and composite material synthesis [Figure 2].

The morphology control methods of 2D materials can be divided into two categories. The first pertains to the manipulation of single-layer nanosheets and includes size modulation and the introduction of holes. The second approach involves crafting hierarchical architectures that are composed of multiple nanosheets. Unlike other techniques, morphology control is aimed primarily at amplifying the number of active sites within a material to bolster its overall catalytic efficacy. Several studies have verified that cathode catalysts featuring large active surfaces are conducive to the deposition and decomposition of solid discharge products, thereby enhancing both capacity and reversibility. Furthermore, the migration of constituents such as O₂, electrolyte ions, reaction intermediates, by-products, and primary discharge products within MABs directly influences the catalytic efficiency of the cathode. The constructed hierarchical structures frequently feature many voids and conduits that significantly enhance charge transfer and facilitate mass transport.

Two-dimensional materials with high surface activity provide a favorable platform for the formation and evolution of defects. Ultrathin 2D materials are believed to possess higher surface energy and abundant coordination-unsaturated sites as compared to their bulk counterparts, facilitating the development of vacancies, lattice dislocations, and distortions. Therefore, extensive investigation into defect engineering has been conducted to finely tune the physical and chemical attributes of 2D nanomaterials. Previous investigations have demonstrated that thoughtfully designed defects can proficiently modulate carrier concentration and energy band structures, thereby augmenting electrical conductivity for energy-related applications. Furthermore, a spectrum of defect engineering strategies can be harnessed to invigorate

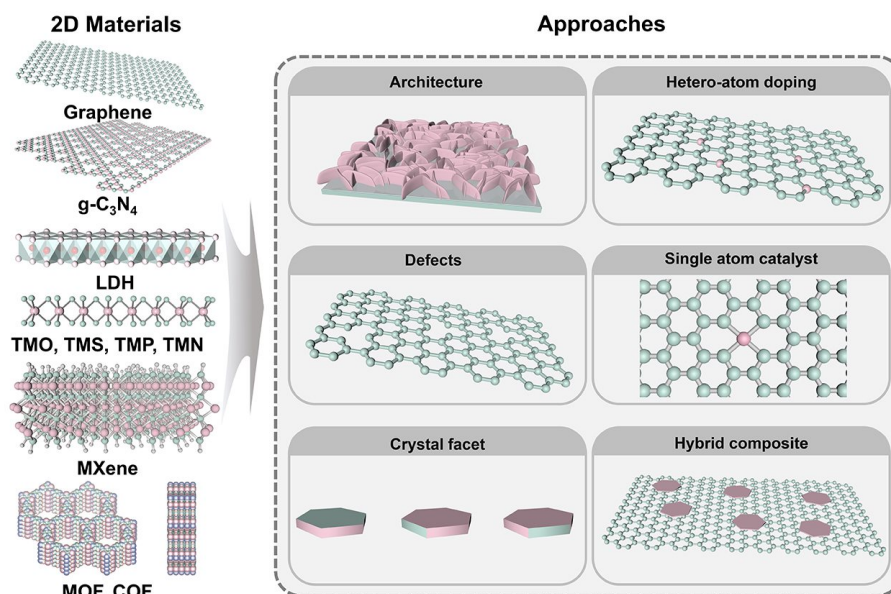


Figure 2. Schematic representation of different 2D materials and approaches to mitigating the challenges associated with MABs.

surface chemical activity and diminish reaction energy barriers within electrode materials. This approach also engenders additional active adsorption/storage sites associated with defects, thereby amplifying catalytic and electrochemical performance.

The properties of heterogeneous catalysis are intricately linked to the atomic arrangement of the exposed surfaces and geometric sites. The meticulous engineering of surface structures at the atomic level offers a means to precisely control the exposure of active sites, thereby amplifying electrocatalytic activities. Consequently, the targeted modification of material chemical and physical attributes through selective facet engineering has emerged as a pivotal research domain to optimize performances across diverse applications. Different crystal planes manifest distinct catalytic properties, including surface stability, oxygen vacancy formation energy, and interactions with surface molecules. For instance, the crystal plane effect of Co_3O_4 as a cathode catalyst for LOBs has garnered substantial attention in recent years. Su *et al.* successfully synthesized high-quality single-crystalline Co_3O_4 nanocrystals, including $\{110\}$ facets exposed Co_3O_4 nanosheets, $\{112\}$ facets exposed Co_3O_4 nanolaminars, and $\{111\}$ facets exposed hexagonal Co_3O_4 nanoplatelets, and demonstrated that the crystal planes reduce the charge-discharge overpotential in the order: $\{110\} < \{112\} < \{111\}$, in accordance with their respective surface energy rankings^[16].

Doping of 2D materials offers a means to modulate their electrical, optical, and magnetic attributes. Basically, all 2D materials are amenable to doping, and the large specific surface area with abundant exposed active sites facilitates infusion. The various techniques that can be used for doping are broadly categorized into in-situ doping during 2D material synthesis and post-doping following material preparation. Doping atoms can be both nonmetallic and metallic. Incorporating single heteroatoms, such as B, N, S, and F, can significantly reshape the electronic structure and chemical environment of active sites in 2D materials. The electron acceptance or donation between heteroatoms and the adjacent host atoms leads to altered charge distribution in the host interface, consequently influencing the adsorption energy of oxygen intermediates. In contrast to single-atom doping, multi-atom doping often engenders unexpected enhancements in catalyst performance. Dual doping within a carbon framework can yield synergistic coupling between the

two heteroatoms, remarkably boosting oxygen reactivity. Metal elements can also be introduced into the structures of TM compounds as dopants to engineer tunable electrocatalytic abilities. Notably, TMs typically possess empty d orbitals that function as electrophilic sites for electrons; hence, cation doping is the suitable approach to optimizing the energy levels of catalysts for the adsorption and activation of pivotal intermediates during electrocatalysis. Moreover, the doping content significantly influences the catalytic performance of 2D nanomaterials, mirroring the alteration extent in the intrinsic host material structure. To a certain degree, increasing the doping content leads to a rise in the number of unsaturated sites in TM compounds, augmenting electrocatalysis. However, excessively high dopant content can also trigger undesirable effects in both structural and physical properties. The reduced distance between dopants associated with excessive doping can potentially lead to aggregation and even the formation of secondary phases. Therefore, when designing metal-doped catalysts, special attention should be paid to the doping content.

The concept of single-site heterogeneous catalysts was first proposed by John in 2005 when development was initiated with the first preparation of a single-atom Pt catalyst on FeO_x [17,18]. Researchers have discovered that reducing the size of bulk catalysts to a single atom (SA) on a substrate conserves the usage of metal sources and leads to an alteration of their electronic state from a continuous one to discrete features, potentially yielding unique properties. Recent investigations have validated unexpectedly excellent characteristics for SAs loaded onto ultrathin nanosheets as compared to larger-size nanoparticles loaded onto 2D nanosheets or SAs loaded onto 3D bulk carriers. Characteristic SACs that are loaded onto 2D materials exhibit the following traits. First, when compared to 3D materials that support SACs, the SAs confined within 2D structures tend to possess more coordinatively unsaturated states due to vacancies on both sides of the basal plane. This unsaturation renders them more likely to achieve enhanced catalytic performance. Second, the open structure on both sides of the 2D plane facilitates a rapid mass transfer process as compared to SACs on 3D supports, theoretically ensuring the complete exposure of SAs to reactants and maximizing catalytic reaction rates. Third, advanced characterization techniques can accurately probe the local atomic structure and electronic states of the SAs that are confined within 2D materials, not only enabling prediction of the molecular reaction dynamics during catalysis but also facilitating model studies that can investigate the intricate interplay between geometric effects, electronic effects, and catalytic performance. It is worth noting that confined SAs can be either exposed directly for use as active sites on 2D supports or embedded within 2D structures, where they modify the electronic properties of inherently inactive 2D materials to initiate catalytic activity. The strong electronic interaction between confined SAs and the 2D structure fundamentally impacts the catalytic properties of an active site. In essence, precise catalyst control can be attained by manipulating the electronic structure of a SA or the surface chemical environment of a 2D carrier. Taking the example of a SA on graphene, it features atomically dispersed TM centers (e.g., Fe, Co, Ni, Cu, Mn) and their adjacent coordinated atoms confined within carbon frameworks. Additionally, heteroatoms such as N, S, O, and P can be doped into the carbon matrix, referred to as environmental atoms. Moreover, the central metal atoms have unsaturated coordination and can interact further with potential guest groups, including small molecules and inorganic particles. Recent research has also explored the introduction of additional central metal atoms into the system, with the newly developed multi-atom catalysts exhibiting higher intrinsic activity due to the synergistic effects between the adjacent central metal atoms. It should be noted that the construction of SACs does have similarities with metal doping, a fact that can be confusing. When it comes to the definition, doping is the introduction of foreign atoms into the lattice of catalysts, in which the main point is the location of heteroatomic doping. However, the focus of SACs is whether the introduced heteroatom is surrounded by the same metal atom. When the amount of doping is small, the introduced metal atoms can be dispersed separately in the catalyst, and the resulting material can be considered as the SAC. As the content of metal dopants increases, the metal atoms are difficult to isolate, so the catalyst is not the SAC anymore.

Constructing complexes is also a common strategy for enhancing catalyst performance. Since a single material generally cannot simultaneously fulfill the activity, conductivity, and stability requirements, the introduction of another material becomes essential. This is particularly significant in MABs where catalysts need to efficiently facilitate both OER and ORR. Finding an electrocatalyst with high activity for either ORR or OER is usually achievable; however, discovering one that has high activity for both reactions is challenging due to the distinct demands for different active sites or metal-ion valence states. Numerous heterostructures of varying dimensionalities have been synthesized for MABs, including zero-dimensional (0D) nanoparticles loaded onto 2D nanosheets, one-dimensional (1D) nanotubes or nanofibers incorporated into 2D nanosheets, and 2D nanosheets combined with other 2D nanosheets. Developing heterostructures based on 2D materials not only retains the inherent advantages of pristine 2D materials but also can introduce new possibilities to properties of materials such as exceptional mechanical strength, rapid electronic and ionic conductivities, enhanced electrochemical activity, and structural stability.

2D MATERIALS FOR AQUEOUS ZABS

ZABs have gained attention as potential sustainable energy solutions thanks to their notable energy density, cost-efficiency, and safety attributes. However, the dearth of suitable bifunctional catalysts poses a notable hindrance to the progress of ZABs. Among the many alternative materials, 2D materials with large surface area, controllable structure, and unique physicochemical promise to act as high-efficiency bifunctional catalysts in ZABs^[19]. 2D materials, such as graphene, GDY, TMOs/TMOHs, TMDCs, TMPs, MXenes, BP, COFs, and MOFs, have been increasingly utilized in OER and ORR, especially in the last five years^[20]. Despite the fact that the substantial effects of advanced 2D materials have contributed to the development of ZABs, this field of research is still in its infancy. Therefore, it is necessary to summarize the recent advances of various 2D materials in ZABs. Here, we divide 2D nanomaterials into five broad categories. The detailed electrochemical performance, including the overpotential of OER ($E_{j=10}$), the half-wave potential of ORR ($E_{1/2}$), power density, and specific capacity in ZABs, were briefly compared in [Table 1](#). Also, for easier comparison of various catalysts, OER and ORR performance are listed in [Figure 3](#). Then, detailed descriptions of each of these materials applied in ZABs were given below.

2D carbon-based materials

Carbon materials are employed as conductive additives and electrocatalysts for ZABs owing to their excellent conductivity, cost-effectiveness, and customizable structure^[63]. However, the thermodynamically low corrosion potential of pure carbon (+0.207 V vs. NHE) can induce electrochemical corrosion during the cell operation. It will further accelerate the deactivation of catalytic active sites due to the production of some stable oxidative intermediates, such as phenols, lactones, and carboxylic acids, and finally lead to a decline in both the activity and durability of carbon-based materials. To solve the carbon corrosion issue at high anodic potentials, some strategies can be employed, including the modification of its composition utilizing heteroatom-doped carbon, the synergistic cooperation incorporating carbon with other materials via a strong coupling interaction, and the manipulation of the crystal structure enhancing graphitization and reducing defect^[64,65]. In recent years, the 2D graphitic structures, such as graphene and GDY, have been extensively utilized for enhancing the electrocatalytic stability because their tightly packed sp^2 hybridized carbon bonds possess the robustness against the corrosion during the electrochemical cell operation^[66,67]. While 2D carbon-based materials play a vital role as cathode materials in ZABs, there remains a substantial distance in catalytic activity when compared to metal-based materials. So, it is necessary to enhance the catalytic activity, mainly strategies including defect engineering (e.g., topological defects and edges) and heteroatom doping (N, P alternating electron and active sites)^[68].

Table 1. Comparison of different types of 2D electrocatalyst performance for ZABs

	Electrocatalysts	OER	ORR	ZABs				Refs.
		$E_{j=10}$ (V vs. RHE)	$E_{1/2}$ (V vs. RHE)	Electrolyte	Peak power density (mW cm ⁻²)	Specific capacity (mAh g _{Zn} ⁻¹)	Cycling stability	
2D Carbon-based materials	NGM	1.67	0.77	6 M KOH	3	-	-	[21]
	d-pGCS-1000	-	0.82	6 M KOH + 0.2 M Zn(Ac) ₂	182.8	773@5	-	[22]
	NCF	-	0.85	6 M KOH + 0.2 M Zn(Ac) ₂	173	-	-	[23]
	N/biochar-800-7	-	0.9	6 M KOH	125	703@5	60 h at 5 mA cm ⁻²	[24]
	N-GDY-900	1.796	0.83	6 M KOH	84	693@10	Over 300 h (450 cycles)	[25]
	2D-PPCN-2/6	-	0.85	6 M KOH + 0.2 M Zn(Ac) ₂	-	-	1,000 cycles	[26]
	NPC-“Li”	1.559	0.83	6 M KOH + 0.2 M Zn(Ac) ₂	-	733@20	10 min/cycle for 150 cycles	[27]
	NSP-Gra	1.76	0.82	6 M KOH	225	-	40 h	[28]
	NPS-G	-	0.857	6 M KOH + 0.2 M Zn(Ac) ₂	151	686@10	20 h at 10 mA cm ⁻²	[29]
Metal-decorated 2D carbon materials	Co@NCNSs-900	1.59	0.85	6 M KOH + 0.2 M Zn(Ac) ₂	271	-	400 cycles (133 h)	[30]
	CuCo@N-C	1.46	0.81	6 M KOH + 0.2 M Zn(Ac) ₂	170	822@5	300 cycles (about 50 h)	[31]
	Fe-N/C-700	-	0.84	6 M KOH	-	727@5	100 h at 5 mA cm ⁻²	[32]
	FeNC-D0.5	-	0.866	6 M KOH	356	-	25 h at 10 mA cm ⁻²	[33]
	FeMn-DSAC	-	0.922	6 M KOH + 0.2 M Zn(Ac) ₂	184	-	200 cycles (80 h)	[34]
	Zn-SAs/UNCNS	-	0.91	6 M KOH	282	798.6@100	Over 20 h at 10 mA cm ⁻²	[35]
	SA-Fe-SNC@900	1.632	0.876	6 M KOH + 0.2 M Zn(Ac) ₂	218.6	798.7@5	200 h at 10 mA cm ⁻²	[36]
	Fe-N, O/G	-	0.86	6 M KOH	164.7	-	>150 h at 20 mA cm ⁻²	[37]
	A-Fe-NC	-	0.865	6 M KOH + 0.2 M Zn(Ac) ₂	132.2	-	240 h at 10 mA cm ⁻²	[38]
	CoSA/NCs	1.533	0.87	6 M KOH + 0.2 M Zn(Ac) ₂	255	908.7@20	6,000 cycles (- 2,000 h)	[39]
	Fe-SA-NSFC	-	0.91	6 M KOH + 0.2 M Zn(Ac) ₂	247.7	792.1@10	240 h at 10 mA cm ⁻²	[40]
	YN ₄ -Cl	-	0.85	6 M KOH + 0.2 M Zn(Ac) ₂	162	770@200	20 h at 20 mA cm ⁻²	[9]
	Zn-N ₄ -O	-	0.884	6 M KOH + 0.2 M Zn(Ac) ₂	182	796.6@100	160 h at 10 mA cm ⁻²	[41]
	O-PdN ₄ -NGS	-	0.90	6 M KOH + 0.2 M Zn(Ac) ₂	178	793@10	240 h at 10 mA cm ⁻²	[42]
	2D transition metal oxide/hydroxide	Ni-doped CoO NSs	-	-	6 M KOH	377	655@30	> 400 h at 5 mA cm ⁻²
N/P-Cu _{0.1} Co _{0.3} Mn _{0.6} O ₂ /CNTs		1.52	0.82	6 M KOH + 0.2 M Zn(Ac) ₂	108.1	-	> 200 h at 10 mA cm ⁻²	[44]
ODAC-CoO-30		1.549	0.849	6 M KOH + 0.2 M Zn(Ac) ₂	128.5	705.6@20	150 h at 5 mA cm ⁻²	[45]
porous Ni/NiO		1.49	0.76	6 M KOH + 0.2 M Zn(Ac) ₂	225	853@20	120 h at 2 mA cm ⁻²	[46]
NiCo ₂ O ₄ -rGO		1.61	0.78	6 M KOH + 0.2 M Zn(Ac) ₂	125.3	719.8@5	200 cycles at 5 mA cm ⁻²	[47]
NiCo ₂ O ₄ nanosheet		-	0.85	6 M KOH + 0.2 M Zn(Ac) ₂	102.08	-	29 h at 10 mA cm ⁻²	[48]

	NiCo _{2,148} O ₄ PNSs	1.42	-	6 M KOH	83	-	120 h at 2 mA cm ⁻²	[49]
	PBMNC/LDH-20	1.66	-	6 M KOH + 0.2 M Zn(Ac) ₂	65.5	695.6@10	100 h at 5 mA cm ⁻²	[50]
	S-LDH/NG	1.474	0.692	6 M KOH + 0.2 M Zn(Ac) ₂	165	772@5	120 h at 5 mA cm ⁻²	[51]
Other 2D transition metal compounds	CoP@CC	1.53	0.67	6 M KOH + 0.2 M Zn(Ac) ₂	30	-	10 h at 10 mA cm ⁻²	[52]
	Co ₉ S ₈ /FeNC	1.58	0.865	6 M KOH + 0.2 M Zn(Ac) ₂	214.7	780.7@5	300 h at 5 mA cm ⁻²	[53]
	Co ₃ FeN	1.65	0.86	6 M KOH	108	798@5	150 h at 5 mA cm ⁻²	[54]
	Re-Ni ₃ S ₂ /NG/NF	1.477	0.66	6 M KOH + 0.2 M Zn(Ac) ₂	99	731.1@5	833 h at 5 mA cm ⁻²	[55]
	FePSe ₃ -O Ns	1.491	0.797	6 M KOH + 0.2 M Zn(Ac) ₂	38	-	280 h at 10 mA cm ⁻²	[56]
	Pt/NBF-ReS ₂ /Mo ₂ CT _x	1.564	0.911	6 M KOH + 0.2 M Zn(Ac) ₂	117.3	786@50	100 h at 5 mA cm ⁻²	[57]
Other 2D catalysts	BHZ-48	1.40 _{Ej=50}	0.84	6 M KOH + 0.2 M Zn(Ac) ₂	148	-	1,250 h at 5 mA cm ⁻²	[58]
	CFZ	1.50	0.82	6 M KOH + 0.2 M Zn(Ac) ₂	178	-	500 h at 25 mA cm ⁻²	[8]
	FeNi LDH-TpFx	1.84 _{Ej=100}	-	6 M KOH + 0.2 M Zn(Ac) ₂	118	798@139	800 cycles at 5 mA cm ⁻²	[59]
	Co-CNNs _{0.7}	1.67	0.803	6 M KOH + 0.2 M Zn(Ac) ₂	85.3	675.7@10	183 h at 10 mA cm ⁻²	[60]
	Co-NC-900	-	0.838	6 M KOH + 0.2 M Zn(Ac) ₂	160	-	45 h at 10 mA cm ⁻²	[61]
	BP-CN-c	1.66	0.84	6 M KOH + 0.2 M Zn(Ac) ₂	168.3	793.9@5	300 h at 10 mA cm ⁻²	[62]

Early research on modifying carbon materials primarily emphasized surface functionalization or geometric structuring. As a result, the significance of carbon defects is frequently overlooked. Topological defects in carbon-based materials are inevitable, arising from fabrication or occurring naturally due to crystal disorder^[69-71]. Several researchers have verified that introducing topological defects into the carbon framework disrupts the distribution of delocalized orbitals within the initial hexagonal lattice. Theoretical computation and experimental investigations have elucidated that manipulating the electronic structure of the carbon matrix influences its binding affinity and electrochemical performance^[72,73]. Tang *et al.* conducted comprehensive research into the theoretical contribution of topological defects to ORR and OER performances, using free energy diagrams and pertinent overpotentials as the foundation of their study^[21]. Specifically, using natural gelatinized sticky rice as raw material, a graphene catalyst with rich topological defects was designed and synthesized, as seen in Figure 4A. The results revealed that for simplex defect sites, the pentagon-heptagon pair exhibited the lowest overpotential, with the pentagon following closely, surpassing all nitrogen species in terms of performance. Furthermore, the researchers constructed primary ZABs to explore the practical viability of the synthesized nitrogen-doped graphene mesh (NGM). The ZAB with a prepared air electrode exhibited a high open circuit voltage (OCV) of 1.42 V and a peak power density of ~3.0 mW cm⁻² at 6.0 mA cm⁻². Moreover, Yu *et al.* presented a nitrogen-doped graphitic carbon nanosheet with abundant structural defects and hierarchical pores (d-pGCS) via pyrolysis routes^[22]. The ZAB with the optimized d-pGCS-1000 catalyst achieved a high peak power density (182 mW cm⁻²) and large specific capacity (773 mAh g_{Zn}⁻¹), showcasing its potential for practical implementation.

Edge and topological defects dominate the inherent imperfections of carbon materials and are widely accepted as pivotal active sites for ZABs^[72,74]. Owing to the distinct bonding configurations that distinguish edge sites from basal planes, edges typically show diverse electrochemical and thermodynamic

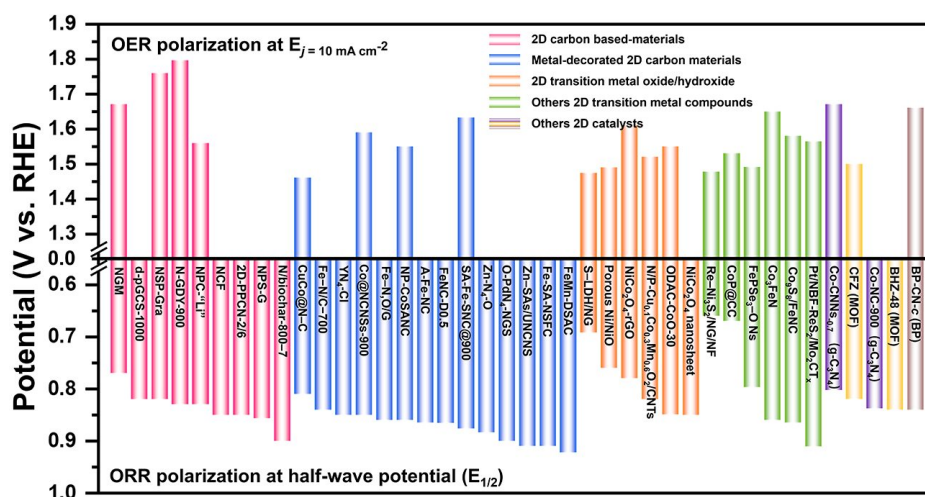


Figure 3. Comparison of different types of 2D electrocatalyst performances in OER and ORR.

characteristics. Tao *et al.* reported edge-rich and dopant-free graphene^[75], demonstrating the crucial role of edge carbon in enabling efficient ZABs without the requirement for external dopants. Additionally, it is noteworthy that of the various types of nanocarbon, 2D carbon nanostructures indisputably offer the most abundant number of edge sites for nitrogen doping. Nevertheless, the edge area of 2D nanocarbons requires further enhancement compared to the basal planes. Consequently, the ORR contribution, which originates in nitrogen in the basal configuration, cannot be extracted, leading to difficulties in assessing the genuine nitrogen-based ORR activity at the edges. In response to these challenges, Zhang *et al.* introduced a creative approach combining graphitization with nitrogen modification^[23]. This strategy effectively yielded novel metal-free carbon nanoflakes (NCF) with enriched edges and a similar structure to graphite^[23]. Benefiting from the synergistic effect of edge-type pyridinic-N/graphitic-N dipole, NCF exhibited high ORR performance with a half-wave potential of 0.85 V. The assembled ZAB delivered a stable OCV of 1.41 V and a high peak power density of 173 mW cm⁻².

Doping is widely acknowledged as an effective strategy for enhancing the intrinsic site activity of carbon-based oxygen electrocatalysts. The method can increase the number and improve the activity of active sites via geometric, electronic, and synergistic influences. Compared to carbon atoms, heteroatoms' distinct radii and electronegativity mean that their incorporation within the carbon framework can activate charge distribution and spin density in the surrounding carbon matrix^[76]. Due to their manifold benefits, nitrogen atoms have gained significant attention from diverse heteroatoms. N-doped carbon nanotubes (CNTs) as catalysts for the ORR were reported in 2009, with notably superior activity compared to pristine CNTs^[77]. Since then, numerous studies have been carried out in this direction. For example, Ma *et al.* obtained N-doped biochar material (N/biochar) via liquid-assisted carbonization with microalgae biomass as the precursor^[24]. The optical N/biochar exhibited remarkable ORR activity with $E_{1/2}$ of 0.90 V due to the active pyridinic N species. Furthermore, the prepared ZAB with N/biochar demonstrated impressive specific capacity (703 mAh g_{Zn}⁻¹) and high stability (60 h). To elucidate the source of this enhanced performance, density functional theory (DFT) calculations were performed. The results suggest that pyridinium-N atoms can modify the band structure of neighboring carbon atoms, thereby facilitating the dissociation of O₂ molecules onto neighboring carbon atoms. After that, Lu *et al.* successfully synthesized nitrogen-doped GDY (N-GDY-900) with pyridinic N as its main nitrogen doping form via a facile pyrolysis route at 900 °C [Figure 4B]^[25]. As a result, the ZAB assembled by N-GDY-900 delivered a high OCV of 1.54V and improved stability for 300 h (450 cycles). DFT calculations have further shown that the N-atoms forming the pyridine

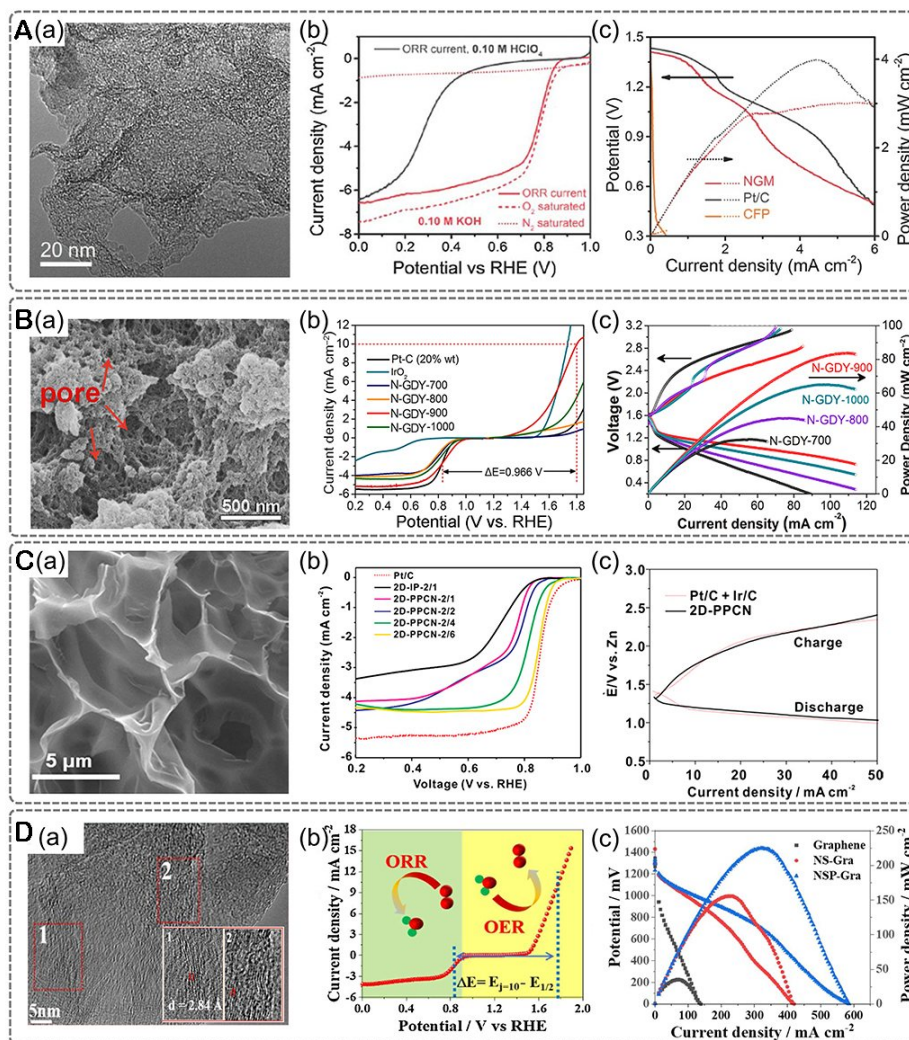


Figure 4. (A) (a) TEM image of graphene layer; (b) LSV curves of ORR for the catalyst at different electrolytes; (c) Polarization and power density curves of ZABs^[21]. Copyright 2016, Wiley-VCH. (B) (a) SEM images of N-GDY-900; (b) ORR and OER performance of four catalysts compared with commercial Pt/C and IrO₂; (c) Charge and discharge polarization curves of N-doped GDY^[25]. Copyright 2021, Elsevier. (C) (a) SEM image of 2D-PPCN; (b) ORR activity of the prepared samples; (c) GCD polarization curves of 2D-PPCN and Pt/C+Ir/C based air electrode^[26]. Copyright 2018, American Chemical Society. (D) (a) TEM image of NSP-Gra; (b) ORR and OER performance of the catalysts; (c) Polarization and power density curves of the primary ZABs^[28]. Copyright 2021, Elsevier.

configuration in GDY can induce a higher positive charge density on the ortho-carbon atoms, resulting in a lower energy barrier. In addition to nitrogen atoms, carbon materials doped with atoms such as B, S, and P also exhibit favorable electrocatalytic activity in oxygen reactions^[78-80]. Lei *et al.* synthesized 2D P-doped porous carbon nanosheets (2D-PPCN) through the multifunctional templating approach [Figure 4C]^[26]. Benefiting from the P doping and porous structure, the ZAB of 2D-PPCN exhibited remarkable performances, including a high OCV (1.40 V) and excellent cycling stability for more than 1,000 charge-discharge cycles. The multiple doping strategy imparts a synergistic influence that further augments the electrocatalytic prowess of metal-free heteroatom-doped carbon catalysts. Both theoretical calculations and experimental studies have verified that incorporating nitrogen atoms into carbonaceous materials can enhance the conductivity of carbon via electron donation by shifting the Fermi level toward the conduction band^[81]. A second nonmetallic heteroatom, such as P, S, or F, associated with N-doped carbons (NCs), can

further modulate the electronegativity and surface polarities, significantly elevating ORR performance. Recently, doping with heteroatoms modulates the electronic surface of carbon and fine-tunes the catalytic activity (such as S and N^[82], P and N^[83-85]) have been broad investigations. For instance, Li *et al.* synthesized N, P co-doped hydrophilic carbon nanosheets (NPC-“Li”)^[27]. The obtained NPC-“Li” exhibited exceptional catalytic performance for both ORR and OER, attributed to the synergistic effect of N and P co-doping with the resulting electronic interactions conducive to the catalytic process. More importantly, ZABs with NPC-“Li” as the cathode demonstrated a high specific capacity (908 Wh kg_{Zn}⁻¹) and long-time cycle stability (150 cycles). Incorporating ternary or multiple heteroatoms into carbon materials has also gained attention^[86,87]. Wang *et al.* obtained N, S, and P tri-doped graphene (NSP-Gra) via a facile wet ball milling method [Figure 4D]^[28]. The defect-engineered graphene, which is mechanically forced to include abundant defects, has proven advantageous in achieving uniform heteroatom doping. The orchestrated doping process facilitates the introduction of numerous active sites and prompts significant alterations in the spin density, thereby bestowing remarkable electrochemical activity for both ORR and OER. The assembled ZAB of NSP-Gra demonstrated a high-power density of 225 mW cm⁻² and long charge-discharge cycling stability for more than 40 h. Furthermore, Zheng *et al.* synthesized heteroatomic N, P, and S-doped graphene-like carbon (NPS-G) catalysts^[29], exhibiting outstanding ORR catalytic activity. This exceptional performance can be attributed to the favorable chemisorption of oxygen species, reduced intrinsic charge transfer resistance, and a porous 2D structure. Notably, the ZAB equipped with NPS-G delivered a high-power density (151 mW cm⁻²) and specific capacities (686 mA h g_{Zn}⁻¹). Heteroatom doping can endow carbon materials with enhanced electrical, electromagnetic, and physicochemical structural features, all affecting the catalytic activity^[28].

Metal-decorated 2D carbon materials

At present, the development of low-cost metal catalysts to replace traditional commercial Pt/C applications in aqueous ZABs is an inevitable way to achieve the widespread popularity of ZABs. Recently, it has been reported that abundant and cost-effective TMs, such as Ni, Mn, Co, Fe, and Mo, exhibit promising catalytic activities for both the OER and ORR. Furthermore, TM-based catalysts exhibit remarkably similar catalytic activity to noble metal-based catalysts and demonstrate significantly enhanced corrosion resistance compared to metal-free catalysts. While challenges such as low intrinsic activity, limited conductivity, and inadequate stability persist, their relatively strong catalytic performance and exceptional selectivity render them promising candidates for bifunctional electrocatalysts and even potential applications in ZABs^[88-90]. Thus, considerable efforts have been directed towards TM-based catalysts in the past decade. According to the geometric size reduction principle to increase the number of active sites, the research of metal nanoparticles, clusters, and SA catalysts has been greatly developed.

Metal nanoparticles or alloy-modified carbon nanomaterials also demonstrate exceptional electrocatalytic activity, promoting the development of ZABs^[91-93]. Zheng *et al.* synthesized a hybrid of NC nanosheets encapsulating Co nanoparticles (Co@NCNSs)^[30]. The optimized hybrids Co@NCNSs-900 demonstrate excellent catalytic performances in OER and ORR due to the high surface area and the synergistic effect between Co nanoparticles and NC nanosheets. As a result, the assembled ZAB of Co@NCNSs-900 showed a higher power density (271 mW cm⁻²), and no degradation was found after 400 cycles. The synergistic effect between metal nanoparticles can regulate the local electron density of the catalyst and produce abundant active sites. As shown in Figure 5A, a bifunctional electrocatalyst with ultrahigh activity, composed of Cu and Co nanoparticle-co-decorated N-doped graphene nanosheets (CuCo@N-C), were synthesized through a template-free strategy by Liu *et al.*^[31]. The CuCo@N-C possesses good ORR activity ($E_{1/2} = 0.81$ V) and an outstanding overpotential of 1.46 V at the current density of 10 mA cm⁻², indicating the strong electron transfer between Cu and Co enhanced reaction kinetics, promoting catalytic activity. Meanwhile, when CuCo@N-C was employed as the cathode, the prepared ZAB presented a high open circuit potential

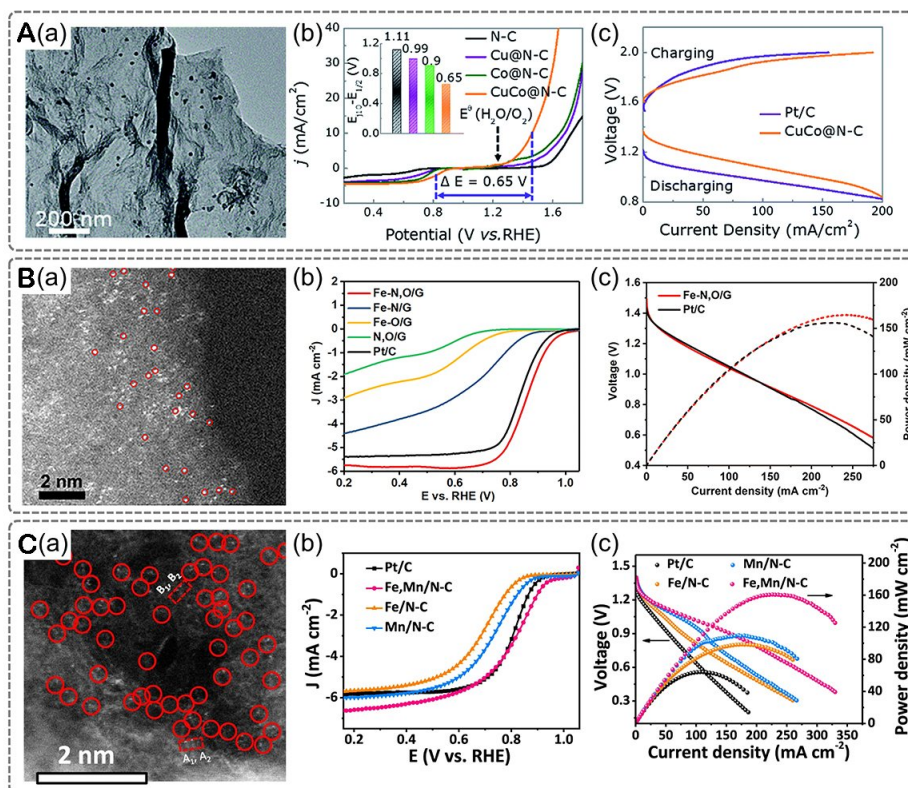


Figure 5. (A) (a) TEM image of CuCo@N-C; (b) ORR and OER curves of CuCo@N-C, Co@N-C, Cu@N-C and N-C; (c) Charge-discharge curves of Pt/C and CuCo@N-C^[31]. Copyright 2019, the Royal Society of Chemistry. (B) (a) SEM image of Fe-N, O/G; (b) LSV tests curves of the ORR for the Fe-N,O/G and other electrocatalysts; (c) Discharge polarization curves and power densities^[37]. Copyright 2023, the Royal Society of Chemistry. (C) (a) HAADF-STEM image of the Fe-SA-NSFC; (b) ORR polarization curves of the Fe-SA-NC, Fe-SA-NSC, Fe-SA-NSFC, and Pt/C; (c) Discharge polarization curves and power density curves^[40]. Copyright 2020, Springer Nature.

(1.51 V) and an ultrahigh power density (170 mW cm^{-2}). More importantly, many studies have demonstrated that alloys can achieve better catalytic performance than individual metals because alloying changes the surface electronic structures, adjusting the effective catalytic active sites and reducing the kinetic energy barriers^[94,95]. It was verified experimentally by Xu *et al.*, who designed a core-shell alloy covered by nitrogen-doped porous carbon nanosheets (FeCo/NUCSs)^[96]. The NUCSs with porous structures facilitated the effective and smooth mass transfer to the active FeCo species encapsulated within a PBA-derived carbon, improving the ORR stability. Furthermore, the ZAB with FeCo/NUCSs as the air electrode exhibited ultrahigh specific capacity ($791.86 \text{ mAh g}^{-1}$) and good cycling stability of 102 h.

Following the principle of enhancing active sites through a geometric size reduction, SACs offer the potential to expose a wealth of active sites, maximizing atomic utilization and displaying distinctive physicochemical properties^[97,98]. A representative study by Qiao *et al.* in 2011 involved the atomic dispersal of Pt atoms onto iron oxide, where they catalyzed the CO oxidation reaction^[18]. The proposed SACs exhibit unique merits, such as maximum atomic efficiency across the entire catalytic process. Since then, substantial efforts have been dedicated to synthesizing and utilizing the family of SACs.

In developing SACs, significant effort has been devoted to enlarging noble metals' atomic utilization efficiency and achieving efficient catalytic activity in high-performance ZABs. Most SACs designed as

oxygen electrocatalysis are anchored onto nitrogen-doped carbon-based materials with a typical M-N-C structure^[99]. Several studies have demonstrated that regulating the guest groups and the central metal, coordination, and environmental atoms can significantly enhance the intrinsic electrocatalytic activity of M-N-C SACs.

Usually, when tuning the intrinsic catalytic activity of SACs, the most direct and effective strategy is to select a suitable central metal atom. For example, during the ORR process, the d orbitals of the central metal atom can interact with the p-orbital electrons of the oxygen intermediate, facilitating the adsorption and decomposition of O₂ molecules. However, achieving precise control over the structure of SACs has proved difficult, and the direct derivation of SACs with excellent ORR electrocatalytic activity is challenging. To address this problem, a novel theoretical simulation approach to the ORR, pioneered by Nørskov *et al.*, provided a convenient way to compare the intrinsic ORR activities of SACs under different center metal atoms^[100]. The intrinsic ORR activity was proved by Peng and Zheng *et al.* The experiment with theoretical calculation indicated that follows the sequence Fe > Co > Cu > Mn > Ni^[101,102]. For example, Yang *et al.* obtained highly active self-supporting iron-coordinating nitrogen-doped carbon catalysts (Fe-N/C) through pyrolysis of the iron coordination complex precursor^[32]. The optimized catalyst Fe-N/C-700 exhibits a half-wave potential ($E_{1/2} = 0.84$ V vs. RHE) for the ORR. Besides, the ZAB with the Fe-N/C-700 as the cathode catalyst shows a high specific capacity of 727 mAh g⁻¹ and an energy density of 965 Wh kg⁻¹ at 5 mA cm⁻². To obtain more active Fe-N₄ sites, Shao *et al.* achieved petal-like porous carbon nanosheets with densely accessible Fe-N₄ sites through the pyrolysis of a novel iron complex derived from diethylenetriaminepentaacetic acid (DTPA) and melamine (FeNC-D)^[33]. The optimal catalyst FeNC-D0.5 has numerous active sites and can enable exposure to more originally inaccessible sites due to the special fluffy petaloid nanosheet structure. Furthermore, the FeNC-D0.5-based ZAB can achieve a remarkable power density of 356 mW cm⁻². Cui *et al.* successfully obtained a catalyst with Fe-Mn dual-metal sites anchored on ultrathin 2D NC nanosheets with a porous structure (FeMn-DSAC)^[34]. The synergistic effect of the Fe-Mn dual-sites can enhance active site exposure and thus improve mass transfer over the porous 2D nanosheet structure. FeMn-DSAC was found to exhibit exceptional bifunctional activity, enabling ZABs to function efficiently even at ultra-low temperatures of -40 °C, with an ultrahigh peak power density of 184 mW cm⁻².

The coordination atoms (such as N, C, and O) can directly bond with the central metal atoms during synthesis. Therefore, regulating the ligand structure can directly affect the central metal atom and thus can promote/inhibit the performance of OER and ORR. Specifically, modifying the coordination structure by altering the coordination number and atoms present can lead to substantial changes in the electronic configuration of the central atom. The efficacy and simplicity of this approach have been progressively demonstrated in the enhanced ORR/OER activity of SACs^[103-105]. For example, Zhang *et al.* studied the effect of the coordination environment of single Zn atoms on the ORR activity by constructing single Zn atoms on ultrathin 2D NC nanosheets (Zn-SAs/UNCNS) via pyrolysis of Zn-tetrakis(4-carboxyphenyl)porphyrin nanosheets at 900 °C^[35]. DFT calculations demonstrated that the electronic states of the divacancy Zn-N₃C-C₈ sites near the Fermi level differ from other sites, significantly improving the performance of catalysts in ZABs, such as an enhanced peak power density of 282 mW cm⁻² and a higher OCV of 1.43 V. In addition to the prevalent coordination of N and C, researchers have also explored the incorporation of novel coordinated atoms such as O, S, and P, among others. Chen *et al.* engineered highly active SACs featuring M-N₄-S sites, with M representing Fe, Cu, and Co, by employing lignosulfonate as a multifunctional bioligand^[36]. The S doping induced the charge redistribution around Fe-N₄ sites, leading to excellent performance for the ORR and OER. The assembled ZAB further demonstrated a high specific capacity of 798.7 mA h g⁻¹ and long-term stability. Li *et al.* developed Fe SAs confined in a graphene

framework (Fe-N, O/G) via calcining the Fe-MOF/graphene precursor in the argon atmosphere [Figure 5B]^[37]. The resulting Fe-N,O/G catalyst exhibits a higher onset potential ($E_{\text{onset}} = 1.00$ V) and half-wave potential ($E_{1/2} = 0.86$ V) in ORR. DFT calculations demonstrate that N, O symmetric double-coordination configuration can effectively regulate the coordination environment of Fe SAs. The Fe-N,O/G-based ZAB delivers a high peak discharge power density of 164.7 mW cm^{-2} and outstanding discharge stability of > 150 h at 20 mA cm^{-2} .

In addition to replacing N atoms, changing the coordination number of the central metal atoms has been identified as a viable approach to directly regulating the electronic structure of a metal atom toward efficient catalytic activity^[106-108]. Shang *et al.* adopted a "coordination design strategy" to prepare a catalyst (A-Fe-NC) by anchoring single-atom Fe on nitrogen-doped carbon nanosheets^[38]. X-ray absorption spectroscopy revealed a coordination number of 5 for the Fe atom, suggesting that five N coordination atoms are coordinated with the central Fe atom. Benefiting from the Fe-N₅ and the unique 2D sheet structure, the flexible ZABs based on the well-designed catalyst exhibit a peak power density of 132.2 mW cm^{-2} and significant charge-discharge cycling stability (240 h). Li *et al.* constructed bifunctional CoN₃ catalytic sites, which present a template method that was dispersed onto N-doped graphitic carbon nanosheets (CoSA/NCs)^[39], with the experimental and theoretical modeling results confirming that the single-atomic dispersed CoN₃ has better catalytic activity than CoN₄. The CoSA/NCs-based ZABs show a significant peak power density (255 mW cm^{-2}) and excellent long-term stability. Modifying the coordination structure of SACs thus plays a crucial role in effectively manipulating the electronic structure of the central metal atoms.

Environmental atoms are substrate atoms that do not establish direct bonds with central metal or ligand atoms. The planar arrangement of active sites and carbon substrates induces significant long-range interactions among the d/p electrons of various atoms within distinct domains. Consequently, incorporating heteroatoms such as S, B, or P into the carbon-based substrate can indirectly impact catalytic activity. Zhou *et al.* presented a method to anchor a SA in nitrogen-, sulfur- and fluorine-co-doped graphitized carbons (M = Fe, Co, Ru, Ir, and Pt) via an effective ligand-stabilized pyrolysis strategy. Among them, Fe-N-Cs with S and F-co-doping (Fe-SA-NSFC) electrocatalysts demonstrated the highest ORR activity with a positive half-wave potential of 0.91 V, as shown in Figure 5C^[40]. S, F co-doping significantly decreases the free energy barrier on the FeN₄ active sites. Therefore, Fe-SA-NSFC shows a good performance in ZABs, with a large peak power density of 247.7 mW cm^{-2} and long-term stability over 240 h. In others, Li *et al.* used high-temperature pyrolysis to synthesize single-atom iron-loaded boron-nitrogen-doped carbon catalysts (Fe-N₄-B)^[109]. The as-designed Fe-N₄-B SAC exhibited high ORR activity with a half-wave potential of 0.859 V. Additionally, the notable bifunctional activity achieved by Fe-N₄-B can be attributed to the effective modulation of the d-band Fe center through B atoms, which optimizes the adsorption behavior of oxygenated species.

Guest groups can be introduced to interact with the central metal atoms in the M-N-C SAC host, effectively acting as ligands that coordinate with the active sites of the SAC. Generally, the d orbitals of the central metal atoms oriented perpendicular to the M-N-C plane are often incompletely occupied, allowing for potential interactions with small-molecule ligands. Consequently, external ligands can coordinate with central metal atoms, thereby regulating the electronic structures of M-N-C sites and modulating intrinsic ORR and OER activity. For instance, chloride ions possess strong coordination capabilities with TM atoms. Ji *et al.* introduced Cl ions to modify the original yttrium single-atom (YN₄) active sites^[9], and the resulting YN₄-Cl moieties embedded within the carbon framework displayed a notable half-wave potential of 0.85 V in ORR, delivering a peak power density of 162 mW cm^{-2} and long-term stability in ZABs. The chlorine atom serves as a suitable axial ligand, forming a YN₄-Cl covalent bond with a moderate coupling between its

3p orbital and the 4d orbital of Y. This bond adapts to elongate self-adaptively, aiding in facilitating intermediate binding during the ORR process. Similarly, M-N-C, with M-N₄ sites modified by O (MN₄-O-MN₄), exhibited higher ORR activity than normal M-N₄ sites such as O-Zr-N-C and Zn-N₄-O^[41,110]. Zhou *et al.* employed a molten-salt strategy to synthesize a palladium SAC featuring planar PdN₄ moieties modulated by an axial oxygen ligand. These active sites were anchored on nitrogen-doped graphene nanosheets, forming the O-PdN₄-NGS catalyst^[42]. The axial O ligand significantly increases the O₂ adsorption energy at the Pd center, activating the PdN₄ sites for O-O bond cleavage. This enhances the catalytic activity and selectivity of the 4e⁻ ORR process. The as-prepared O-PdN₄-NGS electrocatalysts show outstanding ORR performance with a high E_{1/2} of 0.90 V and a low Tafel slope of 74 mV dec⁻¹. The O-PdN₄-NGS-based ZAB delivers a high peak power density of 178 mW cm⁻² at 227.5 mA cm⁻² and long-time cycling stability of 240 h.

2D transition metal oxide/hydroxide

The abundant availability of TMOs and TMOHs holds substantial promise for enhancing the performance of rechargeable ZABs. Currently, catalysts based on precious metals or metal oxides, such as Pt, IrO₂, or RuO₂, have been extensively explored in ZABs. However, the scarcity and high costs of these materials restrict the broad utilization of these catalysts. Numerous cost-effective alternatives using earth-abundant materials have been devised to address these challenges and enable the widespread implementation of ZABs. In the ZABs, both OER and ORR activity should be considered in the selection of matrix metal oxides. In catalyzing oxygen evolution, ΔG_O-ΔG_{OH} was widely employed as the descriptor of metal oxide activity^[111]. Out of the precious metal-based oxides, FeNi or FeCo bimetallic oxides show the best values and are listed at the top of the volcanic plot. Experiments also bore out this view according to [Table 1](#). However, in the ORR, there are few such widely accepted theoretical studies for metal oxides. According to the recent reports, the commonly used oxide-based ORR catalysts mainly include Co- and Mn-based oxides. In the practical approach, not only the choice of metal oxide for the catalysts but also the modification of their functional activities should be carried out to achieve high-performance bifunctional catalysts with excellent performance and stability.

Cobalt oxides (CoO_x) are promising for advancing ZABs due to their remarkable bifunctional catalytic capabilities, particularly the spinel-type oxide Co₃O₄^[112,113]. Typically, the tetrahedral sites in Co₃O₄ are occupied by Co²⁺ ions, while the octahedral sites host Co³⁺ ions^[114]. Catalysts that feature a surface enriched with Co²⁺ ions have been found to display improved ORR performance, while OER activity benefits from the presence of more Co³⁺ sites on the surface. This heightened catalytic activity can be attributed to the enhanced adsorption of O₂ and OH⁻ at the Co²⁺ and Co³⁺ sites, respectively^[115]. For instance, He *et al.* synthesized an ultrathin Co₃O₄ nanofilm that was only approximately 1.8 nm thick^[116]. The ultrathin nanosheets or nanofilms altered the adsorption/desorption behaviors of the oxygen-containing species, enhanced the intrinsic conductivity, and dramatically promoted the reaction kinetics. Enriching the 2D nanostructure surface with Co³⁺ ions promoted the kinetics of the catalytic reaction. Moreover, the Co₃O₄ nanofilm enabled the production of rechargeable ZABs with a low overpotential of 0.72 V, higher round-trip efficiency (62.7%), and excellent cycling stability (175 cycles).

Despite the various advantages of Co₃O₄ nanosheets, the electrocatalytic performance might be impeded due to the inherent low electronic conductivity of Co₃O₄, as reported previously^[117,118]. Carbon materials with high electronic conductivity promote efficient electron transfer from the electrode material to the reaction interface. Therefore, as shown in [Figure 6A](#), Li *et al.* reported a thin mesoporous nanosheet Co₃O₄/nitrogen-doped reduced graphene oxide (Co₃O₄/N-rGO) as a bifunctional catalyst^[119]. The hybrid ZAB exhibited superior discharge and charge polarization properties owing to the strong synergetic effect between the atomically thin Co₃O₄ and N-rGO. Doping is a similarly effective strategy that can further enhance the

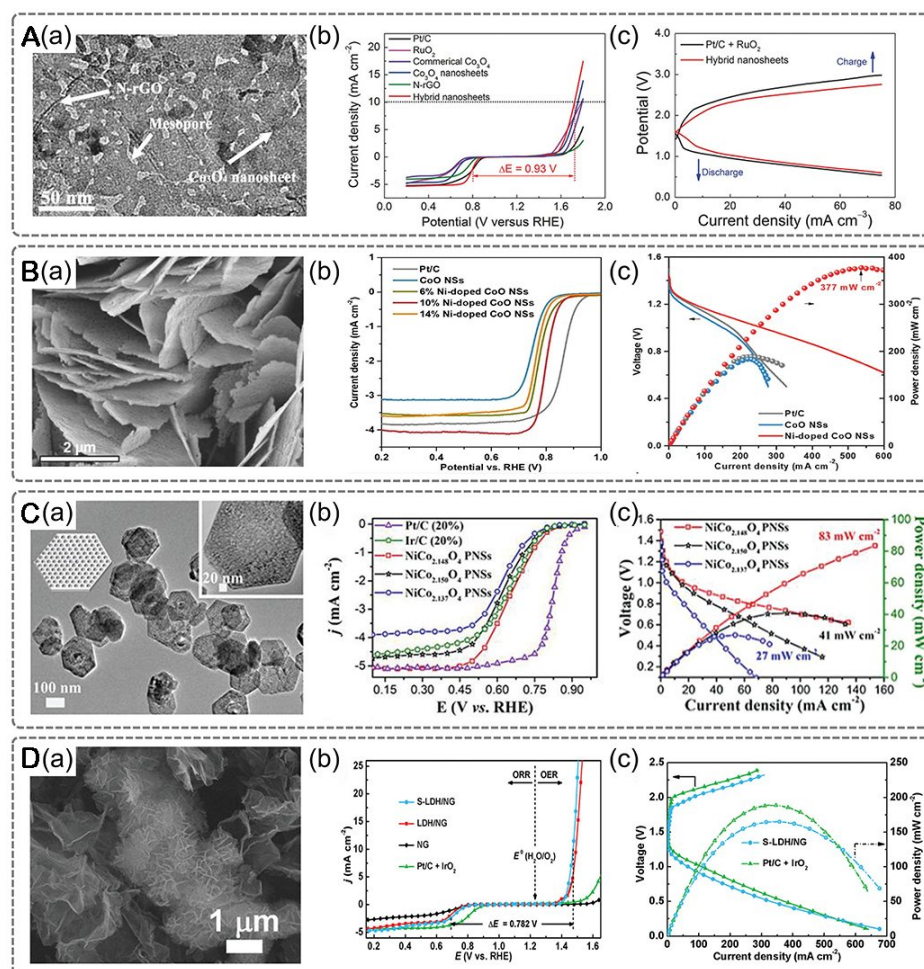


Figure 6. (A) (a) TEM image of the hybrid nanosheets; (b) ORR and OER polarization curves; (c) Discharge and charge polarization curves of the ZABs^[119]. Copyright 2018, Wiley-VCH. (B) (a) SEM image of CoO NSs; (b) ORR polarization curves of pristine CoO NSs, CoO NSs with different Ni dopant concentrations and Pt/C; (c) Polarization curves and corresponding power density plots^[43]. Copyright 2018, Wiley-VCH. (C) (a) TEM image of NiCo_{2,148}O₄ PNSs; (b) ORR polarization curves of Pt/C, Ir/C, NiCo_{2,148}O₄, NiCo_{2,150}O₄, and NiCo_{2,137}O₄ PNSs; (c) Discharge voltage curve corresponding power density plot of NiCo_{2,148}O₄, NiCo_{2,150}O₄, and NiCo_{2,137}O₄ PNSs^[49]. Copyright 2020, Wiley-VCH. (D) (a) SEM image of S-LDH/NG; (b) ORR and OER polarization curves of S-LDH/NG, LDH/NG, Pt/C + IrO₂, and NG; (c) Charge/discharge polarization curves and power density plots of the S-LDH/NG- and Pt/C+IrO₂-based ZABs^[51]. Copyright 2023, Wiley-VCH.

activity of TMOs^[120-122]. For instance, Li *et al.* synthesized Ni-doped CoO nanosheets (Ni-doped CoO NSs) through a straightforward cation exchange process, employing ZnO nanosheets as sacrificial templates^[43]. They demonstrated that uniform Ni doping effectively modulates the binding energy of the intermediate species in the ORR process, thereby enhancing the intrinsic ORR activity at each active site [Figure 6B]^[43]. The Ni-doped CoO NSs were integrated into ZABs, resulting in a high peak power density of 377 mW cm⁻² and long-term stability for more than 400 h under a current density of 5 mA cm⁻². Li *et al.* successfully obtained a high-performance bifunctional catalyst through doping Cu, N, and P into the precursor of the cobalt manganese oxides nanosheets/CNTs (N/PCu_{0.1}Co_{0.3}Mn_{0.6}O₂/CNTs)^[44]. The effective modulation of the Cu, P, and N atoms on the number and the intrinsic activity of the active Co catalytic sites meant that the as-formed N/PCu_{0.1}Co_{0.3}Mn_{0.6}O₂/CNTs functioned as a bifunctional catalyst in ZABs. The creation of oxygen vacancies emerges as an appealing approach to modify the surface chemistry of TMOs, thereby enhancing their electrocatalytic performance^[123-125]. Oxygen vacancies lead to an augmentation in electron density

within neighboring metal atoms, thereby improving the conductivity of TMOs and facilitating charge transfer during the ORR and OER^[126,127]. Tian *et al.* successfully synthesized nanosheets of oxygen-defective amorphous-crystalline CoO (ODAC-CoO) by fast calcination of Co(OH)₂ under vacuum conditions^[45]. The abundant active sites offered by its 2D structure and the incorporation of the amorphous phase led to an amorphous structure that effectively lowered the energy required to form oxygen vacancies, facilitating the creation and stabilization of these vacancies. Most importantly, the moderate oxygen vacancy content observed in ODAC-CoO-30 resulted in enhanced electrical conductivity and diminished energy barriers during ORR and OER processes. Consequently, the ODAC-CoO-30-based ZAB delivered a high peak power density of 128.5 mW cm⁻² and a specific capacity of 705.6 mAh g⁻¹. Except for the usual approaches to improve the catalytic properties of materials, the interfaces also play a pivotal role in enhancing the electrocatalytic properties of a nanocomposite catalyst, and both the heterojunction and fine-tuning of the electronic structure of the interface can be exploited. Liu *et al.* designed a mesoporous Ni/NiO (Porous Ni/NiO) nanosheet, and the assembled ZAB showed a high power density of 225 mW cm⁻² and long-term cycling stability of over 120 h^[46]. In addition, other heterojunctions such as Ru-RuO₂^[128], Cu/Fe₂O₃^[129], and Fe₂O₃/Fe₅C₂/Fe-N-C^[130] also show excellent activity in ZABs.

Considering that the introduction of additional metal ions can lead to the creation of more active sites, polymetallic oxides are anticipated to exhibit greater intrinsic oxygen electrochemistry activity as compared to single metal oxides^[131]. Furthermore, the activity of polymetallic oxides can be readily enhanced by adjusting the respective metallic elements' crystalline structure, valence, and electronic states^[132]. Typical spinel polymetallic oxides in the form A_xB_{3-x}O₄ mainly include CoMn₂O₄, NiCo₂O₄, FeCo₂O₄, ZnCo₂O₄, and ZnMn₂O₄^[133]. Of these, NiCo₂O₄, a representative spinel-structured oxide, continues to present limitations for application in ZABs, with many researchers attempting to improve its electrocatalytic performance. Li *et al.* used morphology engineering to fabricate hierarchical NiCo₂O₄ with different nanostructures^[47]. The best performance was found on the NiCo₂O₄ nanosheets, and the prepared ZAB showed a relatively high peak power density of 125.3 mW cm⁻². Liu *et al.* developed a high-performance NiCo₂O₄ nanosheet with abundant oxygen vacancies^[48]. The produced ZAB of ultrathin nanosheets exhibited a high-power density of 102.08 mW cm⁻² and superior stability of 29 h. Additionally, porous structures, such as mesopores, provide these materials with unique properties in terms of catalytic reaction by facilitating electron transport rates and mass transport^[45,134,135]. Inspired by this, Yin *et al.* synthesized a series of mesoporous nanosheets based on NiCo₂O₄ (NiCo₂O₄ PNSs) by oxygen vacancies engineering, thus obtaining different Co valence states and mesopore sizes, as shown in Figure 6C^[49]. With the transition of the Co coordination environment from tetrahedral to octahedral, the optimized NiCo_{2.148}O₄ PNSs displayed a favorable average Co valence state of 2.3, abundant oxygen vacancies, and uniform 4 nm mesopores. These PNSs exhibited remarkable OER and ORR activity, along with exceptional stability. These enhancements are attributed to the crucial role of Co²⁺ in the system. The ZAB assembled by NiCo_{2.148}O₄ PNSs possessed a high-power density of 83 mW cm⁻² and excellent stability (no evident weakening after 20 h).

TMOs, particularly those with perovskite structures, have been extensively explored as bifunctional electrocatalysts in ZABs due to their affordability, diverse compositions, structural stability, and promising potential^[136-138]. However, pristine perovskite materials are still limited by their small active surfaces and fewer active sites. To further enhance their electrocatalytic activities, one effective strategy that can be used to promote electrocatalytic activity involves the introduction of other materials. Mondal *et al.* constructed the heterostructure of 2D Pr_{0.5}Ba_{0.5}Mn_{1.8-x}Nb_xCo_{0.2}O_{6-δ} double perovskite oxide nanosheet (PBMNC) and NiFe LDH for ZABs^[50]. The resulting PBMNC/LDH-20 cathode exhibited a high-power density of 65.5 mW cm⁻² and superb charge-discharge capability of more than 35 h.

LDHs possess a distinctive layered structure that consists of positively charged layers with negatively charged anions in the interlayer region. However, the practical utilization of LDHs in rechargeable ZABs is hindered by their limited ORR catalytic activity and low conductivity. Thus, Hui *et al.* designed MXene/Zn-LDH-array@PVA composite for use in ZABs^[139]. The NiFe LDH with the best activity was modified by chemical induction to produce oxygen vacancies. The integrated interfacial structure of the MXene/Zn electrode and LDH-array@PVA electrolyte ensures sufficient interfacial contact with good compatibility and stability, reducing the interfacial impedance and limiting zinc dendrite growth. The assembled ZAB exhibited a promising peak power density (92.3 mW cm^{-2}), and only a negligible voltage loss was found after continuous operation for 50 h. Oxygen vacancies modify the structure of active materials on an electrode/electrolyte interface without sacrificing the crystal stability^[140,141], and experimental and DFT calculations have demonstrated that oxygen vacancies enhance the activity of a material for oxygen reactions^[142]. Furthermore, for atomic adjustment, the core principle is optimizing the electronic structure at the active site^[143,144]. For example, Han *et al.* configured atomic-level sulfur-incorporated NiFe-LDHs that were deposited in situ on nitrogen-doped graphene (S-LDH/NG) [Figure 6D]^[51]; the atomic-level sulfur incorporation resulted in a customized topological microstructure and adjusted electronic structure, leading to enhanced catalytic activity and durability of bifunctional electrocatalyst. Moreover, the theoretical calculations revealed that adjusting the electronic structure will impact the conductivity and increase the density of carriers, thereby significantly reducing the Fe-S site reaction energy barrier of zigzag edge structures. Consequently, S-LDH/NG-based ZABs demonstrated a high peak power density of 165 mW cm^{-2} and an energy density of $772 \text{ Wh kg}_{\text{Zn}}^{-1}$.

Other 2D transition metal compounds

The distinct interlayer structure of 2D materials, such as TMSs, TMNs, and TMPs, have good electrical conductivity, corrosion resistance, and platinum-like electronic structures, highly desired properties for rechargeable ZABs. However, despite their excellent physical and chemical properties, they are prone to suffer from aggregation during synthesis, corrosion of catalyst supports, and catalytic instability during OER/ORR processes. To address these concerns, various methods have been explored to enhance their performance, such as regulation of reaction surface area, intrinsic catalytic activity, and conductivity^[89,145,146].

During charging and discharging, the ORR and OER processes occur at the electrocatalyst's surface, giving rise to a triple interface region. To enhance the reactive surface area, many structures have been developed to promote the exposure of active sites. For instance, Cheng *et al.* synthesized carbon cloth-supported cobalt phosphide (CoP@CC) by *in situ* thermal phosphorylation^[52]. As illustrated in Figure 7A, the crisscrossing sheets promote mass transfer between reactants and intermediates, thus avoiding aggregation of the CoP nanosheets that provide the active sites. Notably, the ZAB assembled with CoP@CC catalyst delivered a superior OCV of 0.6 V and a power density of 30 mW cm^{-2} . Compared with CNTs and carbon nanofibers (CNFs), graphene, the classic 2D material, possesses a higher specific surface area and better stability and is an ideal substrate for new high-performance bifunctional catalysts. Ultrathin 2D NiCo_2S_4 nanosheets with a reduced graphene oxide hybrid material ($\text{NiCo}_2\text{S}_4/\text{rGO}$) structure possessed good electrocatalytic activity for OER and ORR^[147]. The hybrid catalyst shows a unique hierarchical structure with a large surface area. The ZAB of $\text{NiCo}_2\text{S}_4/\text{rGO}$ showed a high-power density of 262.6 mW cm^{-2} and remains stable even after 750 cycles. Moreover, assembling active species into an interconnected superstructure featuring hierarchical porosity and high crystallinity enables ample material contact, establishing a rapid electron and mass transfer route and a substantial ion-accessible surface area. Lan *et al.* constructed a 2D holey sheet superstructure composed of interconnected hollow nanoparticles of cobalt sulfide and iron-nitrogen-carbon ($\text{Co}_9\text{S}_8/\text{FeNC}$) via a self-template strategy^[53]. The corresponding superstructure offered a wealth of accessible active sites, robust electron transport routes, and short ion diffusion distances, accelerating the kinetics. As a result, $\text{Co}_9\text{S}_8/\text{FeNC}$ exhibits excellent high-power density and stability in rechargeable ZABs. As shown in

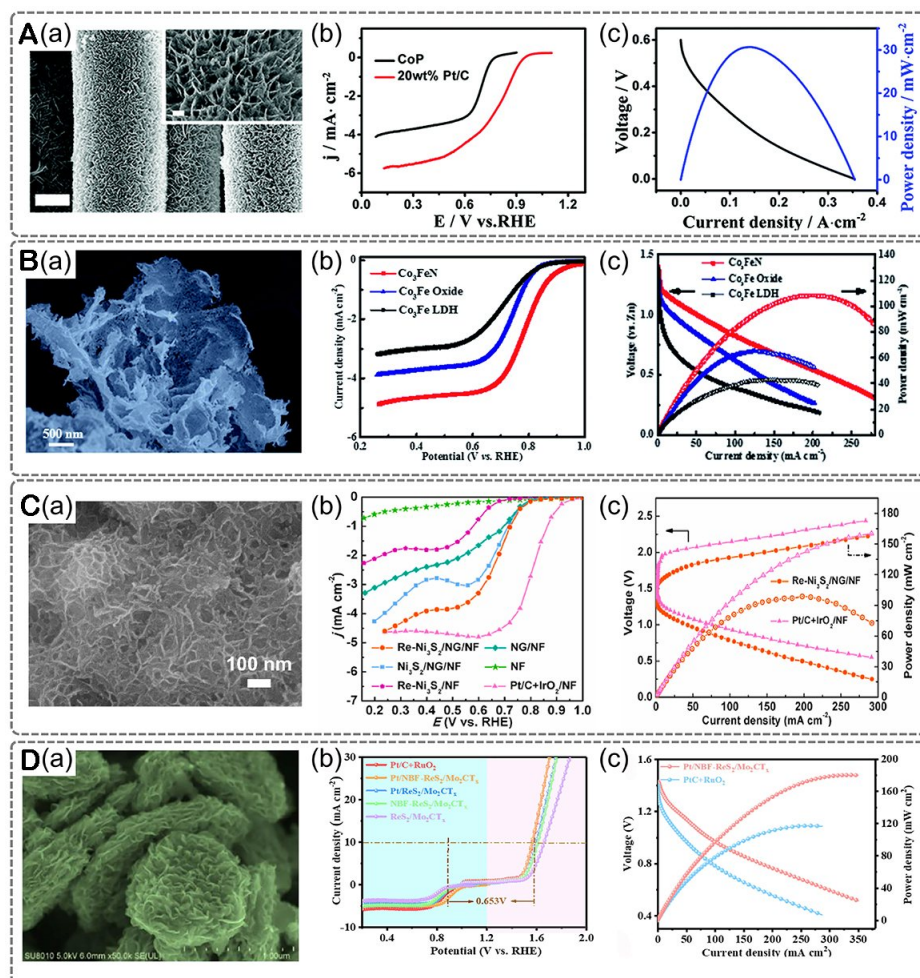


Figure 7. (A) (a) SEM image of Co(OH)₂@CC; (b) ORR performance of CoP and commercial Pt/C; (c) Discharge polarization curve and corresponding power density in ZABs^[52]. Copyright 2017, the Royal Society of Chemistry. (B) (a) SEM image of Co₃FeN nanosheets; (b) LSV curves of different samples for ORR; (c) Discharge polarization curves and corresponding power density curves of different samples^[54]. Copyright 2019, the Royal Society of Chemistry. (C) (a) SEM image of Re-Ni₃S₂/NG/NF; (b) ORR polarization curves of samples; (c) Charge/discharge polarization curves and power density plots Re-Ni₃S₂/NG/NF and Pt/C + IrO₂/NF based ZABs^[55]. Copyright 2022, Elsevier. (D) (a) SEM image of Pt/NbF-ReS₂/Mo₂CT_x; (b) ORR and OER polarization curves of the different samples; (c) Discharge polarization curves and related power density plots in ZABs^[57]. Copyright 2021, Elsevier.

Figure 7B, Guo *et al.* designed 2D Co₃FeN nanosheets via nitrogenization of silk-like Co₃Fe-LDH. The prepared Co₃FeN nanosheets with a holey-structured architecture comprised numerous active sites on a large surface area with superior gas and electrolyte penetration ability^[54]. When the 2D holey-structured metallic Co₃FeN nanosheets were utilized as the cathode, the ZAB demonstrated superior properties, including a power density of 108 mW cm⁻² and good stability for 900 charge-discharge cycles arising from their exceptional electrical conductivity and optimal architecture.

Apart from maximizing the active surface area, effective manipulation of the intrinsic properties of active sites is crucial to enhance electrocatalyst performance. The introduction of heteroatoms is a widely used strategy to modulate atomic and electronic structures, which can affect the adsorption energy. As shown in **Figure 7C**, Han *et al.* reported a novel Re-doped Ni₃S₂ nanosheet array on N-doped graphene-modified nickel foam substrate (Re-Ni₃S₂/NG/NF) through via a simple hydrothermal strategy^[55]. The unique structure endows Re-Ni₃S₂/NG/NF with a large active surface area and numerous electroactive sites. The

incorporation of Re modulated the electronic structural states of Ni_3S_2 , leading to a significant enhancement in electrocatalytic performance. As a result, the Re- Ni_3S_2 /NG/NF-based ZAB exhibited a high-power density of 99 mW cm^{-2} and can be operated for 5,000 cycles. Similarly, Xu *et al.* designed Co atom-doped tungsten sulfides (Co- WS_2) via a filtration and annealing process in the H_2 atmosphere^[148]. Co doping effectively regulates the electron structure of WS_2 , significantly boosting the ORR and OER performance, and the assembled rechargeable ZABs produced by Co- WS_2 exhibited a high-power density of 211 mW cm^{-2} . Two-dimensional materials offer a convenient platform for the modulation of surface/interfaces, resulting in enhanced OER and unleashed ORR activities. Robust interface interactions, unsaturated coordination, and doping with 2D materials can substantially alter the catalyst's electronic structure, thereby driving improvements in electrocatalytic performance. A rechargeable aqueous ZAB using the 2D NiFeMn nitride stabilized by Ti_3C_2 sheets as an air cathode endowed with a high specific capacity of $630 \text{ mAh g}_{\text{Zn}}^{-1}$ and excellent cycling stability over 120 cycles^[149]. This is attributed to enhanced active site exposure, charge redistribution, and the emergence of new active sites at the M-N-C or M-N-e interfaces, contributing to the notable OER activity and unlocked ORR reactivity.

Given that catalytic reactions transpire at the surface/interface of catalysts and inherently involve charge transfer, achieving swift and efficient charge transfer can mitigate polarization effects and expedite kinetic processes^[150,151]. For instance, ultrathin oxygen-doped FePSe_3 ($\text{FePSe}_3\text{-O}$) nanosheets exhibit notable reorganization of surface atoms, resulting in the formation of multiple crystalline-amorphous interfaces that enhance the kinetics of the OER^[56]. DFT calculations suggest that oxygen doping can also influence the electronic states at the Fermi level, leading to a reduced band gap that contributes to improved electrocatalytic performance. Moreover, 2D Co/Ce bimetallic nitrogen-doped carbon nanosheets ($\text{Co}_9\text{S}_8/\text{CeO}_2/\text{Co-NC}$)^[152]. It benefits from the synergetic effect and heterostructure. When assembled in rechargeable ZABs, $\text{Co}_9\text{S}_8/\text{CeO}_2/\text{Co-NC}$ exhibited an outstanding peak power density of $164.24 \text{ mW cm}^{-2}$.

The discovery of 2D MXenes dates back to 2011^[153]. The hydrophilic surfaces and high metallic conductivities of MXenes have led to their extensive utilization in various applications such as photodetectors^[154,155], metal-ion batteries^[156], metal-sulfur batteries, supercapacitors, and water splitting^[157,158]. As emerging 2D nanosheets, MXenes have received extensive attention and are widely applied as effective catalysts in ZABs. For example, Chen *et al.* designed a composite by combining exfoliated V_2C nanosheets with FeNi-LDH nanosheets, wherein the hypophosphite groups were introduced as intercalated anions in the LDHs layers (referred to as $\text{H}_2\text{PO}_2^-/\text{FeNi-LDH-V}_2\text{C}$)^[159]. The strong interfacial interaction and electronic coupling between the LDHs and V_2C nanosheets guarantee fast charge transfer kinetics and a stable structure. The assembled ZAB of $\text{H}_2\text{PO}_2^-/\text{FeNi-LDH-V}_2\text{C}$ showed a superior OCV of 1.42 V, a high-power density (137 mW cm^{-2}), and long durability. In others, Zou *et al.* proposed a novel hierarchical porous Ni-Co-mixed metal sulfide (NiCoS) on $\text{Ti}_3\text{C}_2\text{T}_x$ MXene via a MOF-based approach^[160]. Taking advantage of the unique structure and strong interfacial interaction of NiCoS and $\text{Ti}_3\text{C}_2\text{T}_x$, the hybrid material demonstrates notable electrical conductivity, facilitating efficient electron transport. Consequently, the assembled ZABs that utilize the $\text{NiCoS}/\text{Ti}_3\text{C}_2\text{T}_x$ material exhibit a small charging/discharging voltage gap and excellent durability for long-term operation. MXenes are usually used in forming composite materials with other compounds or SAs. Yi *et al.* synthesized N, B, and F atom-doped ReS_2 , which is grown evenly on the surface of MoC_2T_x MXene, followed by a uniform loading of single-atom Pt on NBF- ReS_2 ($\text{Pt/NBF-ReS}_2/\text{Mo}_2\text{CT}_x$) electrocatalysts, and utilizing the 2D morphology of ReS_2 to offer an extensive surface area for the incorporation of individual Pt atoms^[57], as seen in Figure 7D. In addition, the introduction of N, B, and F increases the number of active sites. The assembled ZAB with the $\text{Pt/NBF-ReS}_2/\text{Mo}_2\text{CT}_x$ electrode exhibited a narrow charge-discharge gap, a higher peak power density of 180.2 mW cm^{-2} , and excellent cycle stability.

Others 2D catalysts

Apart from the aforementioned 2D nanomaterials, other 2D materials, such as MOFs, COFs, C_3N_4 , and BP, have also been applied in the development of ZABs. For example, 2D MOFs can be synthesized from the strong coordination covalent bonds that form between metal-containing nodes and active organic components and can function as the active air cathode in aqueous ZABs. Recently, Jiang *et al.* incorporated ligand vacancies and hierarchical pores into cobalt-zinc heterometal imidazole frameworks (BHZ-48) to regulate their electronic states and structural porosity [Figure 8A]^[58]. In the synthesized BHZ-48, the orbital configuration of active sites is influenced by both near-range interactions with ligand vacancies and distant interactions with the Co-Zn alliance. This combination results in optimized adsorption/desorption energy for the reactive intermediates, effectively lowering the energy barrier for the potential-determining step. When employed as an air electrode, the BHZ-48-based ZAB exhibited a high-power density (148 mW cm^{-2} at 250 mA cm^{-2}) and excellent durability (1,250 h). In addition, because a single catalyst alone cannot achieve optimal activities for ORR and OER, it is essential to devise strategies that effectively balance the absorption and desorption energies of oxygen intermediates in bifunctional catalysts so that ORR and OER can be facilitated simultaneously. Jiang *et al.* alter the intermediate adsorption free energy on the Co-Fe zeolitic imidazolate framework (CFZ)^[8]. Both the experimental results and DFT calculations demonstrate that the electron-withdrawing characteristic of the sulfur group finely tunes the energy level of the d-orbital in the cobalt, regulating the free energy of OH^* adsorption and desorption (ΔG_{OH^*}) and leading to exceptional catalytic activity. The assembled ZAB exhibits remarkable long-term durability of 525 h.

In addition to the electronic structure of the MOF, the morphology of the utilized material has been identified as a critical factor in enhancing catalytic activity. Franco *et al.* synthesized an ultrathin 2D Cu-based MOF (2DCIF) that demonstrated remarkably high ORR activity^[161]. Moreover, the presence of uniformly distributed Cu- N_4O units within a stable 2D framework allows successful utilization of the 2D coordination-included frameworks as air electrodes in aqueous ZABs with outstanding specific capacity and power density values. This success underscores the excellent attributes of 2D Cu-based MOFs as electrocatalysts for energy storage devices. Additionally, integrating specific conductive substrates with MOFs has been explored to effectively enhance the electron migration, further augmenting the ZABs properties. In a representative study, a composite was fabricated by Zhao *et al.* by in situ hybridizing stable, hydrophilic, and conductive MXene nanosheets with 2D cobalt 1,4-benzenedicarboxylate ($\text{Ti}_3\text{C}_2\text{T}_x\text{-CoBDC}$)^[162]. The resulting catalyst exhibited remarkable electrocatalytic performance because of its high surface area, porous structures, and active Co species. The $\text{Ti}_3\text{C}_2\text{T}_x\text{-CoBDC}$ composite-based ZABs also indicate their promise for practical application. After that, Zheng *et al.* prepared hybrid materials (CoNi-MOF/rGO) by synthesizing bimetallic CoNi-MOF nanosheets on reduced graphene oxide through a straightforward surfactant-assisted method^[163]. Benefiting from the multitude of exposed active sites, the improved electron conductivity, and the synergistic effect, the CoNi-MOF/rGO hybrids exhibited outstanding catalytic performance in the ORR and the OER, and the assembled ZAB showed a high peak power density of 97 mW cm^{-2} and excellent stability.

Two-dimensional COFs are constructed using symmetric organic building blocks and are self-assembled through π - π stacking interactions. Their structural adjustability, finely tuned porosity, and strong chemical stability render them promising catalysts for application in aqueous ZABs^[164,165]. Cao *et al.* designed a novel fluorinated COF engineering strategy to develop a high-performance catalyst for rechargeable ZABs^[59]. As shown in Figure 8B, fluorinated COF (TpFx-COF) *in situ* was grown on the hydrophilic FeNi LDH to obtain the FeNi LDH-TpFx and showed high O_2 affinity and several nanopores. The TpFx-COF with well-defined channels can act as the aerophilic “nano-islands” for the transportation of O_2 on the FeNi-LDH electrocatalyst surface. This arrangement effectively segregates the mass O_2 and water transport pathways on the nanoscale, substantially increasing the three-phase boundary area and significantly enhancing the mass

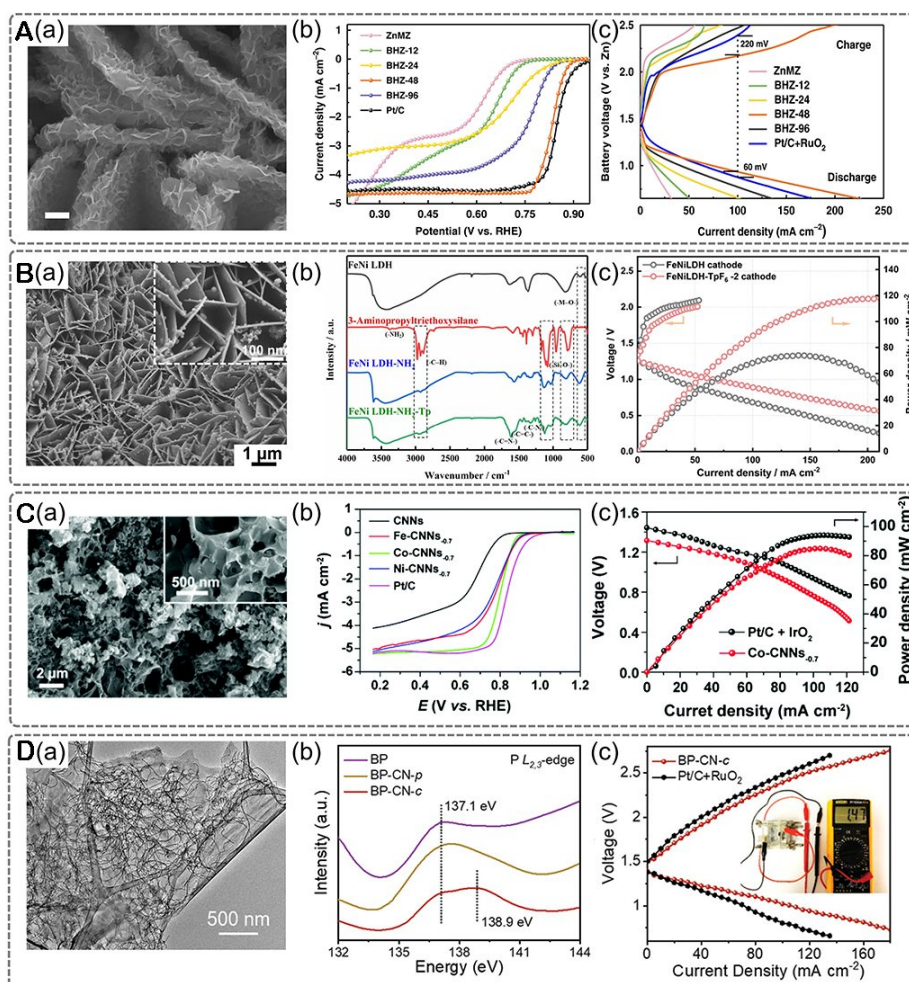


Figure 8. (A) (a) SEM image of BHZ-48; (b) ORR LSV curves for comparison of different samples; (c) Charge and discharge polarization curves^[58]. Copyright 2020, Springer Nature. (B) (a) SEM image of FeNi LDH-TpF6-2; (b) FT-IR spectra; (c) Discharge and charge polarization and power density curves^[59]. Copyright 2023, Wiley-VCH. (C) (a) SEM image of Co-CNNs_{0.7}; (b) ORR polarization curves for various catalysts; (c) Polarization and power density curves^[60]. Copyright 2020, the Royal Society of Chemistry. (D) (a) TEM image of BP-CN-c; (b) P $L_{2,3}$ -edge XANES spectra of BP, BP-CN-p, and BP-CN-c; (c) Discharge/charge polarization curves of ZABs assemble with BP-CN-c and Pt/C+RuO₂^[62]. Copyright 2021, Wiley-VCH.

transfer efficiency. The assembled ZAB of TpFx-COF exhibited a narrow charge/discharge voltage gap of 0.64 V, a peak power density of 118 mW cm⁻², and stable cyclability.

A 2D material that is composed of periodic aromatic units consisting of sp²-hybridized carbon and nitrogen atoms, g-C₃N₄, is characterized by a low surface area and inadequate conductivity, which hampers its viability as an effective electrocatalyst for ORR and OER. Therefore, the design of a g-C₃N₄-based electrocatalyst with high electron mobility for the efficient catalysis of ORR and OER in ZABs remains unfulfilled^[166,167]. Recently, Niu *et al.* synthesized graphitic carbon nitride embedded with TM nanocrystals (M-CNN) through a general solid-phase pyrolysis method [Figure 8C]^[60]. The coordination bond between the metallic Fe, Co, Ni, and N in the M-CNNs_x composites resulted in more defective and disordered graphitic structures than CNNs. Moreover, the ZAB with the Co-CNNs_{0.7} composite as an air cathode demonstrated a notable peak power density of 85.3 mW cm⁻² and a specific capacity of 675.7 mA h g⁻¹. Since then, other g-C₃N₄-based composite catalysts with abundant M-N_x active sites, such as Fe-NC&CN^[168],

NGM-CN-Fe^[169], and Co-NC-900^[61], have been developed. The assembled ZABs that use these materials exhibit high specific capacity with stable and persistent discharge performances.

BP was first synthesized in 1914; however, it was only in 2014 that theory and experimentation confirmed the presence of a BP monolayer. This revelation piqued the interest of researchers^[170], and 2D BP as a multifunctional material, which has many merits, including the adjustable bandgap, puckered-honeycomb configuration, and high charge carrier mobility, attracted much attention in the energy storage field^[171-173]. However, challenges such as low catalytic activity and inadequate electrochemical stability currently limit its application. Because of this, Wang *et al.* developed a metal-free bifunctional oxygen electrocatalyst based on BP and g-C₃N₄, denoted as BP-CN-*c*, in which BP nanosheets were covalently bonded to g-C₃N₄. This material was produced by mixing BP nanosheets with g-C₃N₄ and subsequently subjecting the mixture to anneal at 300 °C under a nitrogen atmosphere, as shown in Figure 8D^[62]. The polarized P-N covalent bonds in BP-CN-*c* effectively modulate the electron transfer from BP to graphitic carbon nitride, markedly enhancing the adsorption of OOH* onto phosphorus atoms. Consequently, the ZAB assembled by BP-CN-*c* cathode exhibited a high-power density of 168.3 mW cm⁻² and an energy density of 952.7 Wh kg⁻¹.

2D MATERIALS FOR NONAQUEOUS LOBS

Despite both falling under the category of MABs, the reaction mechanisms of LOBs and ZABs significantly differ due to variations in the electrolyte composition. In ZABs, the reduction of oxygen to hydroxide during discharge and the oxidation of water to release oxygen during charging are the most critical reactions, and their slow kinetics restrict the development of batteries. However, to LOBs, the development is mainly subject to the generation and decomposition of Li₂O₂, which affects round-trip efficiency, degraded capacity, and cyclability. In response, substantial research endeavors have been directed towards the exploration and application of efficient 2D materials as potent electrocatalysts in response to these challenges. In this context, diverse 2D catalysts, including carbon-based materials, metal-decorated 2D carbon structures, TMOs/TMOHs, other TM compounds, C₃N₄-based materials, and 2D MOF/COFs, have been employed in LOBs, yielding varying degrees of success. The detailed electrochemical performances of these materials as catalysts in LOBs are listed in Table 2.

2D carbon-based materials

Since the first application of graphene nanosheets^[210], various 2D carbon materials have been employed as cathodes in LOBs. These 2D carbon materials mainly include graphene, precursor-derived carbon, and graphylene^[13,211,212]. This choice is not only driven by the cost-effectiveness, abundant availability, and low mass density of carbon-based 2D materials but is also due to their inherent ORR activity. However, it is important to acknowledge that the further development of these 2D carbonaceous materials still faces challenges related to their architectural design. Without advanced architecture, the smooth promotion of mass transfer for all reactants becomes compromised, and chemical pathways are susceptible to blockage due to the deposition of insoluble discharge products.

To address these challenges, substantial endeavors have been directed towards the development of porous carbon materials with advanced structures. Broadly speaking, these approaches fall into two broad categories, the first of which involves manipulating the in-plane structure of monolayer graphene. Lin *et al.* achieved holey graphene via facile air oxidation methods and further designed air electrodes with porous structures^[213]. When employed in LOBs, the high mass loading air cathode exhibits ultrahigh areal capacity reaching approximately 40 mA cm⁻². Another technique involves adjusting the hierarchical structure of 2D nanosheets. Jung *et al.* developed a free-standing film with robust geometric characteristics by non-stacked graphene that could function as a cathode in LOBs^[174]. The considerable porosity confirmed by Brunauer-

Table 2. Comparison of different types of 2D electrocatalyst performances in LOBs

	Catalysts	Electrolyte	Discharge specific capacity (mAh g ⁻¹)	Current density (mA g ⁻¹)	Limited capacity@current density (mAh g ⁻¹ @mA g ⁻¹)	Cycle number	Refs.
2D Carbon-based materials	NS-rGO	1 M LiTFSI/TEGDME	3,320	0.24	1,000@ 0.24 mA cm ⁻²	14	[174]
	NS-G-700	1 M LiTFSI/TEGDME	1,000	100	1,000@600	25	[175]
	s-BNC	1 M LiTFSI/TEGDME	8,397	1,500	1,000@500	160	[176]
	S-doped graphene	1 M LiTFSI/TEGDME	10,400	200	1,000@300	100	[177]
	B-hG-700	1 M LiTFSI/TEGDME	19,698	100	1,000@100	120	[178]
	GDY/Fc	1 M LiTFSI/TEGDME	14,231	200	500@200	183	[13]
Metal-decorated 2D carbon materials	Ru/N-rGO	1 M LiTFSI/TEGDME	17,074	500	1,000@100	100	[179]
	Pt-HGNs	1 M LiTFSI/TEGDME	5,600	100	1,000@100	54	[180]
	Ir-rGO	1 M LiTFSI/TEGDME	9,500	100	1,000@100	40	[181]
	CoCu/graphene	1 M LiTFSI/TEGDME	14,821	200	1,000@500	122	[182]
	PVP-C@LDO	1 M LiTFSI/TEGDME	4,333	100	1.3 mAh cm ⁻² @100	70	[183]
	Co-SAs/N-C200	1 M LiTFSI/TEGDME	11,098	1,000	1,000@200	260	[184]
	Co-SA-rGO	1 M LiTFSI/TEGDME	12,760	100	1,000@100	220	[185]
	Ru _{NC} /Co _{SA} -3DNG	1 M LiTFSI/TEGDME	25,632	100	1,000@200	300	[186]
2D transition metal oxide/hydroxide	1% Ir ₁ /Co ₃ O ₄	1 M LiTFSI/TEGDME	16,861	200	500@200	180	[187]
	CoFeCe-2 oxide	1 M LiTFSI/TEGDME	12,340	100	1,000@100	2,900 h at 100 mA g ⁻¹	[188]
	SeZnO ₃ nanosheets	1 M LiTFSI/DMSO	13,200	500	1,000@500	140	[189]
	LaFeO _{3-x} NS	1 M LiTFSI/TEGDME	14,983	100	1,000@100	60	[190]
Other 2D transition metal compounds	NiS ₂ -NSs	1.0 M LiNO ₃ in DMA	22,500	1,000	1,000@1,000	300	[191]
	Co ₃ O ₄ -NS	1 M LiTFSI in TEGDME	5,917	100	500@100	25	[192]
	H-2D-Co ₉ S ₈	1 M LiTFSI in TEGDME	3,500	100	500@100	100	[193]
	NiS ₂ -CoS ₂ @NC	1 M LiTFSI/TEGDME	14,551	1,000	500@500	490	[194]
	CuCo ₂ S ₄ @Ni	1 M LiTFSI/TEGDME	9,763	100	500@200	164	[195]
	2D Bi ₂ Te ₃	1 M LiNO ₃ /DMSO	21,172	500	600@500	188	[196]
	MoS ₂ /AuNPs	1 M LiTFSI/TEGDME	3,567	600	-	50	[197]
	MoS _{2-x} @CNTs	1 M LiTFSI/TEGDME	19,989	200	1,000@200	105	[198]
	Ni/Mn-MoS ₂	1 M LiTFSI/DMSO	28,195	100	1,000@200	118	[199]
	Pd-TMS/CT	1 M LiTFSI/TEGDME	7,441	500	1,000@500	622	[200]

	6Ag-SnSe ₂	1 M LiTFSI/DMSO	16,871	100	1,000@1,000	144	[201]
	Co ₂ P/acetylene black	1 M LiTFSI/DMSO	5,102	0.1 mA cm ⁻²	500@0.1 mA cm ⁻²	132	[202]
	N-TiO ₂ /Ti ₃ C ₂ T _x	1 M LiTFSI/TEGDME	15,298	100	500@500	200	[203]
Other 2D catalysts	2D Mn-MOF	1 M LiTFSI/TEGDME	9,464	100	1,000@100	200	[204]
	Co-MOF/MXene	1 M LiTFSI/TEGDME	34,763	1000	1,000@1,000	278	[205]
	CMT@MXene	1 M LiTFSI/TEGDME	6,850	200	1,000@500	247	[206]
	Ni-TAPP-Co	1 M LiTFSI/TEGDME	17,104	500	1,000@200	200	[207]
	Pt-CNHS	1 M LiTFSI/TEGDME	17,059.5	100	600@100	70	[208]
	Ag/g-C ₃ N ₄ /Co ₃ O ₄	1 M LiTFSI/TEGDME	7,723	100	1,000@100	51	[209]

Emmett-Teller (BET) surface area measurement led to significantly improved electrochemical performance in terms of discharge capacity. In light of the aforementioned findings, 2D carbon materials with advanced architecture inherently provide abundant voids and spaces that facilitate oxygen-related reactions, ensure convenient access to the electrolyte, and enable swift oxygen diffusion. These effects hold the potential to further elevate the overall electrochemical efficiency of LOBs.

However, the intrinsic limitations of pure 2D carbonaceous materials in effectively catalyzing the formation and decomposition of Li₂O₂ have constrained their application within LOBs. The low kinetic and thermodynamic activity of those untreated carbon-based catalysts will lead to a large overpotential and induce an irreversible capacity fading, which may lead to the battery failure. Also, the common carbon electrode in LOBs still suffers from the inevitable side effects, such as the nucleophilic attack with Li₂O₂, further forming Li₂CO₃. Fortunately, the incorporation of heteroatoms, such as N, P, B, O, and S, presents a viable solution to improve the surface electronic structure of pristine materials and establish new active sites^[175,176,178,211,212,214]. This approach offers a promising opportunity to boost the ORR/OER catalytic performance of carbon materials. Also, it is demonstrated to mitigate the side effects. In the case of N doping, the presence of electron-accepting N atoms introduces a higher positive charge density to the neighboring carbon atoms. Computational and experimental studies have indicated that introducing nitrogen atoms enhances the electrocatalytic activity of nanostructured carbon materials toward oxygen reduction^[77]. Distinct from N atom doping, doping graphene with B not only expedites the kinetics of the ORR but also affects the decomposition of Li₂O₂. According to first-principle thermodynamics calculations, B-doped graphene can reduce the rate-determining barrier to further improve the charge rate of LOBs^[215]. Furthermore, recent investigations have demonstrated that the simultaneous incorporation of multiple heteroatoms into graphene yields hybrid structures with supplementary catalytic properties attributed to their synergistic coupling effects^[175,176].

Based on the research findings presented, it becomes evident that combining porous 2D carbon materials with hierarchical structures and heteroatom-doping holds significant promise and may potentially pave the way for the development of advanced LOBs. For example, Han *et al.* demonstrated that the synergistic effect of chemical doping and 3D porous configuration substantially improved the reaction kinetics of electrodes^[177]. Nitrogen and sulfur-doped nanoporous graphene, while retaining its lightweight nature, ample accessible surface area, and high conductivity, exhibited substantial capacity and excellent cycling stability in rechargeable LOBs. In another study, Liu *et al.* designed an edge-rich porous carbon structure

that resembled stacks of holey graphene via COF pyrolysis, which was denoted COF₈₀₀ [Figure 9A]^[212]. Heating led to the decomposition of nitrogen-containing groups within the COF to produce graphitic and pyridinic nitrogen species. The uniform nitrogen doping and edge sites in the endowed COF₈₀₀ resulted in heightened intrinsic catalytic activity toward ORR. Meanwhile, the COF₈₀₀-based LOB also exhibited a high discharge specific capacity of 2,558 mAh g⁻¹. Similarly, boron-doped holey graphene (B-hG-700), with a significant number of holes and a high boron doping level of 6 at.%, was reported to exhibit exceptional performance in LOB including a high capacity of 19,698 mA h g⁻¹ at 100 mA g⁻¹, and remarkable cycling stability over 120 cycles [Figure 9B]^[178]. Both experimentation and DFT calculations indicated a preference for Li₂O₂ nucleation and vertical growth near the hole/edge sites, facilitating isolated and uniformly distributed Li₂O₂. This process effectively reduces Li₂O₂ agglomeration and creates abundant space to accommodate Li₂O₂, thereby enhancing oxygen reduction and evolution kinetics.

Besides, 2D carbon materials can also be employed to mitigate severe redox shuttling. A novel carbon family, namely the GDY matrix, was introduced by Li *et al.* for this purpose [Figure 9C]^[13]. The GDY framework anchored with ferrocene (GDY/Fc) serves as a stationary soluble redox mediator that preserves the redox-mediating ability of ferrocene while promoting the oriented 3D growth of Li₂O₂, effectively mitigating the shuttle effects that are associated with the redox process. LOBs based on the GDY/Fc electrode demonstrated a high discharge specific capacity of 14,231 mA h g⁻¹ and long-term cycle stability of more than 183 cycles.

Metal-decorated 2D carbon materials

Even if element doping and porous structure construction strategies are used to improve the properties of 2D carbon materials, they are still insufficient to promote the ORR and OER kinetics in LOBs, which may result in high overpotential, low reversibility and poor rate capability. To address these challenges, the incorporation of metals with varying sizes into 2D-based carbon materials has been pursued. This approach can be categorized into three types: ultrasmall nanoparticles, SAs, and combinations of ultrasmall nanoparticles with SAs.

Considering the challenge of dispersing metal nanoparticles, 2D carbon materials are highly suitable as carriers for precious metals due to their abundant active sites, which facilitate the anchoring and growth of precious metals. Sabatier's principle suggests that noble metal catalysts (Ru, Ir, Pt, and Pd) are ideal for promoting the O₂/Li₂O₂ redox reaction in MABs due to their moderate binding energy with LiO₂ intermediates^[216]. Therefore, tremendous noble metal nanoparticles anchored on functionalized carbon nanosheet catalysts have been designed^[179-181,217,218]. Among them, crystalline Pd, situated near the apex of the "volcano plot," demonstrates optimal interactions with LiO₂ for ORR in LOBs. Both flexible Pd nanodendrites on graphene nanoplatelet^[219] and Pd nanoparticles coordinated with rGO^[217] exhibited significantly reduced overpotentials in nonaqueous LOBs. Similarly, Ru possesses strong adsorption energy for LiO₂ intermediates and effectively promotes the decomposition of discharge and side products, aligning with the design principles for efficient Li-O₂ catalysts. Dai *et al.* designed N-doped reduced graphene oxide anchored by ultra-dispersed Ru nanoparticles for LOBs^[179]. The Ru active centers and strong metal-support interactions were found to facilitate a viable process of forming and decomposing discharge products by influencing the surface adsorption of lithium superoxide intermediates and the nucleation and growth of lithium peroxide species. According to these advantages, this electrode exhibited better performance in the LOB, including enhanced discharge capacity of 17,074 mA h g⁻¹, decreased charge overpotential, and long-term stability. Other precious metal-2D carbon materials are also emerging in the field of LOBs. With a strong oxygen absorption ability, Pt nanoparticles with ultrasmall sizes coated onto hollow graphene nanocages act as catalytic nucleation sites of Li₂O₂^[180]. The distinctive matrix of hollow graphene nanocages serves a dual purpose: it not only furnishes a plethora of nanoscale tri-phase regions, serving as active sites

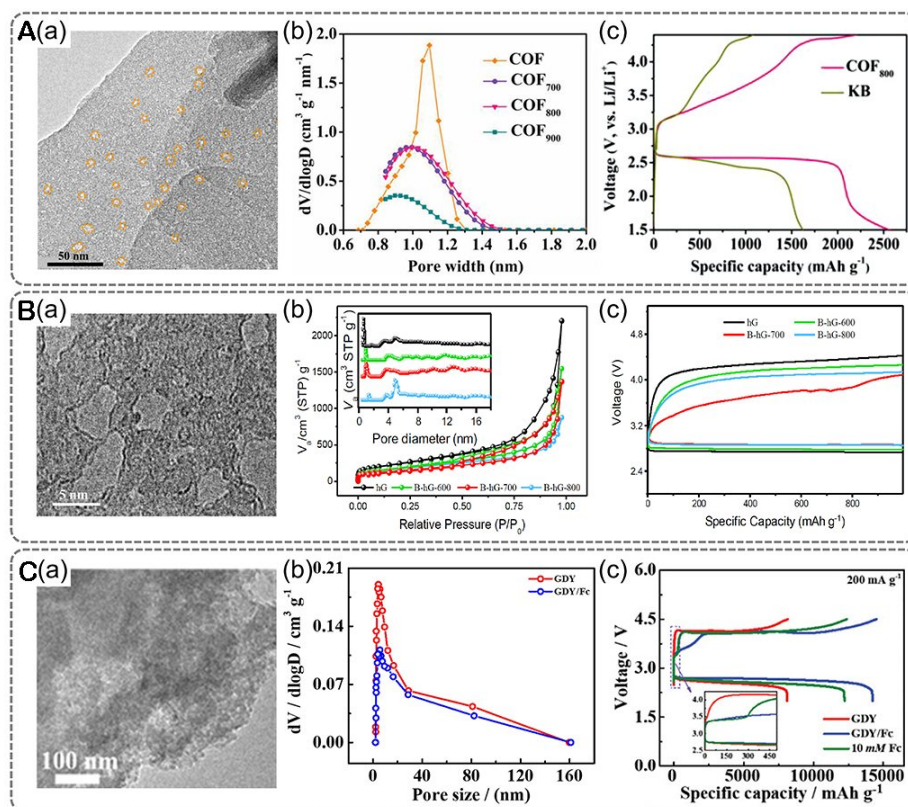


Figure 9. (A) (a) TEM images of COF_{800} ; (b) Pore size distribution curves of the COF and COF treated at different temperatures; (c) Initial GCD profiles of LOBs based on COF_{800} and Ketjen Black at 0.05 mA cm^{-2} [212]. Copyright 2021, Wiley-VCH. (B) (a) TEM image of B-hG-700; (b) Nitrogen adsorption-desorption curves of samples; (c) Initial discharge-charge curves of different cathodes at 100 mA g^{-1} [178]. Copyright 2022, Elsevier. (C) (a) TEM image of GDY/Fc; (b) Pore size distribution curves of samples; (c) GCD curves between 2.0 and 4.5 V at 200 mA g^{-1} [13]. Copyright 2022, Wiley-VCH.

for efficient oxygen reduction, but also provides an ample quantity of mesoscale pores, facilitating rapid oxygen diffusion. The catalysts finally lead to the subsequent formation of Li_2O_2 in a favorable form characterized by small size and an amorphous state, facilitating more efficient decomposition. Iridium incorporated into deoxygenated hierarchical graphene [220] and Ir-rGO composites [181] are also demonstrated as the advanced catalysts to accelerate the formation of Li-based intermediate and oxygen evolution. Nevertheless, the cost and scarcity of these metals limit their use as catalysts in commercial LOBs and have led to the exploration of non-precious metal nanoparticles on 2D carbon substrates, particularly cobalt-based catalysts. The 3D metal of Co, strongly bonded to LiO_2 , has demonstrated superior catalytic activity toward Li_2O_2 formation and decomposition [182,183]. In addition, it was demonstrated that bimetallic catalysts comprising two distinct metals may show exceptional catalytic activity, leveraging the synergy between the metals. Cobalt-copper bimetallic nanoparticles supported on graphene as cathode materials in LOBs exhibited superior rate capability, long cyclability, and outstanding coulombic efficiency due to the synergy of Co and Cu on graphene, enhancing both oxygen reduction and evolution kinetics [182]. Co and CoFe alloy nanoparticles decorated 2D NC also exhibited outstanding ORR/OER performances and durability in LOBs [183].

Compared to solid nanoparticles, SAs have garnered considerable attention in catalytic systems owing to their exceptional properties, which encompass abundant non-saturated atomic coordination sites, efficient

utilization of active atoms, and uniform active centers. Notably, in LOBs, single metal active sites are beginning to exhibit substantial potential in accelerating reaction kinetics and enhancing active species utilization effectively. An exemplary instance involves the synthesis of ultrathin nitrogen-rich carbon with embedded isolated cobalt atoms (Co-SAs/N-C) as the catalyst for LOBs [Figure 10A]^[184]. The produced catalyst full of exposed atomic active sites demonstrates a favorable capacity to control the formation and decomposition of ultra-distributed Li_2O_2 during ORR and OER. These benefits stem from the abundant Co-N-C catalytic sites, leading to significantly enhanced kinetics and reduced overpotentials. Notably, theoretical simulations have revealed that the plentiful cobalt-nitrogen moieties can substantially increase the affinity of active species during reaction. This adjustment completely modulates the formation mechanism of the final product Li_2O_2 in terms of size and distribution. Accordingly, the LOB with Co-SAs/N-C cathodes achieved an excellent discharge capacity of $20,105 \text{ mAh g}^{-1}$ and a long-term cyclability of 260 cycles. Recently, it has been found that LOBs with LiOH redox chemistry hold great promise for practical applications with an improved energy density and cyclic lifetime^[221,222]. Also, LiOH, as a discharge product, exhibits greater chemical stability than Li_2O_2 . Single-atom Co-N_4 /graphene catalysts (Co-SA-rGO) derived from MOFs were introduced and underwent $4e^-$ catalytic reactions with the product LiOH while mitigating water shuttling^[185]. The 3D networks of Co-SA-rGO deliver substantial surface area and mesoporous structures, facilitating both the capture of $\approx 12 \text{ wt\%}$ H_2O molecules and rapid pathways for O_2 diffusion and Li^+ transportation. Additionally, the Co-N_4 center demonstrates enhanced activity toward proton-coupled electron transfer, favoring the $4e^-$ formation of LiOH. With these unique features, the LOB based on Co-SA-rGO achieves a high discharge voltage platform of 2.83 V and a substantial discharge capacity of $12,760 \text{ mAh g}^{-1}$.

Through precise manipulation, both metal SAs and particles can coexist on the surface of 2D materials, showcasing broad prospects in the catalysis field. For instance, Ru nanoclusters were integrated onto N-doped 3D rGO alongside single Co atoms ($\text{Ru}_{\text{NC}}/\text{Co}_{\text{SA}}\text{-3DNG}$), resulting in highly efficient cathode catalysts for LOBs [Figure 10B]^[186]. The catalyst exhibited outstanding performance, including low charge potential, high discharge capacity ($25,632 \text{ mA h g}^{-1}$), and superior cycling stability (300 cycles). The study revealed that the introduction of single Co atoms resulted in the charge transfer between Ru clusters and other atoms and finally led to the electron-deficient Ru. The unique chemical environment of Ru enabled effective adsorption and activation of negatively charged O_2^{2-} ions in Li_2O_2 , further improving the OER activity. Additionally, the well-dispersed Ru clusters facilitated the generation of Co-N-C with enhanced ORR and OER activities, thereby leading to excellent cathodic performance in LOBs.

2D transition metal oxide/hydroxide

According to the studies, both 2D noble metal oxides^[223,224] and TMOs^[16,225-230] with 2D morphology are promising candidates as catalysts in LOBs. However, a critical challenge lies in the scarcity of precious metal resources on our planet, which hinders its large-scale application in LOBs. The high cost of these materials, coupled with their susceptibility to degradation due to metal poisoning or leaching, further complicates the issue. Consequently, the subsequent discussion will concentrate on efficient TMO catalysts for LOBs. Of all TMOs, Co_3O_4 nanosheets in which Co^{2+} and Co^{3+} ions occupy the tetrahedral and octahedral sites have been most thoroughly studied in terms of geometry^[231], crystal plane control^[227,232], and crystal structures. With more research on SACs, Co_3O_4 nanosheets loaded with single-atomic metals ($\text{M-Co}_3\text{O}_4$) were devised and demonstrated as high-performance cathode catalysts [Figure 11A]^[187]. The incorporation of single-atomic metals can effectively replace the central Co atom in the octahedral coordination structure, maintaining its structural integrity. This alteration offers an electron promotion effect, thereby exposing more active Co^{3+} sites, which, in turn, provides more nucleation locations for Li_2O_2 deposition. Furthermore, the introduced metal atoms can spatially segregate the active Co^{3+} centers, thereby regulating Li_2O_2 dispersion to yield a sheet-like morphology that facilitates subsequent charge cycle decomposition. Meanwhile, MnO_2 ^[225],

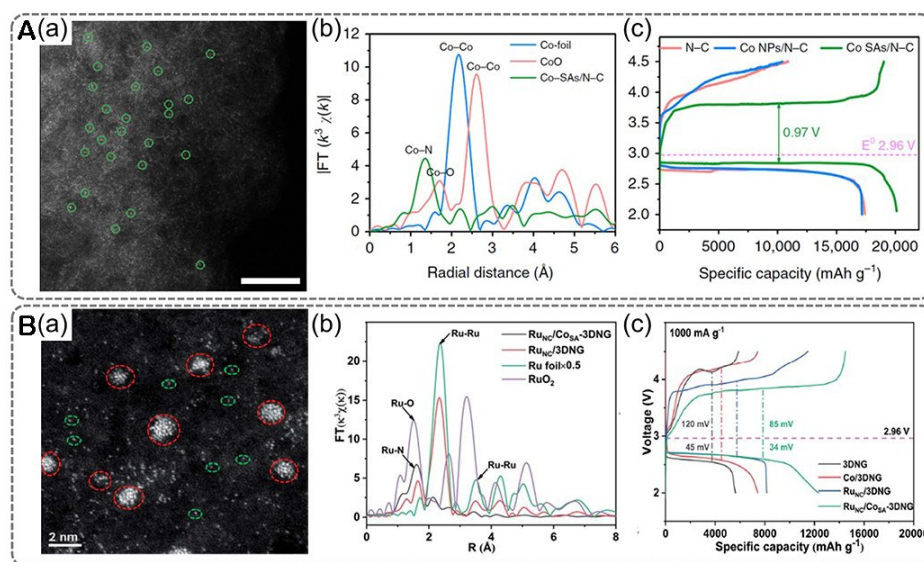


Figure 10. (A) (a) Zoom-in HAADF-STEM image of the Co-SA/NC catalyst; (b) K-edge FT-EXAFS in R space for related samples; (c) Initial deep GCD curves of related samples^[184]. Copyright 2020, Springer Nature. (B) (a) HAADF-STEM images of Ru_{NC}/Co_{SA}-3DNG; Fourier-transform EXAFS spectra for (b) Ru K-edge; (c) Initial discharge-charge profiles (voltage: 2.0-4.5 V, current density: 1,000 mA g⁻¹) of different electrodes^[186]. Copyright 2021, the Royal Society of Chemistry.

Nb₂O₅^[233], NiO^[230,234], and TiO₂^[235] are all considered as the promising candidates for LOBs. In addition, ternary spinel oxides (e.g., NiCo₂O₄, CuCr₂O₄, and MnCo₂O₄) with 2D morphology have garnered significant attention as potential electrocatalysts for LOBs due to their good electronic conductivity and catalytic activity^[236-238]. Trimetallic oxides with a high valence metallic element can effectively modulate the electronic structure and further optimize the adsorption energy of reaction intermediates, thus enhancing catalytic activity in LOBs. An illustrative case is the designed trimetallic CoFeCe oxide, which features amorphous/crystalline heterostructures as cathodes in LOBs [Figure 11B]^[188]. The LOB based on the most successful CoFeCe oxide cathode exhibits the highest initial discharge capacity (12,340 mAh g⁻¹) and maintains over 2,900 h at 100 mA g⁻¹. Combining the experimental outcomes with DFT analysis disclosed the pivotal role of unique heterostructure with minimized lattice mismatch and amorphous-crystalline domains in enhancing LiO₂ intermediate adsorption. These factors collectively contribute to the improvement of the electrocatalytic activity of CoFeCe oxide in LOBs.

Perovskite materials possess adjustable physical and chemical properties and can catalyze both ORR and OER, rendering them promising and cost-effective alternatives to noble metals for cathode catalyst application. Guided by the design principle of an eg-filling with a value of ~1 for maximum ORR activity^[239] and recognizing the inherent low conductivity of perovskite, a meso-LaSrMnO layer supported on graphene nanosheet was synthesized as a catalyst for LOBs. This well-designed system capitalizes on its structural elements: the interstitial space between nanosheets facilitates diffusion of O₂ and Li⁺, the mesoporous structure provides an extensive surface area for electrolyte penetration and discharge product deposition, the perovskite catalyst phase reduces reactive overpotential, and the graphene component establishes a conductive pathway for electron transport. The introduction of oxygen defects has been considered a significant approach to enhancing the catalytic performance and electrical conductivity of 2D perovskites^[189,240]. It has been demonstrated that oxygen vacancies in SeZnO₃ not only increase the number of catalytically active sites but also enhance electrical conductivity, thereby further elevating the catalytic efficacy for LOBs^[189]. LOBs employing oxygen vacancy-enriched LaFeO_{3-x} nanosheets (LaFeO_{3-x} NS) as

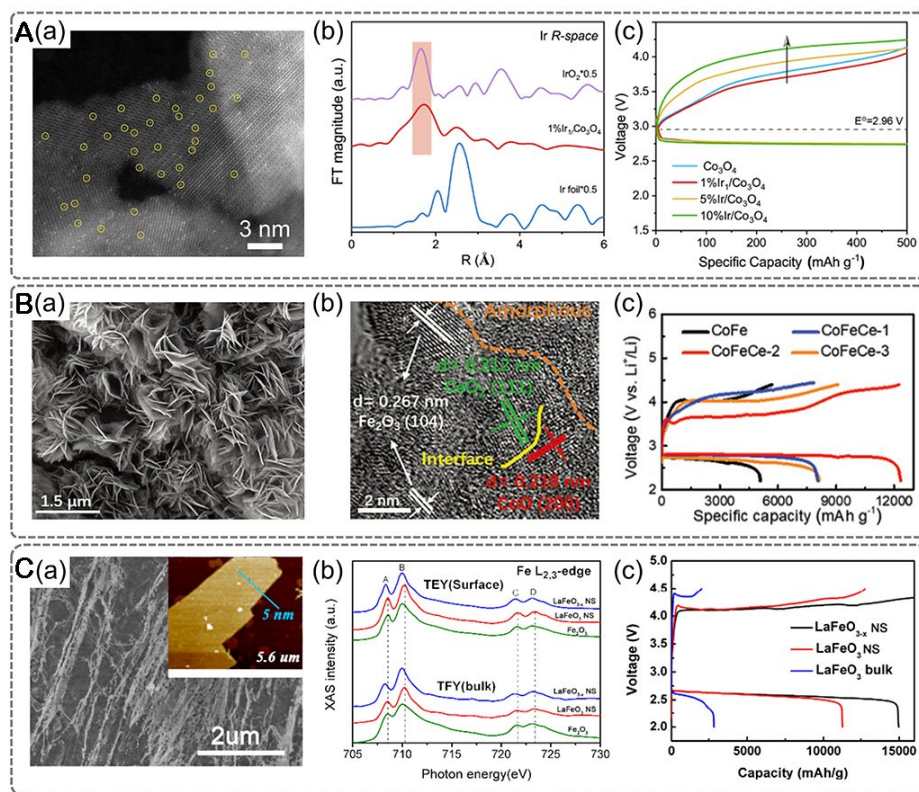


Figure 11. (A) (a) SEM image of Ir/Co₃O₄; (b) Fourier-transform EXAFS spectra of R space; (c) First discharge/charge curves^[187]. Copyright 2023, Wiley-VCH. (B) (a) SEM image of CoFeCe oxide; (b) HRTEM image of CoFeCe oxide; (c) Full first discharge/charge curves of as-prepared catalyst-based LOBs at 100 mA g⁻¹ under a potential of 2.2–4.4 V (vs. Li⁺/Li)^[188]. Copyright 2021, Wiley-VCH. (C) (a) SEM images of LaFeO_{3-x} NS; The Fe L-edge (b) and O K-edge (c) The initial capacity of samples at the current density of 100 mA g⁻¹^[190]. Copyright 2020, Elsevier.

catalysts exhibited remarkable attributes such as low overpotential, high specific capacity (14,983 mAh g⁻¹), and prolonged cycle stability (60 cycles) [Figure 11C]^[190]. These advantages stem from the synergistic interplay of engineering of 2D nanosheets, oxygen defects, and modulation of Fe valence. The choice of metal oxides is mainly concentrated in the oxides of iron, cobalt, nickel, and manganese from Table 2; among these, Co₃O₄ has been intensively studied. It is widely known that the high performance with enhanced long-term stability is hard to obtain with monometallic oxide materials without any further modifications, including both the modification of geometric and atomic structures. In the pursuit of high-efficiency catalysts for LOBs, TMOHs also play a significant role. TMOHs, especially LDHs, have garnered substantial attention owing to their tunable chemical properties and distinct 2D structures. While the limited catalytic prowess of TMOHs has historically hindered advancements in electrochemical performance, various strategies have been employed to overcome this limitation. These include the creation of metal vacancies^[241], manipulation of crystal phases^[242], and integration with conductive substrates^[243,244]. Furthermore, Lu *et al.* successfully synthesized materials with a superlattice structure that comprised CoNiFe LDH and RuO_{2.1} nanosheets, demonstrating exceptional performance in LOBs^[245]. The CoNiFe LDH carrying a positive charge and the negatively charged RuO_{2.1} are intricately arranged at the molecular level, forming superlattice-like hybrids through electrostatic interactions under specific conditions. This observed performance can be attributed to the unique superlattice structure, which facilitates robust interfacial electronic coupling, improved electrical conductivity, and the mitigation of side reactions often observed with conventional carbon-based materials.

Other 2D transition metal compounds

In addition to metal oxides, other compounds within the oxygen group (such as metal sulfides^[191-195,246-249], selenide^[250], and telluride^[196,251]) and the nitrogen group (including metal nitrides and phosphides^[202,252,253]) exhibit remarkable catalytic properties in LOBs. Among the oxygen group compounds, metal sulfides are the most widely studied. Following the initial investigation of NiS as a novel cathode catalyst for LOBs, numerous other TMSs have been explored and reported^[254]. Binary metal sulfides have emerged as notable candidates for energy conversion and storage applications due to their affordability, abundant availability, heightened electron conductivity, and enhanced electrochemical activities.

As an example, single-crystalline NiS₂ nanosheets (NiS₂-NSs) have been synthesized and demonstrated as efficient electrocatalysts for high-performance LOBs^[191]. These single-crystalline NiS₂-NSs can effectively facilitate the reversible Li₂O₂ formation and decomposition, respectively. Furthermore, 2D Co₃S₄ with the nano-thin sheet-like structure was fabricated via the simple hydrothermal method^[192]. The nanosheets with distinctive mesopores exhibited exceptional electrochemical performance in LOBs with a first discharge capacity of approximately 5,917 mAh g⁻¹ and a high reversibility of 95.72%. Moreover, flower-like copper sulfide^[246] and defect-rich holey Co₉S₈^[193] also exhibited significant performance in controlling the deposition of nanoscale Li₂O₂. Following the d-band center theory, the elevation (or reduction) of the d-band position corresponds to a heightened (or diminished) occupancy of the anti-bonding state, thereby resulting in a more potent (or weakened) adsorption of intermediates due to the less filling of the adsorbate-metal anti-bonding states. Consequently, adjusting the adsorption capacity by manipulating the d-band center has emerged as an efficacious approach to bolstering the electrocatalytic performance. Li *et al.* proved that an isomorphic structure, as illustrated by the cobalt/nickel pyrite composite (NiS₂-CoS₂@NC), can effectively customize the d-band center, thereby enhancing the adsorption ability of intermediates in LOBs [Figure 12A]^[194]. The heterostructure NiS₂-CoS₂ exhibited remarkable capability in facilitating the reversible Li₂O₂ formation and decomposition, resulting in an exceptional electrochemical performance featuring high initial specific capacities, extended cycle life, and outstanding rate performance. Beyond binary metal sulfides, ternary spinel sulfides with 2D morphology, characterized by structures and properties akin to ternary spinel oxides, have shown considerable promise for catalytic applications due to their narrow band gap, abundant electron transport channels, and more extensive redox coupling. Gradient-porous ultrathin FeCo₂S₄ nanosheets^[247], 2D spinel CuCo₂S₄ nanosheets^[255], free-standing 3D CuCo₂S₄ nanosheet array^[195], mesoporous MnCo₂S₄ nanosheet arrays^[248], and porous hollow ZnCo₂S₄ nanosheet arrays^[249] are demonstrated to be beneficial in achieving a high energy efficiency and long-term cycle life in LOBs. Long *et al.* successfully engineered a pioneering free-standing cathode that is composed of CuCo₂S₄ nanosheets (CuCo₂S₄@Ni), which exhibits remarkable catalytic activity in aprotic LOBs^[195]. This ingeniously devised oxygen electrode demonstrates a reduced overpotential (0.82 V), elevated specific capacity (9,673 mA h g⁻¹ at 100 mA g⁻¹), and extended cycle life (164 cycles) in contrast to conventional carbonaceous electrodes. The observed performance enhancement can be attributed to the exceptional structure of CuCo₂S₄, wherein both Cu and Co present abundant redox properties, thereby effectively enhancing the kinetics of ORR and OER. Both layered selenide and telluride are also suitable candidates for ORR/OER catalysis. Zhang *et al.* prepared a series of 2D materials, such as SnSe^[250], Bi₂Te₃^[196], and Ag₂Te^[251], as the cathode catalysts for LOBs, and they all exhibited good catalytic performance. For example, 2D Bi₂Te₃, consisting of five Te-Bi atom layers in its stacked configuration, exhibited superior specific capacity and excellent cycling stability^[196]. It is revealed that the (001) plane of the stack surface contributes to exceptional catalytic ability, creating an efficient pathway for the transformation from LiO₂ to Li₂O₂ and preventing the formation of undesired by-products.

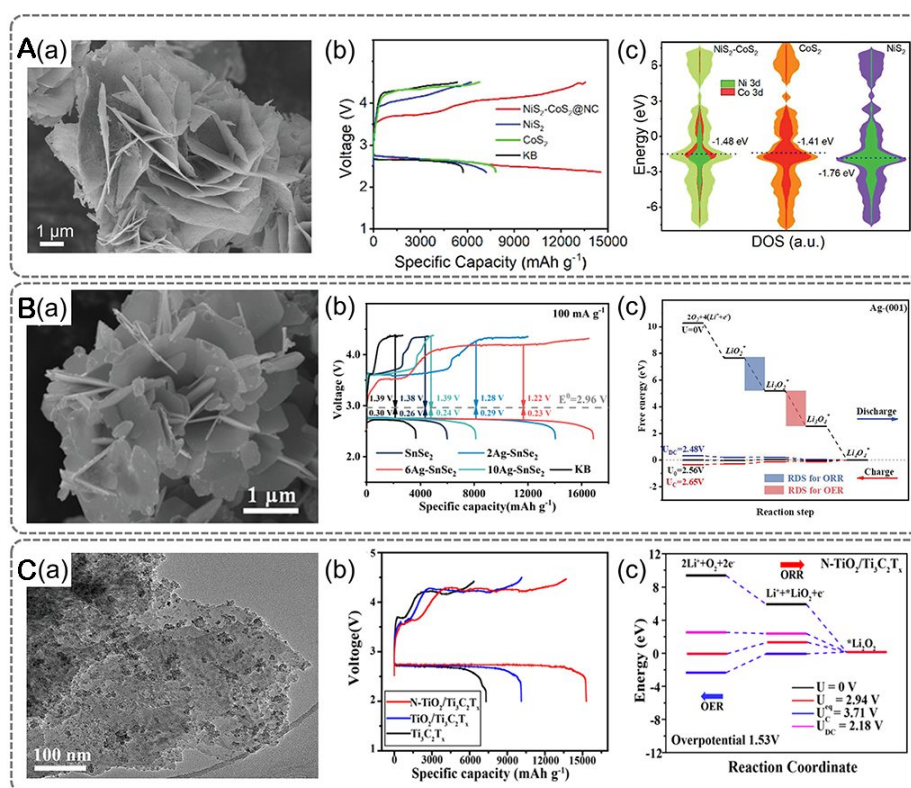


Figure 12. (A) (a) SEM image of $\text{NiS}_2\text{-CoS}_2\text{@NC}$; (b) Initial discharge/charge curves; (c) Density of states with dotted lines identified as the d-band centers of different catalysts^[194]. Copyright 2023, Wiley-VCH. (B) (a) SEM image of Ag-SnSe_2 ; (b) Initial discharge/charge profiles of different cathodes at 100 mA g^{-1} with a voltage range from 2.35 to 4.35 V; (c) Calculated energy diagram of Ag-(001) plane in ORR and OER processes^[201]. Copyright 2022, Wiley-VCH. (C) (a) TEM image of $\text{N-TiO}_2/\text{Ti}_3\text{C}_2\text{T}_x$; (b) Discharge-charge curves of the first cycle in various samples; (c) Gibbs free energy diagrams for $\text{N-TiO}_2/\text{Ti}_3\text{C}_2\text{T}_x$ ^[203]. Copyright 2022, the American Chemical Society.

TMDCs, a typical 2D material, are also widely used in LOBs. Although they are not widely used in ZABs, they are considered to be excellent catalysts for the formation and decomposition of L_2O_2 due to their different reaction mechanisms. In 2015, MoS_2 nanosheets decorated with gold nanoparticles ($\text{MoS}_2/\text{AuNPs}$) were initially introduced as promising cathode materials for LOBs^[197]. Since then, research on TMDCs for LOBs has been ongoing, mainly focusing on various aspects, including their integration with other materials, defect engineering, doping strategies, and phase modulation. As a typical inorganic compound, conductivity is the key problem that hinders the application of TMDCs in the battery field. Therefore, conductive carriers are often used to construct complexes to improve this situation, such as core-shell nanostructured $\text{MoSe}_2\text{@CNT}$ ^[256], 2D MoS_2 nanosheets anchored on hollow carbon spheres (MoS_2/HCS) composites^[257], and graphene-like MoSe_2 nanosheets anchored on hollow CNFs^[258]. As far as defects are concerned, the dominant focus is on the study of the non-metallic vacancy^[198,259]. For example, $\text{MoS}_{2-x}\text{@CNT}$ composites were synthesized through the hydrothermal process followed by annealing and NaBH_4 reduction^[198]. In this composite, defective MoS_2 nanoflakes are uniformly coated onto 3D CNT webs. The surface engineering strategy creates a favorable charge redistribution on the MoS_2 nanoflakes with sulfur vacancies, significantly enhancing the reaction kinetics. Simultaneously, the highly conductive CNT network facilitates mass transfer and offers enough area for cathodes, avoiding the volume expansion. Notably, the unique structure ensures comprehensive coverage of defective MoS_2 nanoflakes on CNT surfaces that allow for direct contact between CNTs and the electrolyte, effectively suppressing side reactions. Besides, heteroatom doping engineering can effectively modify the electronic structure of MoS_2 to

activate its inert surface and enhance its inherent catalytic performance. Cao *et al.* synthesized Ni and Mn co-doped MoS₂ through a facile one-pot hydrothermal method, which demonstrated rapid reaction kinetics in LOBs^[199]. Moreover, phase transition conversion has proven a promising strategy for enhancing catalytic efficiency. The band gap of MoS₂ can be tuned through phase engineering. In contrast to the semiconducting 2H-TMDC, metallic 1T phase TMDC possesses favorable electronic structures that facilitate swift reaction kinetics, high electrical transport rates, and abundant catalytic active sites. This configuration significantly elevates the intrinsic catalytic activity in the field of electrocatalysis. For instance, metallic 1T-MoS₂ was combined with activated CNTs to create free-standing oxygen electrodes^[260]. The prepared electrode exhibited remarkable performance, which can be attributed to the active surfaces of 1T-MoS₂, accessible to both Li⁺ and O₂. Hu *et al.* engineered a Pd-doped 1T-MoS₂ nanosheet array characterized by distinctive electronic structures that confer the electrode with rapid reaction kinetics, a high electrical transport rate, and an abundance of catalytic active sites^[200]. These attributes culminated in remarkable enhancement of the inherent catalytic performance in LOBs^[200]. Mo-based TMDCs are commonly employed, and as research advances, numerous emerging TMDC materials have been identified and utilized. Introducing Ag ions into the layered structure of 1T SnSe₂ (Ag-SnSe₂) has successfully modulated the electronic states along the stack edge planes, resulting in an enhancement of the catalytic capacity of 2D SnSe₂ [Figure 12B]^[201]. Consequently, the LOB with Ag-intercalated SnSe₂ cathodes demonstrated a remarkable specific capacity of 16 871 mAh g⁻¹ and exceptional cycle stability over 2,300 h at 100 mA g⁻¹, along with 144 cycles at 1,000 mA g⁻¹. This enhancement can be attributed to the intercalation of Ag, which effectively accelerates charge transfer and mitigates passivation on the 2D plane during ORR/OER.

Metal phosphide, included in nitrogen group compounds, such as Co₂P^[202], Ni₂P^[252], and MoP^[253], possess an intrinsic metallic nature, facilitating excellent electrical conductivity and rapid electron transfer at the electrode/electrolyte interface. These attributes position them as highly promising alternatives for oxygen electrode materials in LOBs. Huang *et al.* developed porous cobalt phosphide nanosheets with a high surface area using an environmentally benign hydrothermal approach^[202]. The resulting Co₂P/acetylene black composite exhibited improved electrochemical performances, featuring high capacities of 2,551 mA h g⁻¹ based on the total weight of active materials and a robust cycle life exceeding 1,800 cycles. In addition, regulating the heterogeneous interfaces in the catalytic materials to realize the electronic modulation through interfacial coupling has demonstrated efficacy in optimizing the chemical adsorption of O-containing intermediates and expediting the kinetics of oxygen electrode reactions^[261,262]. Microspheres of NiO@Ni₂P were ingeniously synthesized as efficient catalysts for LOBs^[262]. The unique electron redistribution at the NiO@Ni₂P heterostructure interface enhanced intermediate chemisorption. Additionally, the interpenetration of the P-O bond at the NiO@Ni₂P heterointerface induces an internal doping effect, thereby promoting electron transfer and further enhancing both ORR and OER activities. Consequently, the NiO@Ni₂P electrode demonstrates a remarkably low overpotential, a high specific capacity, and exceptional cycling stability.

2D MXenes (TMCs/TMNs) have emerged as a fascinating candidate for electrodes in LOBs due to their remarkable attributes, such as high electrical conductivity, tunable layered structure, abundant active sites, and adjustable surface groups. Theoretical simulations have indicated that MXene phases, such as Ti₃C₂T_x, hold the potential for superior catalytic performance in LOBs by establishing stable and conductive two-phase interfaces with Li₂O₂. Consequently, extensive research has been devoted to MXenes in the quest for high-performance cathode materials that can effectively catalyze Li₂O₂ deposition and degradation. Among these efforts, controlling the surface terminal functional groups of MXenes has emerged as an effective strategy to enhance their catalytic efficiency. Theoretical calculations have demonstrated a catalytic activity

trend for Ti_3C_2 as follows: $\text{Ti}_3\text{C}_2\text{O}_2 > \text{Ti}_3\text{C}_2\text{F}_2 > \text{Ti}_3\text{C}_2(\text{OH})_2 > \text{Ti}_3\text{C}_2$, highlighting the potential advantages of O-terminated Ti_3C_2 MXene for catalyzing both ORR and OER in LOBs^[263]. Concurrently, experimental evidence has validated that introducing oxygen functional groups to the MXene surface effectively boosts its intrinsic activity^[264-266]. Furthermore, incorporating heteroatoms has been identified as a promising approach to enhancing the catalytic performance of MXene. Another study involved the generation of a single-atom-doped Ti_3C_2 MXene catalyst with isolated semi-metallic selenium atoms^[267]. These isolated selenium atom catalytic centers exhibit active behavior, substantially augmenting the intrinsic LiO_2 absorption capacity. It fundamentally modifies the formation/decomposition mechanism of L_2O_2 , thereby significantly improving redox kinetics and mitigating overpotentials. Constructing complexes has also been recognized as an effective technique to accelerate catalytic reaction kinetics^[203,268,269]. Zheng *et al.* designed nitrogen-doped TiO_2 on $\text{Ti}_3\text{C}_2\text{T}_x$ nanosheets (N- $\text{TiO}_2/\text{Ti}_3\text{C}_2\text{T}_x$) as the oxygen electrode catalyst for LOBs [Figure 12C]^[203]. The heterojunction between TiO_2 and $\text{Ti}_3\text{C}_2\text{T}_x$ nanosheets retained metallic properties and effectively facilitated Li^+ and electron transfer within the electrode. More importantly, precise regulation of active sites at the N- $\text{TiO}_2/\text{Ti}_3\text{C}_2\text{T}_x$ heterojunction optimized the adsorption of LiO_2 and Li_2O_2 , thus accelerating the sluggish kinetics for both ORR and OER. As expected, N- $\text{TiO}_2/\text{Ti}_3\text{C}_2\text{T}_x$ catalyzed LOBs presented a superior specific capacity of 15,298 mAh g^{-1} and could run stably for over 200 cycles.

Other 2D catalysts

In addition to the catalysts described earlier, several other types of 2D materials have also been used in LOBs, such as MOFs, COFs, and $\text{g-C}_3\text{N}_4$. Of these, 2D MOF materials have been extensively investigated due to their notable characteristics, including high porosity, controllable large surface area, tunable structure and chemistry, and versatile chemical functionality achievable by substituting organic linkers and/or TMs. Yuan *et al.* were the pioneers in the application of 2D MOFs in aprotic LOBs^[204]. They employed a straightforward ultrasonic method to prepare a range of MOFs as cathode catalysts, resulting in the desired ultrathin structure. Notably, 2D Mn-MOFs possessed the highest performance among all prepared 2D MOFs, exhibiting a higher initial discharge specific capacity of 9,464 mAh g^{-1} and exceptional cyclability over 200 cycles. This remarkable performance can be attributed to the highly electrocatalytic activity of Mn-O clusters in 2D Mn-MOFs for the decomposition of Li_2O_2 and LiOH , which enhances the reversibility and efficiency of LOBs. Lv *et al.* enhanced the intrinsic activity of 2D MOFs via both doping and spin state manipulation^[270,271]. In the former approach, Ru atoms were incorporated into nickel-hexaminothriphenylene (Ni-HTP), featuring quadrilateral Ni- N_4 units^[270]. The atomically dispersed Ru- N_4 sites exhibited strong adsorption affinity for LiO_2 intermediate due to their adjustable d-band center. This favored the generation of film-like Li_2O_2 , promoting electron transfer and ion diffusion between the cathode and electrolyte and further facilitating Li_2O_2 decomposition during charging. This design allowed the LOBs with NiRu-HTP to achieve significantly reduced overpotential and remarkable cyclability. In the latter approach, the spin state of partial Ni^{2+} metal centers ($t_{2g}^6 e_g^2$) within a conductive nickel catecholate framework (Ni_{III}-NCF) was manipulated to high-valence Ni^{3+} ($t_{2g}^6 e_g^1$) to create Ni_{III}-NCF^[271]. This change of spin state enhanced Ni-O covalency in Ni_{III}-NCF, promoting electron exchange between Ni sites and oxygen adsorbates and accelerating oxygen redox kinetics. The battery employing Ni_{III}-NCF exhibited notably reduced discharge/charge voltage gaps, superior rate capability, and extended cycling stability. Furthermore, MXenes are frequently employed to form complexes with MOFs, enabling the catalysis of L_2O_2 formation and degradation. Zhang *et al.* prepared a free-standing flexible Co-MOF/MXene film as a cathode for LOBs^[205]. In this study, 2D Co-MOF nanosheets were strategically intercalated between the MXene layers. This arrangement effectively prevented the self-aggregation of MXene layers, significantly increased the interlayer spacing within the Co-MOF/ Ti_3C_2 hybrid film, and established enhanced pathways for the expansion of Li^+ and O_2 species. Nam *et al.* introduced a novel approach by directly growing a bimetallic cobalt-manganese organic framework (CMT) onto a $\text{Ti}_3\text{C}_2\text{T}_x$ MXene sheet via solvothermal treatment [Figure 13A]^[206]. Leveraging ligand chemistry, the carboxyl acids present in

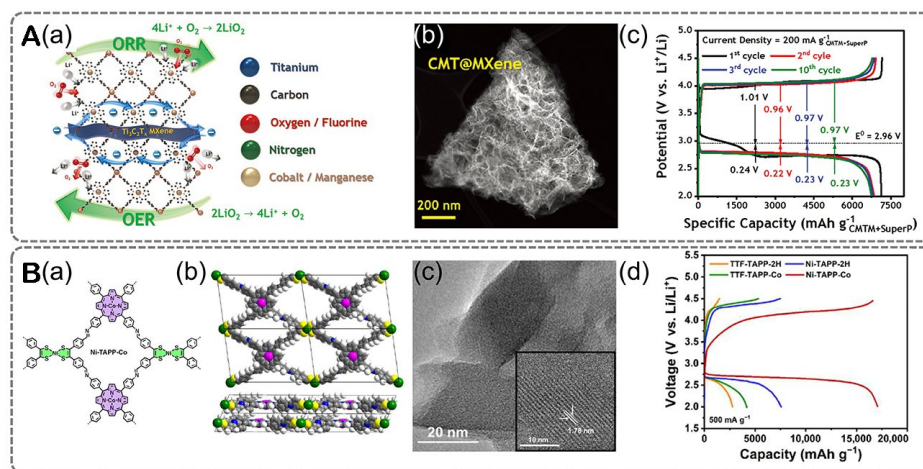


Figure 13. (A) (a) Working principle of CMT@MXene bifunctional electrocatalyst with an electron hopping mechanism; (b) SEM image of CMT@MXene; (c) Charge-discharge profiles of samples^[206]. Copyright 2023, Wiley-VCH. (B) (a) Molecular structures of Ni-TAPP-Co; (b) Top view of Ni-TAPP-Co; (c) SEM image of Ni-TAPP-Co; (d) Galvanostatic profiles for samples^[207]. Copyright 2023, the American Association for the Advancement of Science.

tetrakis(4-carboxyphenyl) porphyrin, serving as an organic linker, were grafted onto the surface terminations of $\text{Ti}_3\text{C}_2\text{T}_x$ MXenes using Fischer esterification and fluorine substitution reactions. This tailored modification notably bolstered antioxidation stability. Moreover, the solvothermal treatment prompted the generation of metalloporphyrin structures and unpaired electrons at the interface of CMT and $\text{Ti}_3\text{C}_2\text{T}_x$ MXenes. These features improved electrocatalytic performance, endurance, and electrical conductivity through an electron hopping mechanism. Consequently, CMT@MXene composites exhibited impressive stability as bifunctional electrocatalysts, maintaining a fixed specific capacity of $1,000 \text{ mAh g}^{-1}$ and a current density of 500 mA g^{-1} for 247 cycles in LOBs. Unlike MOFs, COFs are constructed by strong covalent bonds, which align well with the stability requirements of LOBs. However, in their pristine state, COFs lack exceptional catalytic performance due to the absence of metal sites. To address this, bimetallic COFs (Ni-TAPP-Co) were engineered through the assembly of Ni(bded)₂ (bded=bis[1,2-di(4-formylphenyl)ethylene-1,2-dithiolate]) and 5,10,15,20-tetrakis(4-aminophenyl)-porphyrinocobalt [Figure 13B]^[207]. This collaboration gave rise to a bimetallic Ni/Co-COF featuring a notable BET surface area, remarkable chemical stability, reasonably good electrical conductivity, and bifunctional activity as a cathode material for LOBs. The battery incorporating the Ni-TAPP-Co cathode exhibited a minimal discharge/charge potential gap and displayed consistent cycling performance over 200 cycles. The superior performance primarily stems from the morphology modulation of Li_2O_2 nanosheets facilitated by the Ni/Co sites during both discharge and charge processes.

As a semiconductor, the progress of $\text{g-C}_3\text{N}_4$ is constrained by its limited electronic conductivity and inadequate intrinsic activity for catalytic processes. In response to these challenges, strategies have been implemented to address these issues. To fix the problems mentioned, a conductive substrate, such as graphene, was first introduced to increase the number of electrons accumulated on the $\text{g-C}_3\text{N}_4$ surface, thereby enhancing the density of active sites^[272,273]. However, the problem of low activity to $\text{g-C}_3\text{N}_4$ remained. To this end, efforts have been directed towards enhancing the catalytic activity of $\text{g-C}_3\text{N}_4$, encompassing approaches such as doping engineering, the integration of SAs, and the fabrication of composite materials in conjunction with other active substances. Upon investigating the ORR mechanism on the surfaces of $\text{g-C}_3\text{N}_4$ and its derivatives doped with S, O, and P, it was observed that S-doped $\text{g-C}_3\text{N}_4$ exhibited the highest intrinsic catalytic activity. DFT calculations revealed an overpotential of 0.41 V for S-doped $\text{g-C}_3\text{N}_4$ during

the discharge process and 0.84 V for S-doped g-C₃N₄/Li, indicating the promising potential of S-doped g-C₃N₄ in LOBs^[274]. Theoretical calculations have also been applied to predict high performance g-C₃N₄ loaded by ultra-dispersed metal atoms, which can be considered SACs. Through combined electronic analysis and thermodynamic calculations, the electrocatalytic mechanism of TM/g-C₃N₄ SACs in LOBs has been clarified. The strong interactions between TMs and the g-C₃N₄ substrate anchor the metal atom durably at the unsaturated pyridine N site, thus contributing to the extended cycling stability of the oxygen electrode^[14]. Among the fifteen investigated candidates, Ru/g-C₃N₄ SACs exhibited the lowest discharge and charge overpotentials. This behavior was attributed to the synergistic interplay between the mobile d electrons of Ru and electron-rich N coordinators, leading to significant interfacial charges, metallic electrical conductivity, and substantial spin magnetic moments within the RuN₂ active center. Experimental evidence also supports the advantage of single-atom supported g-C₃N₄ in LOBs. A single-atom Pt catalyst supported on holey ultrathin g-C₃N₄ nanosheets (Pt-CNHS) was synthesized via a facile liquid-phase reaction^[208]. This catalyst exhibited high Pt dispersibility, promoting utilization efficiency and enhancing electrochemical activity. As a cathode catalyst, Pt-CNHS demonstrated remarkable electrocatalytic activity in LOBs, attributed to its large surface area, enhanced electrical conductivity, and efficient interfacial mass transfer facilitated by Pt atoms and the porous structure of CNHS. The composite strategy, commonly used in catalyst construction, is not merely additive; the structure-activity relationship between two catalysts is also worth studying. Metal oxides^[209,275,276] and selenides^[277] are often good composite objects due to their high activity. For instance, a Co₃O₄-modified Ag/g-C₃N₄ nanocomposite was designed as the cathode electrode in LOBs^[209]. The g-C₃N₄ substrate prevented the aggregation of Ag and Co₃O₄ nanoparticles, with Ag NPs enhancing the surface area and electronic conductivity of g-C₃N₄. Also, this synergistic effect led to improved oxygen reduction/evolution capabilities of Co₃O₄. The Ag/g-C₃N₄/Co₃O₄ nanocomposite exhibited higher catalytic activity for the ORR/OER in Li-O₂ cells compared to individual constituents of Co₃O₄ or Ag/g-C₃N₄.

CONCLUSION AND OUTLOOK

MABs hold the promise of meeting the high energy density requirements of power batteries while offering benefits such as flexibility, portability, and enhanced safety. However, substantial challenges must be overcome if large-scale commercialization is to be achieved, including limited rate capabilities, high overpotential, insufficient cycling stability, uncontrolled side reactions, and unpredictable reaction mechanisms. This review begins by elucidating the operational mechanisms of ZABs and LOBs, which represent aqueous and nonaqueous batteries, respectively. The focus then shifts to 2D materials with significant potential as oxygen electrode catalysts in MABs. Material modification approaches and their respective functions are then summarized, and a comprehensive account of the latest advancements in 2D catalysts within MABs is provided. Confronting these challenges, the outlooks on the development of advanced MABs are as follows:

(I) Highly efficient bifunctional catalysts

The primary challenge lies in the rational design of effective, stable, and cost-efficient bifunctional catalysts that can replace unstable and expensive precious metal materials in MABs. Unlike traditional catalysts that mainly accelerate a single reaction, the cyclic nature of OER and ORR on the air electrode during charge and discharge necessitates catalysts for MABs to concurrently lower the energy barriers of both reactions. Therefore, the effective integration of active sites becomes a promising strategy. Unfortunately, despite substantial efforts, an optimal solution remains elusive. In pursuit of commercial viability, the second challenge pertains to catalyst stability, encompassing the catalyst's natural storage stability and its stability while functioning as a catalyst. In large-scale production, the ease of material storage becomes a pivotal

consideration. For instance, MXenes, exceptional 2D carriers, are promising as efficient catalysts for both ZABs and LOBs when modified. Nevertheless, their susceptibility to oxidation in air or water solutions poses a significant hindrance, limiting their widespread application. Catalyst stability during reactions is another crucial concern. The causes of instability can result from the degradation of active sites and detachment from the electrode. The former is related to the reaction mechanism, which may be due to changes in the catalyst itself or result from the adsorption of by-products that cover the active site. The latter can be attributed to weak adhesion between catalyst and support and can be improved using binders or by allowing the catalyst to grow on the carrier. In terms of practical application, economic viability is unavoidable, which is also one of the reasons why precious metal catalysts are not suitable for widespread use. Similarly, intricate preparation processes, stringent conditions, and low yields can render catalysts impractical. The path ahead for catalyst development, therefore, remains long and complex.

(II) Means to regulate 2D nanomaterials

As for the modification means of 2D materials, they are mainly divided into two kinds according to their functions. One is the design of a hierarchical structure. The designed hierarchical structure is often rich in holes of different sizes, enhancing the contact between the catalyst and the electrolyte and facilitating the acceleration of the mass transfer and electron transfer as well. Moreover, such a stable structure can prevent the agglomeration of 2D structured materials during the reaction process to a certain extent. The second is surface environment adjustment of 2D nanomaterials, including the introduction of heteroatoms, the manipulation of defect structures, the adjustment of the interface, and so on. These methods have been demonstrated to change the Fermi level of 2D materials, and the newly constructed active site can affect the adsorption energy of the material surface with the reaction intermediates, thereby reducing the reaction energy barrier. However, the current research only focuses on one side, so the prepared catalysts still have various deficiencies. We propose to combine these two methods to improve the catalyst simultaneously in terms of multistage structure and atomic structure optimization. This will be the main design direction of 2D bifunctional catalysts in the future.

(III) Definite mechanism

The current understanding of the mechanism for MABs, although improving, remains partial and incomplete. Continued endeavors are essential to monitor the intricate processes of oxygen catalysis, aiming to attain a profound comprehension of the reaction mechanisms pertinent to both MABs and LOBs. The mechanism underpinning oxygen-catalyzed reactions is dynamic and subject to alteration by various factors such as temperature, electrolyte composition, and even electrode material, all of which complicate this area of research. Fortunately, with the development of new scientific equipment, more in-depth research can be performed. For instance, advanced in-situ characterization techniques, such as in-situ XRD, XPS, Raman, FTIR, and HRTEM, offer a real-time understanding of the evolution of crucial reaction intermediates. These techniques aid in unraveling essential information concerning reaction pathways, surface/interface behaviors, and performance degradation. We call on the premise of excellent battery system performance through the observation of intermediate products to deduce the experimental mechanism. Subsequently, a comprehensive analysis of a wealth of data is undertaken to thoroughly grasp the factors influencing the mechanism. This information is then looped back into the experimental design, encompassing catalyst development, to further enhance our understanding and guide future research directions.

(IV) Standard measurement

The battery performance is affected by various factors, including reaction temperatures, electrolytes, the area of electrodes, the mass loading of catalysts, or the concentration of O₂. Hence, the establishment of criteria for assessing battery performance becomes imperative to identify the main factors. Only in this way can the comparison of catalysts be meaningful. Lastly, while conducting tests at low current levels is advantageous for comprehending reaction mechanisms, it is equally crucial to explore testing under high current conditions to cater to commercialization requirements.

In conclusion, the journey to develop advanced MABs is still far-reaching. We believe that this review provides some insights into high-efficiency and stable catalysts that can promote the rapid advancement of MABs.

DECLARATIONS

Authors' contributions

Proposed the topic of this review: Kim JK, Park HS

Prepared the manuscript: Pei C, Zhang D, Kim J

Collectively discussed and revised the manuscript: Pei C, Zhang D, Yu X, Sim U, Park HS, Kim JK

Availability of data and materials

Not applicable.

Financial support and sponsorship

This research was supported by the "Regional Innovation Strategy (RIS)" through the National Research Foundation of Korea (NRF) funded by the Ministry of Education (MOE)(2021RIS-002) and the Korea Institute of Energy Technology Evaluation and Planning (KETEP) grant funded by the Korea government (MOTIE) (20214000000500, training program of CCUS for the green growth).

Conflicts of interest

All authors declared that there are no conflicts of interest.

Ethical approval and consent to participate

Not applicable.

Consent for publication

Not applicable.

Copyright

© The Author(s) 2024.

REFERENCES

1. Li Y, Lu J. Metal-air batteries: will they be the future electrochemical energy storage device of choice? *ACS Energy Lett* 2017;2:1370-7. DOI
2. Chen Y, Xu J, He P, et al. Metal-air batteries: progress and perspective. *Sci Bull* 2022;67:2449-86. DOI
3. Chang Z, Xu J, Zhang X. Recent progress in electrocatalyst for Li-O₂ batteries. *Adv Energy Mater* 2017;7:1700875. DOI
4. Cheng F, Chen J. Metal-air batteries: from oxygen reduction electrochemistry to cathode catalysts. *Chem Soc Rev* 2012;41:2172-92. DOI PubMed
5. Zheng X, Yuan M, Zhao Y, et al. Status and prospects of MXene-based lithium-oxygen batteries: theoretical prediction and experimental modulation. *Adv Energy Mater* 2023;13:2204019. DOI
6. Zhu X, Hu C, Amal R, Dai L, Lu X. Heteroatom-doped carbon catalysts for zinc-air batteries: progress, mechanism, and opportunities. *Energy Environ Sci* 2020;13:4536-63. DOI
7. Jana M, Xu R, Cheng X, et al. Rational design of two-dimensional nanomaterials for lithium-sulfur batteries. *Energy Environ Sci*

- 2020;13:1049-75. DOI
8. Jiang Y, Deng YP, Liang R, et al. Linker-compensated metal-organic framework with electron delocalized metal sites for bifunctional oxygen electrocatalysis. *J Am Chem Soc* 2022;144:4783-91. DOI
 9. Ji B, Gou J, Zheng Y, et al. Coordination chemistry of large-sized yttrium single-atom catalysts for oxygen reduction reaction. *Adv Mater* 2023;35:e2300381. DOI
 10. Sun Y, Liu X, Jiang Y, et al. Recent advances and challenges in divalent and multivalent metal electrodes for metal-air batteries. *J Mater Chem A* 2019;7:18183-208. DOI
 11. Abraham KM, Jiang Z. A polymer electrolyte-based rechargeable lithium/oxygen battery. *J Electrochem Soc* 1996;143:1-5. DOI
 12. Lai J, Xing Y, Chen N, Li L, Wu F, Chen R. Electrolytes for rechargeable lithium-air batteries. *Angew Chem Int Ed* 2020;59:2974-97. DOI
 13. Li X, Han G, Qian Z, et al. π -conjugation induced anchoring of ferrocene on graphdiyne enable shuttle-free redox mediation in lithium-oxygen batteries. *Adv Sci* 2022;9:2103964. DOI PubMed PMC
 14. Cheng Y, Dou Y, Kan D, Wang Y, Wei Y. Electrocatalysis in Li-O₂ battery over single-atom catalyst based on g-C₃N₄ substrate. *Appl Surf Sci* 2023;610:155481. DOI
 15. Pei C, Choi MS, Yu X, Xue H, Xia BY, Park HS. Recent progress in emerging metal and covalent organic frameworks for electrochemical and functional capacitors. *J Mater Chem A* 2021;9:8832-69. DOI
 16. Su D, Dou S, Wang G. Single crystalline Co₃O₄ nanocrystals exposed with different crystal planes for Li-O₂ batteries. *Sci Rep* 2014;4:5767. DOI PubMed PMC
 17. Thomas JM, Raja R, Lewis DW. Single-site heterogeneous catalysts. *Angew Chem Int Ed* 2005;44:6456-82. DOI PubMed
 18. Qiao B, Wang A, Yang X, et al. Single-atom catalysis of CO oxidation using Pt₁/FeO_x. *Nat Chem* 2011;3:634-41. DOI
 19. Novoselov KS, Geim AK, Morozov SV, et al. Electric field effect in atomically thin carbon films. *Science* 2004;306:666-9. DOI
 20. Jin H, Guo C, Liu X, et al. Emerging two-dimensional nanomaterials for electrocatalysis. *Chem Rev* 2018;118:6337-408. DOI
 21. Tang C, Wang HF, Chen X, et al. Topological defects in metal-free nanocarbon for oxygen electrocatalysis. *Adv Mater* 2016;28:6845-51. DOI
 22. Yu J, Dai Y, Zhang Z, et al. New nitrogen-doped graphitic carbon nanosheets with rich structural defects and hierarchical nanopores as efficient metal-free electrocatalysts for oxygen reduction reaction in Zn-air batteries. *Chem Eng Sci* 2022;259:117816. DOI
 23. Zhang L, Gu T, Lu K, Zhou L, Li D, Wang R. Engineering synergistic edge-N dipole in metal-free carbon nanoflakes toward intensified oxygen reduction electrocatalysis. *Adv Funct Mater* 2021;31:2103187. DOI
 24. Ma L, Liu W, Hu X, Lam PK, Zeng JR, Yu H. Ionothermal carbonization of biomass to construct sp²/sp³ carbon interface in N-doped biochar as efficient oxygen reduction electrocatalysts. *Chem Eng J* 2020;400:125969. DOI
 25. Lu T, Hu X, He J, et al. Aqueous/solid state Zn-air batteries based on N doped graphdiyne as efficient metal-free bifunctional catalyst. *Nano Energy* 2021;85:106024. DOI
 26. Lei W, Deng Y, Li G, et al. Two-dimensional phosphorus-doped carbon nanosheets with tunable porosity for oxygen reactions in zinc-air batteries. *ACS Catal* 2018;8:2464-72. DOI
 27. Li P, Jang H, Yuan B, Wu Z, Liu X, Cho J. Using lithium chloride as a medium to prepare N,P-codoped carbon nanosheets for oxygen reduction and evolution reactions. *Inorg Chem Front* 2019;6:417-22. DOI
 28. Wang Y, Xu N, He R, Peng L, Cai D, Qiao J. Large-scale defect-engineering tailored tri-doped graphene as a metal-free bifunctional catalyst for superior electrocatalytic oxygen reaction in rechargeable Zn-air battery. *Appl Catal B* 2021;285:119811. DOI
 29. Zheng X, Wu J, Cao X, et al. N-, P-, and S-doped graphene-like carbon catalysts derived from onium salts with enhanced oxygen chemisorption for Zn-air battery cathodes. *Appl Catal B* 2019;241:442-51. DOI
 30. Zheng D, Ci S, Cai P, Wang G, Wen Z. Nitrogen-doped carbon nanosheets encapsulating cobalt nanoparticle hybrids as high-performance bifunctional electrocatalysts. *ChemElectroChem* 2019;6:2683-8. DOI
 31. Liu P, Hu Y, Liu X, et al. Cu and Co nanoparticle-Co-decorated N-doped graphene nanosheets: a high efficiency bifunctional electrocatalyst for rechargeable Zn-air batteries. *J Mater Chem A* 2019;7:12851-8. DOI
 32. Yang ZK, Lin L, Xu AW. 2D nanoporous Fe-N/C nanosheets as highly efficient non-platinum electrocatalysts for oxygen reduction reaction in Zn-air battery. *Small* 2016;12:5710-9. DOI PubMed
 33. Shao C, Zhuang S, Zhang H, et al. Enhancement of mass transport for oxygen reduction reaction using petal-like porous Fe-NC nanosheet. *Small* 2021;17:e2006178. DOI
 34. Cui T, Wang YP, Ye T, et al. Engineering dual single-atom sites on 2D ultrathin N-doped carbon nanosheets attaining ultra-low-temperature zinc-air battery. *Angew Chem Int Ed* 2022;61:e202115219. DOI
 35. Zhang T, Wang F, Yang C, et al. Boosting ORR performance by single atomic divacancy Zn-N₃C-C₈ sites on ultrathin N-doped carbon nanosheets. *Chem Catal* 2022;2:836-52. DOI
 36. Chen Z, Peng X, Chen Z, et al. Mass production of sulfur-tuned single-atom catalysts for Zn-Air batteries. *Adv Mater* 2023;35:2209948. DOI
 37. Li Y, Ding Y, Zhang B, et al. N,O symmetric double coordination of an unsaturated Fe single-atom confined within a graphene framework for extraordinarily boosting oxygen reduction in Zn-air batteries. *Energy Environ Sci* 2023;16:2629-36. DOI
 38. Shang N, Wang C, Zhang X, et al. Atomically dispersed iron on nitrogen-decorated carbon for high-performance oxygen reduction and zinc-air batteries. *Chem Eng J* 2021;426:127345. DOI
 39. Li P, Wang H, Tan X, et al. Bifunctional electrocatalyst with CoN₃ active sites dispersed on N-doped graphitic carbon nanosheets for

- ultrastable Zn-air batteries. *Appl Catal B* 2022;316:121674. DOI
40. Zhou Y, Tao X, Chen G, et al. Multilayer stabilization for fabricating high-loading single-atom catalysts. *Nat Commun* 2020;11:5892. DOI PubMed PMC
 41. Jin Q, Wang C, Guo Y, et al. Axial oxygen ligands regulating electronic and geometric structure of Zn-N-C sites to boost oxygen reduction reaction. *Adv Sci* 2023;10:e2302152. DOI PubMed PMC
 42. Zhou S, Huang S, Wang X, et al. Activating the PdN₄ single-atom sites for 4 electron oxygen reduction reaction via axial oxygen ligand modification. *Chem Eng J* 2023;472:145129. DOI
 43. Li YJ, Cui L, Da PF, et al. Multiscale structural engineering of Ni-doped CoO nanosheets for zinc-air batteries with high power density. *Adv Mater* 2018;30:e1804653. DOI
 44. Li Y, Talib SH, Liu D, et al. Improved oxygen evolution reaction performance in Co_{0.4}Mn_{0.6}O₂ nanosheets through triple-doping (Cu, P, N) strategy and its application to Zn-air battery. *Appl Catal B* 2023;320:122023. DOI
 45. Tian Y, Liu X, Xu L, et al. Engineering crystallinity and oxygen vacancies of Co(II) oxide nanosheets for high performance and robust rechargeable Zn-air batteries. *Adv Funct Mater* 2021;31:2101239. DOI
 46. Liu P, Ran J, Xia B, Xi S, Gao D, Wang J. Bifunctional oxygen electrocatalyst of mesoporous Ni/NiO nanosheets for flexible rechargeable Zn-air batteries. *Nanomicro Lett* 2020;12:68. DOI PubMed PMC
 47. Li Y, Cheng G, Zhou Z, et al. Shape-controlled synthesis of NiCo₂O₄-rGO as bifunctional electrocatalyst for Zn-air battery. *ChemElectroChem* 2019;6:4429-36. DOI
 48. Liu W, Bao J, Xu L, et al. NiCo₂O₄ ultrathin nanosheets with oxygen vacancies as bifunctional electrocatalysts for Zn-air battery. *Appl Surf Sci* 2019;478:552-9. DOI
 49. Yin J, Jin J, Liu H, et al. NiCo₂O₄-based nanosheets with uniform 4 nm mesopores for excellent Zn-air battery performance. *Adv Mater* 2020;32:e2001651. DOI
 50. Mondal S, Majee R, Arif Islam Q, Bhattacharyya S. 2D heterojunction between double perovskite oxide nanosheet and layered double hydroxide to promote rechargeable zinc-air battery performance. *ChemElectroChem* 2020;7:5005-12. DOI
 51. Han X, Li N, Baik JS, et al. Sulfur mismatch substitution in layered double hydroxides as efficient oxygen electrocatalysts for flexible zinc-air batteries. *Adv Funct Mater* 2023;33:2212233. DOI
 52. Cheng Y, Liao F, Shen W, et al. Carbon cloth supported cobalt phosphide as multifunctional catalysts for efficient overall water splitting and zinc-air batteries. *Nanoscale* 2017;9:18977-82. DOI
 53. Lan M, Xie C, Li B, et al. Two-dimensional cobalt sulfide/iron-nitrogen-carbon holey sheets with improved durability for oxygen electrocatalysis. *ACS Appl Mater Interfaces* 2022;14:11538-46. DOI
 54. Guo H, Gao X, Yu N, et al. Metallic state two-dimensional holey-structured Co₃FeN nanosheets as stable and bifunctional electrocatalysts for zinc-air batteries. *J Mater Chem A* 2019;7:26549-56. DOI
 55. Han X, Li N, Xiong P, et al. Rhenium induced electronic structure modulation of Ni₃S₂/N-doped graphene for efficient trifunctional electrocatalysis. *Compos Part B Eng* 2022;234:109670. DOI
 56. Hao Y, Huang A, Han S, et al. Plasma-treated ultrathin ternary FePSe₃ nanosheets as a bifunctional electrocatalyst for efficient zinc-air batteries. *ACS Appl Mater Interfaces* 2020;12:29393-403. DOI
 57. Yi M, Li N, Lu B, Li L, Zhu Z, Zhang J. Single-atom Pt decorated in heteroatom (N, B, and F)-doped ReS₂ grown on Mo₂CT_x for efficient pH-universal hydrogen evolution reaction and flexible Zn-air batteries. *Energy Stor Mater* 2021;42:418-29. DOI
 58. Jiang Y, Deng YP, Liang R, et al. d-Orbital steered active sites through ligand editing on heterometal imidazole frameworks for rechargeable zinc-air battery. *Nat Commun* 2020;11:5858. DOI PubMed PMC
 59. Cao Q, Wan L, Xu Z, et al. A fluorinated covalent organic framework with accelerated oxygen transfer nanochannels for high-performance zinc-air batteries. *Adv Mater* 2023;35:e2210550. DOI
 60. Niu WJ, He JZ, Wang YP, et al. A hybrid transition metal nanocrystal-embedded graphitic carbon nitride nanosheet system as a superior oxygen electrocatalyst for rechargeable Zn-air batteries. *Nanoscale* 2020;12:19644-54. DOI
 61. Zhang S, Shang N, Gao S, et al. Ultra dispersed Co supported on nitrogen-doped carbon: an efficient electrocatalyst for oxygen reduction reaction and Zn-air battery. *Chem Eng Sci* 2021;234:116442. DOI
 62. Wang X, Raghupathy RKM, Querebillo CJ, et al. Interfacial covalent bonds regulated electron-deficient 2D black phosphorus for electrocatalytic oxygen reactions. *Adv Mater* 2021;33:e2008752. DOI
 63. Chen L, Xu X, Yang W, Jia J. Recent advances in carbon-based electrocatalysts for oxygen reduction reaction. *Chin Chem Lett* 2020;31:626-34. DOI
 64. Katsounaros I, Cherevko S, Zeradjanin AR, Mayrhofer KJ. Oxygen electrochemistry as a cornerstone for sustainable energy conversion. *Angew Chem Int Ed* 2014;53:102-21. DOI PubMed
 65. Li FM, Huang L, Zaman S, et al. Corrosion chemistry of electrocatalysts. *Adv Mater* 2022;34:e2200840. DOI
 66. Xiong P, Tan J, Lee H, et al. Two-dimensional carbon-based heterostructures as bifunctional electrocatalysts for water splitting and metal-air batteries. *Nano Mater Sci* 2022. DOI
 67. Sato Y, Yamada N, Kitano S, Kowalski D, Aoki Y, Habazaki H. High-corrosion-resistance mechanism of graphitized platelet-type carbon nanofibers in the OER in a concentrated alkaline electrolyte. *J Mater Chem A* 2022;10:8208-17. DOI
 68. Tang W, Mai J, Liu L, et al. Recent advances of bifunctional catalysts for zinc air batteries with stability considerations: from selecting materials to reconstruction. *Nanoscale Adv* 2023;5:4368-401. DOI PubMed PMC
 69. Zhu J, Mu S. Defect engineering in carbon-based electrocatalysts: insight into intrinsic carbon defects. *Adv Funct Mater*

- 2020;30:2001097. DOI
70. Yan D, Li Y, Huo J, Chen R, Dai L, Wang S. Defect chemistry of nonprecious-metal electrocatalysts for oxygen reactions. *Adv Mater* 2017;29:1606459. DOI PubMed
 71. Jiang Y, Yang L, Sun T, et al. Significant contribution of intrinsic carbon defects to oxygen reduction activity. *ACS Catal* 2015;5:6707-12. DOI
 72. Zeng Z, Yi L, He J, et al. Hierarchically porous carbon with pentagon defects as highly efficient catalyst for oxygen reduction and oxygen evolution reactions. *J Mater Sci* 2020;55:4780-91. DOI
 73. Chen D, Zhu J, Mu X, et al. Nitrogen-Doped carbon coupled FeNi₃ intermetallic compound as advanced bifunctional electrocatalyst for OER, ORR and zn-air batteries. *Appl Catal B* 2020;268:118729. DOI
 74. Zhang LH, Shi Y, Wang Y, Shiju NR. Nanocarbon catalysts: recent understanding regarding the active sites. *Adv Sci* 2020;7:1902126. DOI
 75. Tao L, Wang Q, Dou S, et al. Edge-rich and dopant-free graphene as a highly efficient metal-free electrocatalyst for the oxygen reduction reaction. *Chem Commun* 2016;52:2764-7. DOI
 76. Yang H, Han X, Douka AI, et al. Advanced oxygen electrocatalysis in energy conversion and storage. *Adv Funct Mater* 2021;31:2007602. DOI
 77. Gong K, Du F, Xia Z, Durstock M, Dai L. Nitrogen-doped carbon nanotube arrays with high electrocatalytic activity for oxygen reduction. *Science* 2009;323:760-4. DOI PubMed
 78. Zhang J, Zhao Z, Xia Z, Dai L. A metal-free bifunctional electrocatalyst for oxygen reduction and oxygen evolution reactions. *Nat Nanotechnol* 2015;10:444-52. DOI
 79. Wohlgemuth S, White RJ, Willinger M, Titirici M, Antonietti M. A one-pot hydrothermal synthesis of sulfur and nitrogen doped carbon aerogels with enhanced electrocatalytic activity in the oxygen reduction reaction. *Green Chem* 2012;14:1515-23. DOI
 80. Jiao Y, Zheng Y, Jaroniec M, Qiao SZ. Origin of the electrocatalytic oxygen reduction activity of graphene-based catalysts: a roadmap to achieve the best performance. *J Am Chem Soc* 2014;136:4394-403. DOI PubMed PMC
 81. Zhang S, Cai Y, He H, et al. Heteroatom doped graphdiyne as efficient metal-free electrocatalyst for oxygen reduction reaction in alkaline medium. *J Mater Chem A* 2016;4:4738-44. DOI
 82. Feng Z, Ma Y, Li Y, Li R, Tang Y, Dai X. Charge-compensated co-doping of graphdiyne with boron and nitrogen to form metal-free electrocatalysts for the oxygen reduction reaction. *Phys Chem Chem Phys* 2020;22:1493-501. DOI
 83. Li R, Wei Z, Gou X. Nitrogen and phosphorus dual-doped graphene/carbon nanosheets as bifunctional electrocatalysts for oxygen reduction and evolution. *ACS Catal* 2015;5:4133-42. DOI
 84. Hu C, Liang Q, Yang Y, et al. Conductivity-enhanced porous N/P co-doped metal-free carbon significantly enhances oxygen reduction kinetics for aqueous/flexible zinc-air batteries. *J Colloid Interface Sci* 2023;633:500-10. DOI
 85. Li M, Wang K, Lv Q. N,P-co-Doped Graphdiyne as efficient metal-free catalysts for oxygen reduction reaction. *Chem Res Chin Univ* 2021;37:1283-8. DOI
 86. Choi CH, Park SH, Woo SI. Binary and ternary doping of nitrogen, boron, and phosphorus into carbon for enhancing electrochemical oxygen reduction activity. *ACS Nano* 2012;6:7084-91. DOI PubMed
 87. Huang B, Liu Y, Huang X, Xie Z. Multiple heteroatom-doped few-layer carbons for the electrochemical oxygen reduction reaction. *J Mater Chem A* 2018;6:22277-86. DOI
 88. Wang J, Hu H, Zhang H, et al. Regulating the catalytically active sites in low-cost and earth-abundant 3D transition-metal-based electrode materials for high-performance zinc-air batteries. *Energy Fuels* 2021;35:6483-503. DOI
 89. Wei L, Ang EH, Yang Y, et al. Recent advances of transition metal based bifunctional electrocatalysts for rechargeable zinc-air batteries. *J Power Sources* 2020;477:228696. DOI
 90. Yang D, Chen D, Jiang Y, et al. Carbon-based materials for all-solid-state zinc-air batteries. *Carbon Energy* 2021;3:50-65. DOI
 91. Fu G, Yan X, Chen Y, et al. Boosting bifunctional oxygen electrocatalysis with 3D graphene aerogel-supported Ni/MnO particles. *Adv Mater* 2018;30:1704609. DOI
 92. Fu G, Wang J, Chen Y, et al. Exploring indium-based ternary thiospinel as conceivable high-potential air-cathode for rechargeable Zn-air batteries. *Adv Energy Mater* 2018;8:1802263. DOI
 93. Liu Y, Chen Z, Li Z, et al. CoNi nanoalloy-Co-N₄ composite active sites embedded in hierarchical porous carbon as bi-functional catalysts for flexible Zn-air battery. *Nano Energy* 2022;99:107325. DOI
 94. Du L, Luo L, Feng Z, et al. Nitrogen-doped graphitized carbon shell encapsulated NiFe nanoparticles: a highly durable oxygen evolution catalyst. *Nano Energy* 2017;39:245-52. DOI
 95. Fu Y, Yu H, Jiang C, et al. NiCo alloy nanoparticles decorated on N-doped carbon nanofibers as highly active and durable oxygen electrocatalyst. *Adv Funct Mater* 2018;28:1705094. DOI
 96. Xu X, Xie J, Liu B, et al. PBA-derived FeCo alloy with core-shell structure embedded in 2D N-doped ultrathin carbon sheets as a bifunctional catalyst for rechargeable Zn-air batteries. *Appl Catal B* 2022;316:121687. DOI
 97. Yang XF, Wang A, Qiao B, Li J, Liu J, Zhang T. Single-atom catalysts: a new frontier in heterogeneous catalysis. *Acc Chem Res* 2013;46:1740-8. DOI
 98. Chen Y, Ji S, Chen C, Peng Q, Wang D, Li Y. Single-atom catalysts: synthetic strategies and electrochemical applications. *Joule* 2018;2:1242-64. DOI
 99. Han J, Bao H, Wang J, et al. 3D N-doped ordered mesoporous carbon supported single-atom Fe-N-C catalysts with superior

- performance for oxygen reduction reaction and zinc-air battery. *Appl Catal B* 2021;280:119411. DOI
100. Nørskov JK, Rossmeisl J, Logadottir A, et al. Origin of the overpotential for oxygen reduction at a fuel-cell cathode. *J Phys Chem B* 2004;108:17886-92. DOI
 101. Peng H, Liu F, Liu X, et al. Effect of transition metals on the structure and performance of the doped carbon catalysts derived from polyaniline and melamine for ORR application. *ACS Catal* 2014;4:3797-805. DOI
 102. Zheng Y, Yang D, Kweun JM, et al. Rational design of common transition metal-nitrogen-carbon catalysts for oxygen reduction reaction in fuel cells. *Nano Energy* 2016;30:443-9. DOI
 103. Zhao C, Li B, Liu J, Zhang Q. Intrinsische elektrokatalytische aktivitätssteuerung von M-N-C-einzelatom-katalysatoren für die sauerstoffreduktionsreaktion. *Angew Chemie Int Ed* 2021;133:4496-512. DOI
 104. Shang H, Zhou X, Dong J, et al. Engineering unsymmetrically coordinated Cu-S₃N₃ single atom sites with enhanced oxygen reduction activity. *Nat Commun* 2020;11:3049. DOI PubMed PMC
 105. Yu L, Li Y, Ruan Y. Dynamic control of sacrificial bond transformation in the Fe-N-C single-atom catalyst for molecular oxygen reduction. *Angew Chem Int Ed* 2021;60:25296-301. DOI
 106. Li L, Chen Y, Xing H, et al. Single-atom Fe-N₃ catalyst for high-performance zinc-air batteries. *Nano Res* 2022;15:8056-64. DOI
 107. Hu L, Dai C, Chen L, et al. Metal-triazolate-framework-derived FeN₄Cl₁ single-atom catalysts with hierarchical porosity for the oxygen reduction reaction. *Angew Chemie Int Ed* 2021;133:27530-5. DOI
 108. Peng L, Yang J, Yang Y, et al. Mesopore-rich Fe-N-C catalyst with FeN₄-O-NC single-atom sites delivers remarkable oxygen reduction reaction performance in alkaline media. *Adv Mater* 2022;34:e2202544. DOI
 109. Li X, Liu J, Cai Q, Kan Z, Liu S, Zhao J. Engineering d-band center of iron single atom site through boron incorporation to trigger the efficient bifunctional oxygen electrocatalysis. *J Colloid Interface Sci* 2022;628:331-42. DOI
 110. Wang X, An Y, Liu L, et al. Atomically dispersed pentacoordinated-zirconium catalyst with axial oxygen ligand for oxygen reduction reaction. *Angew Chem Int Ed* 2022;61:e202209746. DOI PubMed PMC
 111. Seh ZW, Kibsgaard J, Dickens CF, Chorkendorff I, Nørskov JK, Jaramillo TF. Combining theory and experiment in electrocatalysis: insights into materials design. *Science* 2017;355:eaad4998. DOI PubMed
 112. Li H, Zhang Y, Hu X, Liu W, Chen J, Yu H. Metal-organic framework templated Pd@PdO-Co₃O₄ nanocubes as an efficient bifunctional oxygen electrocatalyst. *Adv Energy Mater* 2018;8:1702734. DOI
 113. Dai Y, Yu J, Wang J, et al. Bridging the charge accumulation and high reaction order for high-rate oxygen evolution and long stable Zn-air batteries. *Adv Funct Mater* 2022;32:2111989. DOI
 114. Lee DU, Xu P, Cano ZP, Kashkooli AG, Park MG, Chen Z. Recent progress and perspectives on bi-functional oxygen electrocatalysts for advanced rechargeable metal-air batteries. *J Mater Chem A* 2016;4:7107-34. DOI
 115. Lu Z, Wang H, Kong D, et al. Electrochemical tuning of layered lithium transition metal oxides for improvement of oxygen evolution reaction. *Nat Commun* 2014;5:4345. DOI
 116. He Y, Zhang J, He G, et al. Ultrathin Co₃O₄ nanofilm as an efficient bifunctional catalyst for oxygen evolution and reduction reaction in rechargeable zinc-air batteries. *Nanoscale* 2017;9:8623-30. DOI
 117. Yan K, Qin J, Lin J, et al. Probing the active sites of Co₃O₄ for the acidic oxygen evolution reaction by modulating the Co²⁺/Co³⁺ ratio. *J Mater Chem A* 2018;6:5678-86. DOI
 118. Zhang X, Liu R, Zang Y, et al. Co/CoO nanoparticles immobilized on Co-N-doped carbon as trifunctional electrocatalysts for oxygen reduction, oxygen evolution and hydrogen evolution reactions. *Chem Commun* 2016;52:5946-9. DOI
 119. Li Y, Zhong C, Liu J, et al. Atomically thin mesoporous Co₃O₄ layers strongly coupled with N-rGO nanosheets as high-performance bifunctional catalysts for 1D knittable zinc-air batteries. *Adv Mater* 2018;30:1703657. DOI
 120. Zheng Z, Huang L, Zhou Y, Hu X, Ni X. Large-scale synthesis of mesoporous CoO-doped NiO hexagonal nanoplatelets with improved electrochemical performance. *Solid State Sci* 2009;11:1439-43. DOI
 121. Tan P, Chen B, Xu H, Cai W, He W, Ni M. Growth of Al and Co co-doped NiO nanosheets on carbon cloth as the air electrode for Zn-air batteries with high cycling stability. *Electrochim Acta* 2018;290:21-9. DOI
 122. Qian J, Guo X, Wang T, Liu P, Zhang H, Gao D. Bifunctional porous Co-doped NiO nanoflowers electrocatalysts for rechargeable zinc-air batteries. *Appl Catal B* 2019;250:71-7. DOI
 123. Tian Y, Xu L, Qiu J, Liu X, Zhang S. Rational design of sustainable transition metal-based bifunctional electrocatalysts for oxygen reduction and evolution reactions. *Sustain Mater Technol* 2020;25:e00204. DOI
 124. Ao K, Shi J, Zhang X, Daoud WA. Tuning oxygen vacancies in spinel nanosheets for binder-free oxygen cathodes with superior catalytic activity in zinc-air batteries. *J Power Sources* 2022;521:230918. DOI
 125. Jin W, Chen J, Liu B, et al. Oxygen vacancy-rich in-doped CoO/CoP heterostructure as an effective air cathode for rechargeable Zn-air batteries. *Small* 2019;15:e1904210. DOI
 126. Zhu K, Shi F, Zhu X, Yang W. The roles of oxygen vacancies in electrocatalytic oxygen evolution reaction. *Nano Energy* 2020;73:104761. DOI
 127. Ji Q, Bi L, Zhang J, Cao H, Zhao XS. The role of oxygen vacancies of ABO₃ perovskite oxides in the oxygen reduction reaction. *Energy Environ Sci* 2020;13:1408-28. DOI
 128. Wang N, Ning S, Yu X, et al. Graphene composites with Ru-RuO₂ heterostructures: highly efficient Mott-Schottky-type electrocatalysts for pH-universal water splitting and flexible zinc-air batteries. *Appl Catal B* 2022;302:120838. DOI
 129. Dong Q, Ji S, Wang H, Linkov V, Wang R. Oxygen spillover effect at Cu/Fe₂O₃ heterointerfaces to enhance oxygen electrocatalytic

- reactions for rechargeable Zn-air batteries. *ACS Appl Mater Interfaces* 2022;14:51222-33. DOI
130. Guo X, Liu S, Wan X, et al. Controllable solid-phase fabrication of an Fe₂O₃/Fe₃C₂/Fe-N-C electrocatalyst toward optimizing the oxygen reduction reaction in zinc-air batteries. *Nano Lett* 2022;22:4879-87. DOI
 131. Park J, Risch M, Nam G, et al. Single crystalline pyrochlore nanoparticles with metallic conduction as efficient bi-functional oxygen electrocatalysts for Zn-air batteries. *Energy Environ Sci* 2017;10:129-36. DOI
 132. Yan Y, Xia BY, Zhao B, Wang X. A review on noble-metal-free bifunctional heterogeneous catalysts for overall electrochemical water splitting. *J Mater Chem A* 2016;4:17587-603. DOI
 133. Li C, Han X, Cheng F, Hu Y, Chen C, Chen J. Phase and composition controllable synthesis of cobalt manganese spinel nanoparticles towards efficient oxygen electrocatalysis. *Nat Commun* 2015;6:7345. DOI PubMed PMC
 134. Ni B, Ouyang C, Xu X, Zhuang J, Wang X. Modifying commercial carbon with trace amounts of ZIF to prepare derivatives with superior ORR activities. *Adv Mater* 2017;29:1701354. DOI PubMed
 135. Xu W, Lu Z, Sun X, Jiang L, Duan X. Superwetting electrodes for gas-involving electrocatalysis. *Acc Chem Res* 2018;51:1590-8. DOI PubMed
 136. Wang H, Zhou M, Choudhury P, Luo H. Perovskite oxides as bifunctional oxygen electrocatalysts for oxygen evolution/reduction reactions - a mini review. *Appl Mater Today* 2019;16:56-71. DOI
 137. Liu K, Li J, Wang Q, et al. Designed synthesis of LaCoO₃/N-doped reduced graphene oxide nanohybrid as an efficient bifunctional electrocatalyst for ORR and OER in alkaline medium. *J Alloys Compd* 2017;725:260-9. DOI
 138. Ran J, Wang T, Zhang J, et al. Modulation of electronics of oxide perovskites by sulfur doping for electrocatalysis in rechargeable Zn-air batteries. *Chem Mater* 2020;32:3439-46. DOI
 139. Hui X, Zhang P, Li J, et al. In situ integrating highly ionic conductive LDH-array@PVA gel electrolyte and MXene/Zn anode for dendrite-free high-performance flexible Zn-air batteries. *Adv Energy Mater* 2022;12:2201393. DOI
 140. Zhou D, Xiong X, Cai Z, et al. Flame-engraved nickel-iron layered double hydroxide nanosheets for boosting oxygen evolution reactivity. *Small Methods* 2018;2:1800083. DOI
 141. Yan D, Wang W, Luo X, Chen C, Zeng Y, Zhu Z. NiCo₂O₄ with oxygen vacancies as better performance electrode material for supercapacitor. *Chem Eng J* 2018;334:864-72. DOI
 142. Ambriz-peláez O, Béjar J, Ramos-castillo C, Guerra-balcázar M, Álvarez-contreras L, Arjona N. Defected NiFe layered double hydroxides on N-doped carbon nanotubes as efficient bifunctional electrocatalyst for rechargeable zinc-air batteries. *Appl Surface Sci* 2022;601:154253. DOI
 143. Wang T, Nam G, Jin Y, et al. NiFe (Oxy) hydroxides derived from NiFe disulfides as an efficient oxygen evolution catalyst for rechargeable Zn-air batteries: the effect of surface S residues. *Adv Mater* 2018;30:e1800757. DOI
 144. Jia Z, Shang J, Xue K, et al. N-doped nanocarbon inserted NiCo-LDH nanoplates on NF with high OER/ORR performances for zinc-air battery. *ChemCatChem* 2023;15:e202201469. DOI
 145. Kumar DB, Nie W, Jiang Z, Lee J, Maiyalagan T. Recent progress in transition metal carbides and nitrides based composites as bifunctional oxygen electrocatalyst for zinc air batteries. *J Alloys Compd* 2023;960:170828. DOI
 146. Yu X, Zhou T, Ge J, Wu C. Recent advances on the modulation of electrocatalysts based on transition metal nitrides for the rechargeable Zn-air battery. *ACS Mater Lett* 2020;2:1423-34. DOI
 147. Liang Y, Gong Q, Sun X, Xu N, Gong P, Qiao J. Rational fabrication of thin-layered NiCo₂S₄ loaded graphene as bifunctional non-oxide catalyst for rechargeable zinc-air batteries. *Electrochim Acta* 2020;342:136108. DOI
 148. Xu R, Xu Z, Zhang X, Ling Y, Li M, Yang Z. Cobalt-doped tungsten sulfides as stable and efficient air electrodes for rechargeable zinc-air batteries. *ChemElectroChem* 2020;7:148-54. DOI
 149. Wu Z, Wang H, Xiong P, et al. Molecularly thin nitride sheets stabilized by titanium carbide as efficient bifunctional electrocatalysts for fiber-shaped rechargeable zinc-air batteries. *Nano Lett* 2020;20:2892-8. DOI
 150. Luo M, Koper MTM. A kinetic descriptor for the electrolyte effect on the oxygen reduction kinetics on Pt(111). *Nat Catal* 2022;5:615-23. DOI
 151. Yu J, Li Z, Liu T, et al. Morphology control and electronic tailoring of CoxAy (A = P, S, Se) electrocatalysts for water splitting. *Chem Eng J* 2023;460:141674. DOI
 152. Sun Y, Guan Y, Wu X, et al. ZIF-derived "senbei"-like Co₉S₈/CeO₂/Co heterostructural nitrogen-doped carbon nanosheets as bifunctional oxygen electrocatalysts for Zn-air batteries. *Nanoscale* 2021;13:3227-36. DOI
 153. Naguib M, Kurtoglu M, Presser V, et al. Two-dimensional nanocrystals produced by exfoliation of Ti₃AlC₂. *Adv Mater* 2011;23:4248-53. DOI
 154. Lukatskaya MR, Mashtalir O, Ren CE, et al. Cation intercalation and high volumetric capacitance of two-dimensional titanium carbide. *Science* 2013;341:1502-5. DOI
 155. Ghidiu M, Lukatskaya MR, Zhao MQ, Gogotsi Y, Barsoum MW. Conductive two-dimensional titanium carbide 'clay' with high volumetric capacitance. *Nature* 2014;516:78-81. DOI PubMed
 156. Yue L, Chen L, Wang X, et al. Ni/Co-MOF@aminated MXene hierarchical electrodes for high-stability supercapacitors. *Chem Eng J* 2023;451:138687. DOI
 157. Seh ZW, Fredrickson KD, Anasori B, et al. Two-dimensional molybdenum carbide (MXene) as an efficient electrocatalyst for hydrogen evolution. *ACS Energy Lett* 2016;1:589-94. DOI
 158. kong W, Li L, Yu X, et al. Platinum nickel alloy-MXene catalyst with inverse opal structure for enhanced hydrogen evolution in both

- acidic and alkaline solutions. *Nano Res* 2023;16:195-201. DOI
159. Chen Y, Yao H, Kong F, et al. V₂C MXene synergistically coupling FeNi LDH nanosheets for boosting oxygen evolution reaction. *Appl Catal B* 2021;297:120474. DOI
160. Zou H, He B, Kuang P, Yu J, Fan K. Metal-organic framework-derived nickel-cobalt sulfide on ultrathin mxene nanosheets for electrocatalytic oxygen evolution. *ACS Appl Mater Interfaces* 2018;10:22311-9. DOI
161. Franco A, Salatti-dorado JÁ, García-caballero V, et al. A 2D copper-imidazolate framework without thermal treatment as an efficient ORR electrocatalyst for Zn-air batteries. *J Mater Chem A* 2022;10:24590-7. DOI
162. Zhao L, Dong B, Li S, et al. Interdiffusion reaction-assisted hybridization of two-dimensional metal-organic frameworks and Ti₃C₂T_x nanosheets for electrocatalytic oxygen evolution. *ACS Nano* 2017;11:5800-7. DOI
163. Zheng X, Cao Y, Liu D, et al. Bimetallic metal-organic-framework/reduced graphene oxide composites as bifunctional electrocatalysts for rechargeable Zn-air batteries. *ACS Appl Mater Interfaces* 2019;11:15662-9. DOI
164. Liu M, Liu S, Cui CX, et al. Construction of catalytic covalent organic frameworks with redox-active sites for the oxygen reduction and the oxygen evolution reaction. *Angew Chem Int Ed* 2022;61:e202213522. DOI
165. Yang S, Li X, Tan T, et al. A fully-conjugated covalent organic framework-derived carbon supporting ultra-close single atom sites for ORR. *Appl Catal B* 2022;307:121147. DOI
166. Han X, Zhang W, Ma X, et al. Identifying the activation of bimetallic sites in NiCo₂S₄@g-C₃N₄-CNT hybrid electrocatalysts for synergistic oxygen reduction and evolution. *Adv Mater* 2019;31:e1808281. DOI
167. zheng J, Kang T, Liu B, Wang P, Li H, Yang M. N-doped carbon nanotubes encapsulated with FeNi nanoparticles derived from defect-rich, molecule-doped 3D g-C₃N₄ as an efficient bifunctional electrocatalyst for rechargeable zinc-air batteries. *J Mater Chem A* 2022;10:9911-21. DOI
168. Zhu X, Zhang J, Wang Y, et al. Achieving high-performance oxygen reduction catalyst and Zn-air battery through a synergistic nitrogen doping strategy. *Energy Technol* 2022;10:2200602. DOI
169. Wang C, Zhao H, Wang J, et al. Atomic Fe hetero-layered coordination between g-C₃N₄ and graphene nanomeshes enhances the ORR electrocatalytic performance of zinc-air batteries. *J Mater Chem A* 2019;7:1451-8. DOI
170. Jiang Q, Gan C, Wu X, Liu Z, Tang J. Facile synthesis of black phosphorus directly grown on carbon paper as an efficient OER electrocatalyst: role of interfacial charge transfer and induced local charge distribution. *Adv Powder Technol* 2022;33:103371. DOI
171. Kang J, Wells SA, Wood JD, et al. Stable aqueous dispersions of optically and electronically active phosphorene. *Proc Natl Acad Sci USA* 2016;113:11688-93. DOI PubMed PMC
172. Ling X, Wang H, Huang S, Xia F, Dresselhaus MS. The renaissance of black phosphorus. *Proc Natl Acad Sci USA* 2015;112:4523-30. DOI PubMed PMC
173. Yang S, Zhang K, Ricciardulli AG, et al. A delamination strategy for thinly layered defect-free high-mobility black phosphorus flakes. *Angew Chem Int Ed* 2018;57:4677-81. DOI
174. Jung I, Kwon HJ, Kim M, et al. Rapid oxygen diffusive lithium-oxygen batteries using a restacking-inhibited, free-standing graphene cathode film. *J Mater Chem A* 2019;7:10397-404. DOI
175. Huang H, Zhu J, Zhang W, et al. Controllable codoping of nitrogen and sulfur in graphene for highly efficient Li-Oxygen batteries and direct methanol fuel cells. *Chem Mater* 2016;28:1737-45. DOI
176. Zhang J, Luo X, Li X, et al. Two-dimensional boron and nitrogen dual-doped graphitic carbon as an efficient metal-free cathodic electrocatalyst for lithium-air batteries. *ChemElectroChem* 2021;8:949-56. DOI
177. Han J, Guo X, Ito Y, et al. Effect of chemical doping on cathodic performance of bicontinuous nanoporous graphene for Li-O₂ batteries. *Adv Energy Mater* 2016;6:1501870. DOI
178. Xiao F, Meng Y, Lin Z, et al. Highly boron-doped holey graphene for lithium oxygen batteries with enhanced electrochemical performance. *Carbon* 2022;189:404-12. DOI
179. Dai W, Liu Y, Wang M, et al. Monodispersed ruthenium nanoparticles on nitrogen-doped reduced graphene oxide for an efficient lithium-oxygen battery. *ACS Appl Mater Interfaces* 2021;13:19915-26. DOI
180. Wu F, Xing Y, Zeng X, et al. Platinum-coated hollow graphene nanocages as cathode used in lithium-oxygen batteries. *Adv Funct Mater* 2016;26:7626-33. DOI
181. Lu J, Lee YJ, Luo X, et al. A lithium-oxygen battery based on lithium superoxide. *Nature* 2016;529:377-82. DOI
182. Chen Y, Zhang Q, Zhang Z, et al. Two better than one: cobalt-copper bimetallic yolk-shell nanoparticles supported on graphene as excellent cathode catalysts for Li-O₂ batteries. *J Mater Chem A* 2015;3:17874-9. DOI
183. Xu SM, Liang X, Wu XY, et al. Multistaged discharge constructing heterostructure with enhanced solid-solution behavior for long-life lithium-oxygen batteries. *Nat Commun* 2019;10:5810. DOI PubMed PMC
184. Wang P, Ren Y, Wang R, et al. Atomically dispersed cobalt catalyst anchored on nitrogen-doped carbon nanosheets for lithium-oxygen batteries. *Nat Commun* 2020;11:1576. DOI PubMed PMC
185. Zhang W, Zheng J, Wang R, et al. Water-trapping single-atom Co-N₄/graphene triggering direct 4e⁻ LiOH chemistry for rechargeable aprotic Li-O₂ batteries. *Small* 2023;19:e2301391. DOI
186. Liu M, Li J, Chi B, et al. Integration of single Co atoms and Ru nanoclusters boosts the cathodic performance of nitrogen-doped 3D graphene in lithium-oxygen batteries. *J Mater Chem A* 2021;9:10747-57. DOI
187. Zhang Y, Zhang S, Ma J, Chen X, Nan C, Chen C. Single-atom-mediated spinel octahedral structures for elevated performances of Li-oxygen batteries. *Angew Chem Int Ed* 2023;62:e202218926. DOI

188. Sun Z, Cao X, Tian M, et al. Synergized multimetal oxides with amorphous/crystalline heterostructure as efficient electrocatalysts for lithium-oxygen batteries. *Adv Energy Mater* 2021;11:2100110. DOI
189. Kim YS, Lee G, Sung M, Kim D. Orthorhombically distorted perovskite SeZnO_3 nanosheets as an electrocatalyst for lithium-oxygen batteries. *Chem Eng J* 2021;406:126896. DOI
190. Gao R, Chen Q, Zhang W, et al. Oxygen defects-engineered LaFeO_{3-x} nanosheets as efficient electrocatalysts for lithium-oxygen battery. *J Catal* 2020;384:199-207. DOI
191. Ju B, Song HJ, Lee G, Sung M, Kim D. Nickel disulfide nanosheet as promising cathode electrocatalyst for long-life lithium-oxygen batteries. *Energy Stor Mater* 2020;24:594-601. DOI
192. Sennu P, Christy M, Aravindan V, Lee Y, Nahm KS, Lee Y. Two-dimensional mesoporous cobalt sulfide nanosheets as a superior anode for a Li-ion battery and a bifunctional electrocatalyst for the Li-O₂ system. *Chem Mater* 2015;27:5726-35. DOI
193. Wang G, Li Y, Shi L, Qian R, Wen Z. Realizing the growth of nano-network Li_2O_2 film on defect-rich holey Co_9S_8 nanosheets for Li-O₂ battery. *Chem Eng J* 2020;396:125228. DOI
194. Li D, Zhao L, Wang J, Yang C. Tailoring the d-Band Center over isomorphism pyrite catalyst for optimized intrinsic affinity to intermediates in lithium-oxygen batteries. *Adv Energy Mater* 2023;13:2204057. DOI
195. Long J, Hou Z, Shu C, et al. Free-standing three-dimensional CuCo_2S_4 nanosheet array with high catalytic activity as an efficient oxygen electrode for lithium-oxygen batteries. *ACS Appl Mater Interfaces* 2019;11:3834-42. DOI
196. Feng J, Wang H, Guo L, et al. Stacking surface derived catalytic capability and by-product prevention for high efficient two dimensional Bi_2Te_3 cathode catalyst in Li-oxygen batteries. *Appl Catal B* 2022;318:121844. DOI
197. Zhang P, Lu X, Huang Y, et al. MoS_2 nanosheets decorated with gold nanoparticles for rechargeable Li-O₂ batteries. *J Mater Chem A* 2015;3:14562-6. DOI
198. Li D, Zhao L, Xia Q, et al. Activating MoS_2 nanoflakes via sulfur defect engineering wrapped on CNTs for stable and efficient Li-O₂ batteries. *Adv Funct Mater* 2022;32:2108153. DOI
199. Cao X, Zhang Y, Lu C, et al. Synergistic dual atomic sites with localized electronic modulation enable high-performance lithium-oxygen batteries. *Chem Eng J* 2023;466:143351. DOI
200. Hu A, Shu C, Xu C, et al. Interface-engineered metallic 1T- MoS_2 nanosheet array induced via palladium doping enabling catalysis enhancement for lithium-oxygen battery. *Chem Eng J* 2020;382:122854. DOI
201. Zhang G, Liu C, Guo L, Liu R, Miao L, Dang F. Electronic “bridge” construction via Ag intercalation to diminish catalytic anisotropy for 2D tin diselenide cathode catalyst in lithium-oxygen batteries. *Adv Energy Mater* 2022;12:2200791. DOI
202. Huang HB, Luo SH, Liu CL, Yi TF, Zhai YC. High-Surface-area and porous Co_2P nanosheets as cost-effective cathode catalysts for Li-O₂ batteries. *ACS Appl Mater Interfaces* 2018;10:21281-90. DOI
203. Zheng X, Yuan M, Guo D, et al. Theoretical design and structural modulation of a surface-functionalized $\text{Ti}_3\text{C}_2\text{T}_x$ MXene-based heterojunction electrocatalyst for a Li-oxygen battery. *ACS Nano* 2022;16:4487-99. DOI
204. Yuan M, Wang R, Fu W, et al. Ultrathin two-dimensional metal-organic framework nanosheets with the inherent open active sites as electrocatalysts in aprotic Li-O₂ batteries. *ACS Appl Mater Interfaces* 2019;11:11403-13. DOI
205. Zhang W, Tang S, Chen Z, et al. The controllable construction of nanochannel in two-dimensional lamellar film for efficient oxygen reduction reaction and lithium-oxygen batteries. *Chem Eng J* 2022;430:132489. DOI
206. Nam S, Mahato M, Matthews K, et al. Bimetal organic framework- $\text{Ti}_3\text{C}_2\text{T}_x$ MXene with metalloporphyrin electrocatalyst for lithium-oxygen batteries. *Adv Funct Mater* 2023;33:2210702. DOI
207. Ke SW, Li W, Gu Y, et al. Covalent organic frameworks with Ni-Bis(dithiolene) and Co-porphyrin units as bifunctional catalysts for Li-O₂ batteries. *Sci Adv* 2023;9:eadf2398. DOI PubMed PMC
208. Zhao W, Wang J, Yin R, et al. Single-atom Pt supported on holey ultrathin $\text{g-C}_3\text{N}_4$ nanosheets as efficient catalyst for Li-O₂ batteries. *J Colloid Interface Sci* 2020;564:28-36. DOI
209. Guo Q, Zhang C, Zhang C, et al. Co_3O_4 modified $\text{Ag/g-C}_3\text{N}_4$ composite as a bifunctional cathode for lithium-oxygen battery. *J Energy Chem* 2020;41:185-93. DOI
210. Li Y, Wang J, Li X, Geng D, Li R, Sun X. Superior energy capacity of graphene nanosheets for a nonaqueous lithium-oxygen battery. *Chem Commun* 2011;47:9438-40. DOI
211. Wu G, Mack NH, Gao W, et al. Nitrogen-doped graphene-rich catalysts derived from heteroatom polymers for oxygen reduction in nonaqueous lithium-O₂ battery cathodes. *ACS Nano* 2012;6:9764-76. DOI
212. Liu M, Zhu X, Song Y, et al. Bifunctional edge-rich nitrogen doped porous carbon for activating oxygen and sulfur. *Adv Funct Mater* 2023;33:2213395. DOI
213. Lin Y, Moitoso B, Martinez-Martinez C, et al. Ultrahigh-capacity lithium-oxygen batteries enabled by dry-pressed holey graphene air cathodes. *Nano Lett* 2017;17:3252-60. DOI
214. Shui J, Lin Y, Connell JW, Xu J, Fan X, Dai L. Nitrogen-doped holey graphene for high-performance rechargeable Li-O₂ batteries. *ACS Energy Lett* 2016;1:260-5. DOI
215. Ren X, Zhu J, Du F, Liu J, Zhang W. B-doped graphene as catalyst to improve charge rate of lithium-air battery. *J Phys Chem C* 2014;118:22412-8. DOI
216. Zoubi W, Putri RAK, Abukhadra MR, Ko YG. Recent experimental and theoretical advances in the design and science of high-entropy alloy nanoparticles. *Nano Energy* 2023;110:108362. DOI
217. Kumar S, Kumar S, Kumar D, Sathish N, Singh A, Goswami M. Reduced graphene oxide and Pd nanocomposite as a catalyst for

- oxygen reduction reaction in rechargeable Li-oxygen battery. *ChemistrySelect* 2019;4:8404-9. DOI
218. Su D, Han Seo D, Ju Y, et al. Ruthenium nanocrystal decorated vertical graphene nanosheets@Ni foam as highly efficient cathode catalysts for lithium-oxygen batteries. *NPG Asia Mater* 2016;8:e286. DOI
219. Ye SJ, Kim DY, Kim DW, Park OO, Kang Y. Facile synthesis of palladium nanodendrites supported on graphene nanoplatelets: an efficient catalyst for low overpotentials in lithium-oxygen batteries. *J Mater Chem A* 2016;4:578-86. DOI
220. Zhou W, Cheng Y, Yang X, et al. Iridium incorporated into deoxygenated hierarchical graphene as a high-performance cathode for rechargeable Li-O₂ batteries. *J Mater Chem A* 2015;3:14556-61. DOI
221. Bi X, Li M, Liu C, et al. Cation Additive enabled rechargeable LiOH-based lithium-oxygen batteries. *Angew Chem Int Ed* 2020;59:22978-82. DOI
222. Gallant BM. Unlocking reversibility of LiOH-based Li-air batteries. *Joule* 2020;4:2254-6. DOI
223. Zhang M, Zou L, Yang C, Chen Y, Shen Z, Bo C. An all-nanosheet OER/ORR bifunctional electrocatalyst for both aprotic and aqueous Li-O₂ batteries. *Nanoscale* 2019;11:2855-62. DOI
224. Tang C, Sun P, Xie J, et al. Two-dimensional IrO₂/MnO₂ enabling conformal growth of amorphous Li₂O₂ for high-performance Li-O₂ batteries. *Energy Stor Mater* 2017;9:206-13. DOI
225. Zhang P, He M, Xu S, Yan X. The controlled growth of porous δ-MnO₂ nanosheets on carbon fibers as a bi-functional catalyst for rechargeable lithium-oxygen batteries. *J Mater Chem A* 2015;3:10811-8. DOI
226. Zhang J, Li P, Wang Z, et al. Three-dimensional graphene-Co₃O₄ cathodes for rechargeable Li-O₂ batteries. *J Mater Chem A* 2015;3:1504-10. DOI
227. Song K, Cho E, Kang Y. Morphology and active-site engineering for stable round-trip efficiency Li-O₂ batteries: a search for the most active catalytic site in Co₃O₄. *ACS Catal* 2015;5:5116-22. DOI
228. Liu Q, Xu J, Chang Z, Zhang X. Direct electrodeposition of cobalt oxide nanosheets on carbon paper as free-standing cathode for Li-O₂ battery. *J Mater Chem A* 2014;2:6081-5. DOI
229. Hu X, Cheng F, Zhang N, Han X, Chen J. Nanocomposite of Fe₂O₃@C/MnO₂ as an efficient cathode catalyst for rechargeable lithium-oxygen batteries. *Small* 2015;11:5545-50. DOI
230. Hong M, Choi HC, Byon HR. Nanoporous NiO plates with a unique role for promoted oxidation of carbonate and carboxylate species in the Li-O₂ battery. *Chem Mater* 2015;27:2234-41. DOI
231. Zhang Y, Hu M, Yuan M, et al. Ordered two-dimensional porous Co₃O₄ nanosheets as electrocatalysts for rechargeable Li-O₂ batteries. *Nano Res* 2019;12:299-302. DOI
232. Zheng Y, Gao R, Zheng L, Sun L, Hu Z, Liu X. Ultrathin Co₃O₄ nanosheets with edge-enriched {111} planes as efficient catalysts for lithium-oxygen batteries. *ACS Catal* 2019;9:3773-82. DOI
233. Li JH, Yu YX. How Do oxygen vacancies influence the catalytic performance of two-dimensional Nb₂O₅ in lithium- and sodium-oxygen batteries? *ChemSusChem* 2021;14:5488-98. DOI
234. Long Y, Zhang Z, Zhao L, et al. Bucket effect on high-performance Li-O₂ batteries based on P-doped 3D NiO microspheres with conformal growth of discharge products. *J Mater Chem A* 2022;10:24538-51. DOI
235. Wang G, Zhang S, Qian R, Wen Z. Atomic-Thick TiO₂(B) nanosheets decorated with ultrafine Co₃O₄ nanocrystals as a highly efficient catalyst for lithium-oxygen battery. *ACS Appl Mater Interfaces* 2018;10:41398-406. DOI
236. Wang H, Fan B, Luo Z, Wu Q, Zhou X, Wang F. A unique hierarchical structure: NiCo₂O₄ nanowire decorated NiO nanosheets as a carbon-free cathode for Li-O₂ battery. *Catal Sci Technol* 2021;11:7632-9. DOI
237. Song K, Ai W, Zhang Y, et al. Three-dimensional self-supported CuCo₂O₄ nanowires@NiO nanosheets core/shell arrays as an oxygen electrode catalyst for Li-O₂ batteries. *J Mater Chem A* 2021;9:3007-17. DOI
238. Liu G, Zhang L, Wang S, Ding L, Wang H. Hierarchical NiCo₂O₄ nanosheets on carbon nanofiber films for high energy density and long-life Li-O₂ batteries. *J Mater Chem A* 2017;5:14530-6. DOI
239. Suntivich J, Gasteiger HA, Yabuuchi N, Nakanishi H, Goodenough JB, Shao-Horn Y. Design principles for oxygen-reduction activity on perovskite oxide catalysts for fuel cells and metal-air batteries. *Nat Chem* 2011;3:546-50. DOI PubMed
240. Kim C, Gwon O, Jeon I, et al. Cloud-like graphene nanoplatelets on Nd_{0.5}Sr_{0.5}CoO_{3-δ} nanorods as an efficient bifunctional electrocatalyst for hybrid Li-air batteries. *J Mater Chem A* 2016;4:2122-7. DOI
241. Zhou Y, Yan D, Gu Q, et al. Implanting cation vacancies in Ni-Fe LDHs for efficient oxygen evolution reactions of lithium-oxygen batteries. *Appl Catal B* 2021;285:119792. DOI
242. Sun Z, Lin L, Yuan M, et al. Two-dimensional β-cobalt hydroxide phase transition exfoliated to atom layers as efficient catalyst for lithium-oxygen batteries. *Electrochim Acta* 2018;281:420-8. DOI
243. Zhu J, Metzger M, Antonietti M, Feller TP. Vertically aligned two-dimensional graphene-metal hydroxide hybrid arrays for Li-O₂ batteries. *ACS Appl Mater Interfaces* 2016;8:26041-50. DOI
244. Wang X, Wang Q, Hou X, et al. Facile fabrication of two-dimensional reduced graphene oxide/CoAl-layered double hydroxides nanocomposites for lithium-oxygen battery with improved electrochemical performance. *J Alloys Compd* 2018;744:196-203. DOI
245. Lu X, Sakai N, Tang D, et al. CoNiFe Layered Double Hydroxide/RuO_{2,1} nanosheet superlattice as carbon-free electrocatalysts for water splitting and Li-O₂ batteries. *ACS Appl Mater Interfaces* 2020;12:33083-93. DOI
246. Ding S, Liu S, Li J, Wu L, Ma ZF, Yuan X. Multifunctional catalyst CuS for nonaqueous rechargeable lithium-oxygen batteries. *ACS Appl Mater Interfaces* 2021;13:50065-75. DOI
247. Hou Z, Shu C, Hei P, et al. Configuration of gradient-porous ultrathin FeCo₂S₄ nanosheets vertically aligned on Ni foam as a

- noncarbonaceous freestanding oxygen electrode for lithium-oxygen batteries. *Nanoscale* 2020;12:1864-74. DOI
248. Sadighi Z, Liu J, Ciucci F, Kim JK. Mesoporous MnCo_2S_4 nanosheet arrays as an efficient catalyst for Li-O₂ batteries. *Nanoscale* 2018;10:15588-99. DOI PubMed
249. Zhang P, Hui X, Wang H, Gao X, Yin L. Porous hollow ZnCo_2S_4 nanosheet arrays derived from metal-organic framework as efficient cathode for lithium oxygen batteries. *J Alloys Compd* 2021;860:157656. DOI
250. Zhang G, Li G, Wang J, et al. 2D SnSe cathode catalyst featuring an efficient facet-dependent selective Li₂O₂ growth/decomposition for Li-oxygen batteries. *Adv Energy Mater* 2022;12:2103910. DOI
251. Guo L, Tan L, Xu A, et al. Highly efficient two-dimensional Ag₂Te cathode catalyst featuring a layer structure derived catalytic anisotropy in lithium-oxygen batteries. *Energy Stor Mater* 2022;50:96-104. DOI
252. Ran Z, Shu C, Hou Z, et al. Phosphorus vacancies enriched Ni₂P nanosheets as efficient electrocatalyst for high-performance Li-O₂ batteries. *Electrochim Acta* 2020;337:135795. DOI
253. Wei M, Luo Y, Jin C, et al. MoP nanoflakes as efficient electrocatalysts for rechargeable Li-O₂ batteries. *ACS Appl Energy Mater* 2018;1:331-5. DOI
254. Ma Z, Yuan X, Zhang Z, et al. Novel flower-like nickel sulfide as an efficient electrocatalyst for non-aqueous lithium-air batteries. *Sci Rep* 2015;5:18199. DOI PubMed PMC
255. Hou Z, Long J, Shu C, Liang R, Li J, Liao X. Two-dimensional spinel CuCo_2S_4 nanosheets as high efficiency cathode catalyst for lithium-oxygen batteries. *J Alloys Compd* 2019;798:560-7. DOI
256. He B, Li G, Li J, et al. MoSe₂@CNT core-shell nanostructures as grain promoters featuring a direct Li₂O₂ formation/decomposition catalytic capability in lithium-oxygen batteries. *Adv Energy Mater* 2021;11:2003263. DOI
257. Hu A, Shu C, Qiu X, Li M, Zheng R, Long J. Improved cyclability of lithium-oxygen batteries by synergistic catalytic effects of two-dimensional MoS₂ nanosheets anchored on hollow carbon Spheres. *ACS Sustain Chem Eng* 2019;7:6929-38. DOI
258. Lai Y, Chen W, Zhang Z, Gan Y, Yang X, Li J. Two-dimensional graphene-like MoSe₂ nanosheets anchored on hollow carbon nanofibers as a cathode catalyst for rechargeable Li-O₂ batteries. *RSC Adv* 2016;6:19843-7. DOI
259. Sun Z, He J, Yuan M, et al. Li⁺-clipping for edge S-vacancy MoS₂ quantum dots as an efficient bifunctional electrocatalyst enabling discharge growth of amorphous Li₂O₂ film. *Nano Energy* 2019;65:103996. DOI
260. Sadighi Z, Liu J, Zhao L, Ciucci F, Kim JK. Metallic MoS₂ nanosheets: multifunctional electrocatalyst for the ORR, OER and Li-O₂ batteries. *Nanoscale* 2018;10:22549-59. DOI
261. Wang J, Gao R, Zheng L, et al. CoO/CoP Heterostructured nanosheets with an O-P interpenetrated interface as a bifunctional electrocatalyst for Na-O₂ battery. *ACS Catal* 2018;8:8953-60. DOI
262. Yan Y, Ran Z, Zeng T, et al. Interfacial electron redistribution of hydrangea-like NiO@Ni₂P heterogeneous microspheres with dual-phase synergy for high-performance lithium-oxygen battery. *Small* 2022;18:e2106707. DOI
263. Yang Y, Chen J, Gao Q, Feng Y, Xing F, Yao M. First-principle study on catalytic activity of functionalized Ti₃C₂ MXene as cathode catalyst for Li-O₂ batteries. *Current Appl Phys* 2022;34:24-8. DOI
264. Jiang Y, Tian M, Wang H, et al. Mildly oxidized MXene (Ti₃C₂, Nb₂C, and V₂C) electrocatalyst via a generic strategy enables longevous Li-O₂ battery under a high rate. *ACS Nano* 2021;15:19640-50. DOI
265. Li G, Li N, Peng S, et al. Highly efficient Nb₂C MXene cathode catalyst with uniform O-terminated surface for lithium-oxygen batteries. *Adv Energy Mater* 2021;11:2002721. DOI
266. Li J, Han K, Huang J, et al. Polarized nucleation and efficient decomposition of Li₂O₂ for Ti₃C MXene cathode catalyst under a mixed surface condition in lithium-oxygen batteries. *Energy Stor Mater* 2021;35:669-78. DOI
267. Zhao D, Wang P, Di H, Zhang P, Hui X, Yin L. Single semi-metallic selenium atoms on Ti₃C₂ MXene nanosheets as excellent cathode for lithium-oxygen batteries. *Adv Funct Mater* 2021;31:2010544. DOI
268. Zheng R, Shu C, Hou Z, et al. In Situ Fabricating oxygen vacancy-rich TiO₂ nanoparticles via utilizing thermodynamically metastable Ti atoms on Ti₃C₂T_x MXene nanosheet surface to boost electrocatalytic activity for high-performance Li-O₂ batteries. *ACS Appl Mater Interfaces* 2019;11:46696-704. DOI
269. Zheng R, Shu C, Chen X, et al. Unique intermediate adsorption enabled by anion vacancies in metal sulfide embedded MXene nanosheets overcoming kinetic barriers of oxygen electrode reactions in lithium-oxygen batteries. *Energy Stor Mater* 2021;40:41-50. DOI
270. Lv Q, Zhu Z, Ni Y, et al. Atomic ruthenium-riveted metal-organic framework with tunable d-band modulates oxygen redox for lithium-oxygen batteries. *J Am Chem Soc* 2022;144:23239-46. DOI
271. Lv Q, Zhu Z, Ni Y, Geng J, Li F. Spin-state manipulation of two-dimensional metal-organic framework with enhanced metal-oxygen covalency for lithium-oxygen batteries. *Angew Chem Int Ed* 2022;61:e202114293. DOI
272. Luo WB, Chou SL, Wang JZ, Zhai YC, Liu HK. A metal-free, free-standing, macroporous graphene@g-C₃N₄ composite air electrode for high-energy lithium oxygen batteries. *Small* 2015;11:2817-24. DOI PubMed
273. Yi J, Liao K, Zhang C, Zhang T, Li F, Zhou H. Facile in situ preparation of graphitic-C₃N₄@carbon paper as an efficient metal-free cathode for nonaqueous Li-O₂ battery. *ACS Appl Mater Interfaces* 2015;7:10823-7. DOI PubMed
274. Mehri M, Mousavi-khoshdel S, Molaei M. First-principle calculations study of pristine, S-, O-, and P-doped g-C₃N₄ as ORR catalysts for Li-O₂ batteries. *Chem Phys Lett* 2021;775:138614. DOI
275. Hang Y, Zhang C, Luo X, et al. α-MnO₂ nanorods supported on porous graphitic carbon nitride as efficient electrocatalysts for lithium-air batteries. *J Power Sources* 2018;392:15-22. DOI

276. Wu Y, Wang T, Zhang Y, et al. Electrocatalytic performances of g-C₃N₄-LaNiO₃ composite as bi-functional catalysts for lithium-oxygen batteries. *Sci Rep* 2016;6:24314. [DOI](#) [PubMed](#) [PMC](#)
277. Kumar S, Jena A, Hu YC, et al. Cobalt diselenide nanorods grafted on graphitic carbon nitride: a synergistic catalyst for oxygen reactions in rechargeable Li-O₂ batteries. *ChemElectroChem* 2018;5:29-35. [DOI](#)